

KUNGL. TEKNISKA HÖGSKOLANS
HANDLINGAR

TRANSACTIONS OF THE ROYAL INSTITUTE OF TECHNOLOGY
STOCKHOLM, SWEDEN

Nr 80

1954

UDC 621.385.16:621.518.57
BIBLIOTHEEK
LABORATORIUM VOOR
TECHNISCHE FYSICA
DELFT

DEVELOPMENT OF TROCHOTRONS

BY

J. BJÖRKMAN and L. LINDBERG



STOCKHOLM
AB. HENRIK LINDSTAHL'S BOKHANDEL I DISTRIBUTION

110g-
forsk-
s not
buted

Förteckning över Kungl. Tekniska Högskolans Handlingar:

1. *List of Publications of Members of the Staff of The Royal Institute of Technology, Stockholm.* 270 s. 1947. Kr. 14: —.
2. NYLANDER, HENRIK och HOLST, HANS, *Några undersökningar rörande skivor och höga balkar av armerad betong.* 66 s. 1946. Kr. 2: —. (Meddelanden från Institutionen för Byggnadsstatik).
3. NEOVIUS, GÖSTA, *New Methods of Filter Design by Means of Frequency Transformations.* 41 s. 1946. Kr. 2: —.
4. HELLSTRÖM, NILS, *On Distillates from Wood.* 15 s. 1947. Kr. 1: —.
5. SAMUELSSON, OLOF, *Reinigung von Wasser durch Ausflockung.* 15 s. 1947. Kr. 1: —.
6. HALLÉN, ERIK, *Some Units in the Giorgi System and the C. G. S. System.* 44 s. 1947. Kr. 2: 50.
7. BÄCKSTRÖM, MATTS, *A Peculiar Thermodynamical Analogy.* 12 s. 1947. Kr. 1: —.
8. WERTHÉN, HANS, and NILSSON, BJÖRN, *An Automatic Impedance Meter.* 95 s. 1947. Kr. 4: 50.
9. EGGWERTZ, SIGGE, *Theory of Elasticity for Thin Circular Cylindrical Shells.* 26 s. 1947. Kr. 2: —.
10. NIORDSON, FRITHIOF, I. N., *Buckling of Conical Shells Subjected to Uniform External Lateral Pressure.* 23 s. 1947. Kr. 1: 50.
11. FORSSBLAD, LARS, *Effects of Wind, Waves, and Current on Floating Timber.* 75 s. 1947. Kr. 3: 50.
12. HALLÉN, ERIK, *Iterated Sine and Cosine Integrals.* 6 s. 1947. Kr. 1: —.
13. HALLÉN, ERIK, *On Antenna Impedances.* 18 s. 1947. Kr. 2: —.
14. THAM, PERCY, *Photogrammetric Orientation Data and Determination of their Accuracy.* 38 s. 1947. Kr. 2: 50.
15. MALMQUIST, LARS, *Temperature Measurements in High-Velocity Gas Streams.* 54 s. 1948. Kr. 3: —.
16. BJERHAMMAR, ARNE, *A Method of Combined Centring and Levelling for Surveying Instruments Equipped with Optical Plumb Indicators.* 32 s. 1948. Kr. 2: —.
17. MORTSELL, STURE, *On Accuracy of Sieve Analyses Made by Means of Sieving Machines.* 45 s. 1948. Kr. 3: —.
18. WEIBULL, W., *Waves in Compressible Media.* I. Basic Equations. II. Plane Continuous Waves. 38 s. 1948. Kr. 3: —.
19. MALMLÖW, G., *Thermal Ageing Properties of Cellulose Insulating Materials.* 67 s. 1948. Kr. 3: —.
20. JOHANSSON, C. H., *Theoretical Investigation of the Effect of Capillary Suction on Transfer of Moisture in Hygroscopic Materials.* 16 s. 1948. Kr. 2: —.
21. HELLSTRÖM, NILS, *On Distillates from Fir Stumps.* Part I. Fir Tar and Oils from Fir Tar. Part II. Neutral Substances Present in Fir Tar and Oils from Fir Tar. 54 s. 1948. Kr. 3: 50.
22. ALFVÉN, H., LINDBERG, L., MALMFORS, K. G., WALLMARK, T., and ÅSTRÖM, E., *Theory and Applications of Trochotrons.* 106 s. 1948. Kr. 6: —.
23. JOSEPHSON, BENGT, *Impedance Measurements in Decimetre Wave Band.* 70 s. 1948. Kr. 5: —.
24. FÄLKEMO, CURT, and ADLERCREUTZ, JOHAN, *Model Tests on Single-Step Planing Surfaces.* (Publication No 1/1947 of The Ship Testing Laboratory). 40 s. 1948. Kr. 3: 50.
25. ALM, EMIL, *Physical Properties of Arcs in Circuit Breakers.* 248 s. 1949. Kr. 12: —.
26. MORATH, ERIK, *A Mathematical Theory of Shaded-Pole Motors.* 48 s. 1949. Kr. 4: —.
27. WEIBULL, W., *A Statistical Representation of Fatigue Failures in Solids.* 51 s. 1949. Kr. 4: —.
28. NYLANDER, HENRIK, *Torsional and Lateral Buckling of Eccentrically Compressed I and T Columns.* 33 s. 1949. Kr. 3: —.
29. PETTERSSON, OVE, *Combined Bending and Torsion of Simply Supported Beams of Bissymmetrical Cross Section.* 45 s. 1949. Kr. 3: 50.
30. WÄSTLUND, GEORG, and BERGSTROM, SVEN G., *Buckling of Compressed Steel Members.* 172 s. 1949. Kr. 10: —.
31. BJÖRKMAN, ANDERS, *Studies on Hydrogenation of Sulphite Waste Liquor.* 41 s. 1950. Kr. 4: —.
32. HEUMAN, CARL, *Zur Theorie der elliptischen Integrale.* 58 s. 1950. Kr. 4: 50.
33. REGNELL, STIG, *Wood-Staff Pipes.* 158 s. 1950. Kr. 10: —.
34. ODQVIST, F. K. G. and SCHAUB, C., *The Yield Point of Mild Steel at Non-Homogeneous and Compound Stress Distributions.* 16 s. 1950. Kr. 2: —.
35. HALLERT, B., *Contribution to Theory of Errors for Double Point Intersection in Space.* 80 s. 1950. Kr. 5: —.

VI 7 27

B10

KUNGL. TEKNISKA HÖGSKOLANS
HANDLINGAR

TRANSACTIONS OF THE ROYAL INSTITUTE OF TECHNOLOGY
STOCKHOLM, SWEDEN

Nr 80

1954

UDC 621.385.16:621.318.57

DEVELOPMENT OF TROCHOTRONS

BY

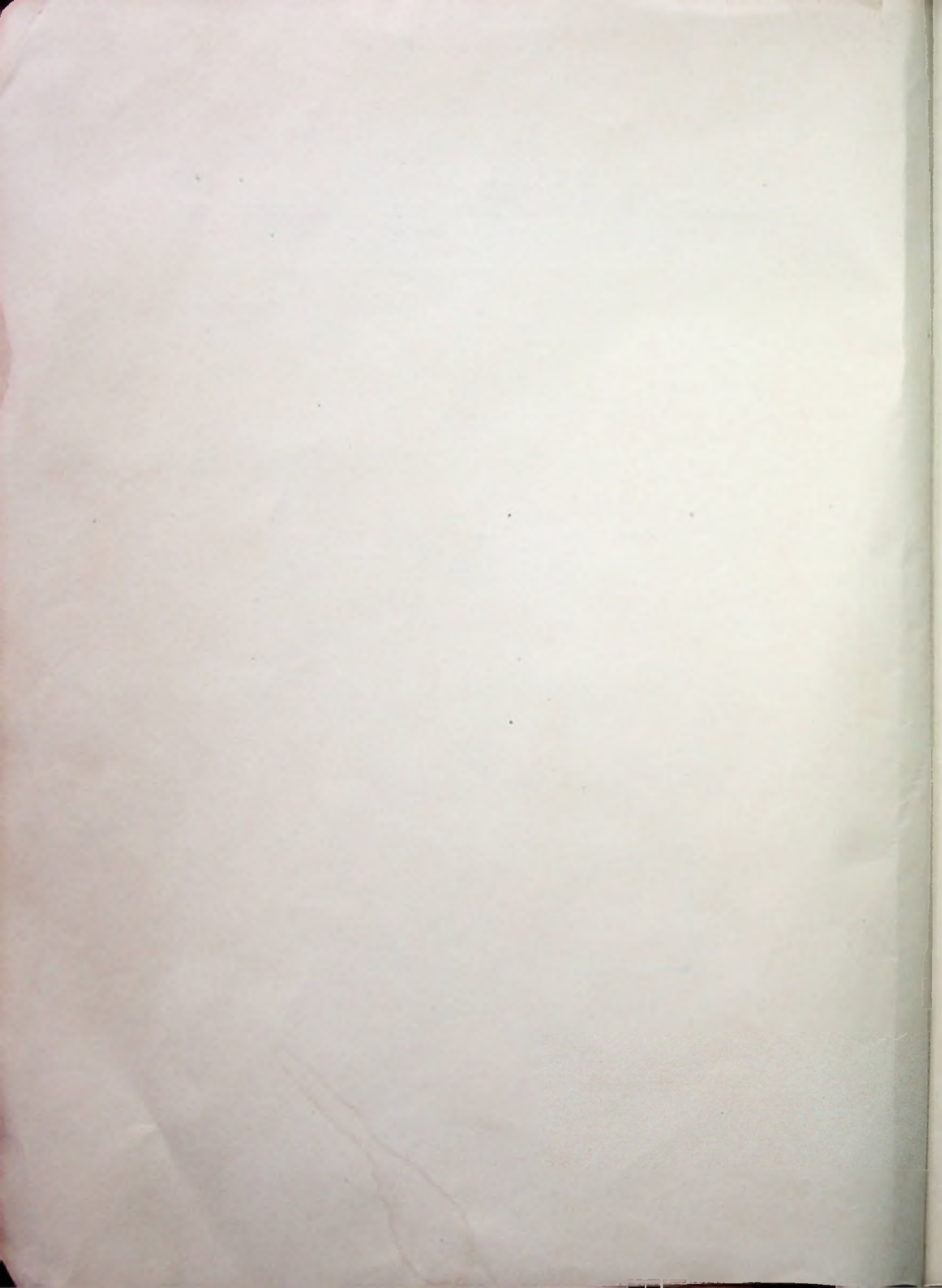
J. BJÖRKMAN and L. LINDBERG



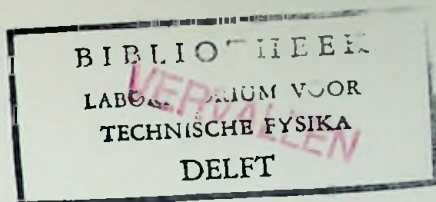
BIBLIOTHEEK
LABORATORIUM VOOR
TECHNISCHE FYSIKA
DELFT

GÖTEBORG 1954
ELANDERS BOKTRYCKERI AKTIEBOLAG

2275



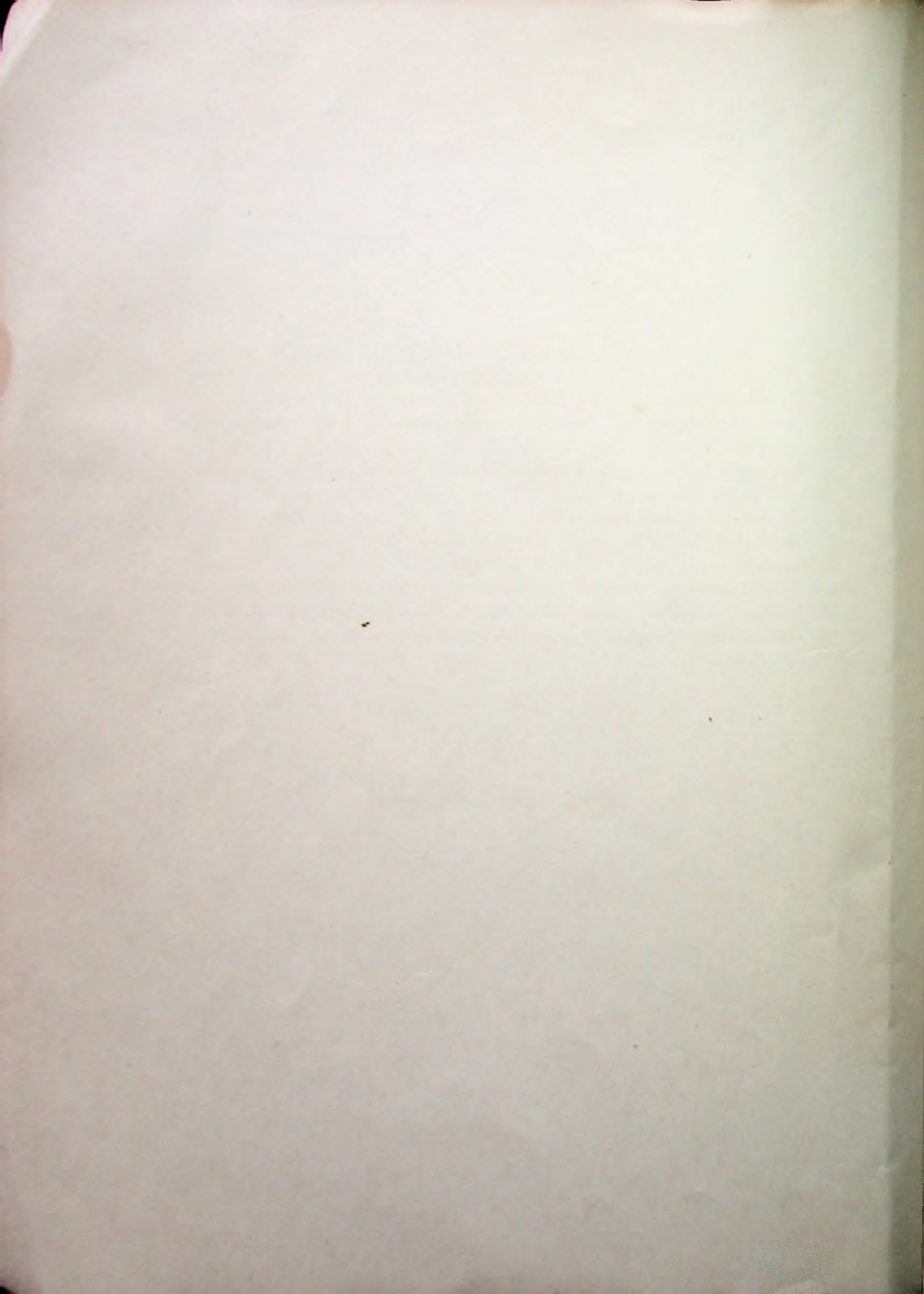
VH . 7. 27



Summary

The trochotron is a multielectrode electron tube working in a magnetic field. A trochoidal beam is formed and can be guided to different electrode boxes forming an electronic switch or selector. Trochotrons of plane design are earlier described. The present work, performed during 1948—1951, describes the development of two new designs, the cylindrical and the binary types. Electronic phenomena, such as space charge effects, noise and oscillations are of great importance. The experimental investigations are described and optimum design and operating conditions are discussed.

The main application of the cylindrical trochotron is as a decade counter for random pulses. It is capable of very high counting rates, 10^7 pulses per second have been reached. The binary trochotron is applicable to calculating machines. A pyramid selector and an adder are described.



7 27

BIBLIOTHEEK
LABORATORIUM VOOR
TECHNISCHE FYSIKA
DELFT

CHAPTER 1.
BASIC TROCHOTRON TECHNICS
BY
J. BJÖRKMAN

1.1. Trochoidal electronic beams

The principle of trochoidal electronic motion is well known and discussed in many textbooks.

An electron, subject to the action of electric and magnetic fields at right angles to each other and at right angles to the initial velocity of the electron, moves in a trochoidal path. The motion of the electron is a combination of a circular motion and a translation, like the motion of a point on a rolling wheel. The centre of the »wheel» follows approximately an electric equipotential line.

Fig. 1.1 shows how a trochoidal electron beam is obtained. A cathode *c* is placed in the electric field between two electrodes *a* and *r*, *a* being positive and *r* negative with respect to the cathode. A homogeneous magnetic field *B*, perpendicular to the plane of the paper, penetrates the electrode assembly. The emitted electrons are confined in a beam consisting of a complex mixture of trochoidal electron orbits filling a narrow equipotential space slightly above

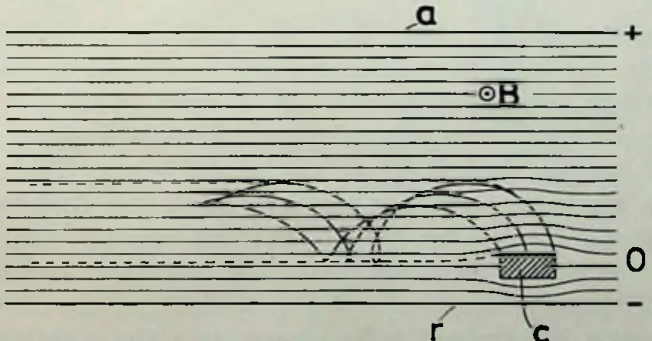


Fig. 1.1. Electron paths forming a trochoidal beam.

the potential of the cathode. As discussed by WALLMARK [ALFVÉN *et al.* 1948, p. 34] a trochoidal beam may have different structure depending on the starting conditions. Some designs of electron source produce principally curtate trochoids, others prolate trochoids. In the recently developed trochotrons having trochoidal beams of very high current density the space charge has a great influence on the electron paths. The space charge tends to straighten the orbits. An ideal case is the laminar flow considered in chapt 3.

The beam can be guided at will by shifting the equipotential lines along which it travels. This is a very important and characteristic property of trochoidal electronic beams. For a mathematical treatment of the problem, see ALFVÉN [1950, chapt. 2].

An electrode can take current from the trochoidal beam mainly in two ways. In the first case the beam hits an electrode at the same potential as the beam itself. In general only part of the beam will be collected in this manner. In the second case the beam is urged to the receiver by a strong electric field. Thus a very efficient method to catch the beam is to guide it into a corner or a narrow slit between a positive and a negative electrode. In the strong electric field then encountered by the beam, the electric forces acting upon the electrons are much greater than the magnetic ones. The electrons are all pulled to the positive electrode and the beam completely collected.

There is also a possibility to take electrons off the beam in the direction of the magnetic field. In the trochotron, however, this method has been used only in a few special cases.

1.2. Trochotrons

The trochotron [ALFVÉN *et al.*, 1947, 1948], an invention of Prof. H. ALFVÉN, is an electron tube utilizing trochoidal beams. It is a multielectrode tube, containing a set of open boxes and operating in a magnetic field. Along electrical equipotential surfaces a trochoidal beam can be guided to any one of the boxes. The trochotron is thus an electronic switch or selector and it may find applications in fields where switching has to be done quickly, *e. g.* in pulse counters, calculating machines, automatic telephony and the like.

Fig. 1.2. shows schematically the electrode structure of three types of trochotrons, *a* the plane, *b* the binary and *c* the cylindrical design. The drawings are crosssections perpendicular to the magnetic field.

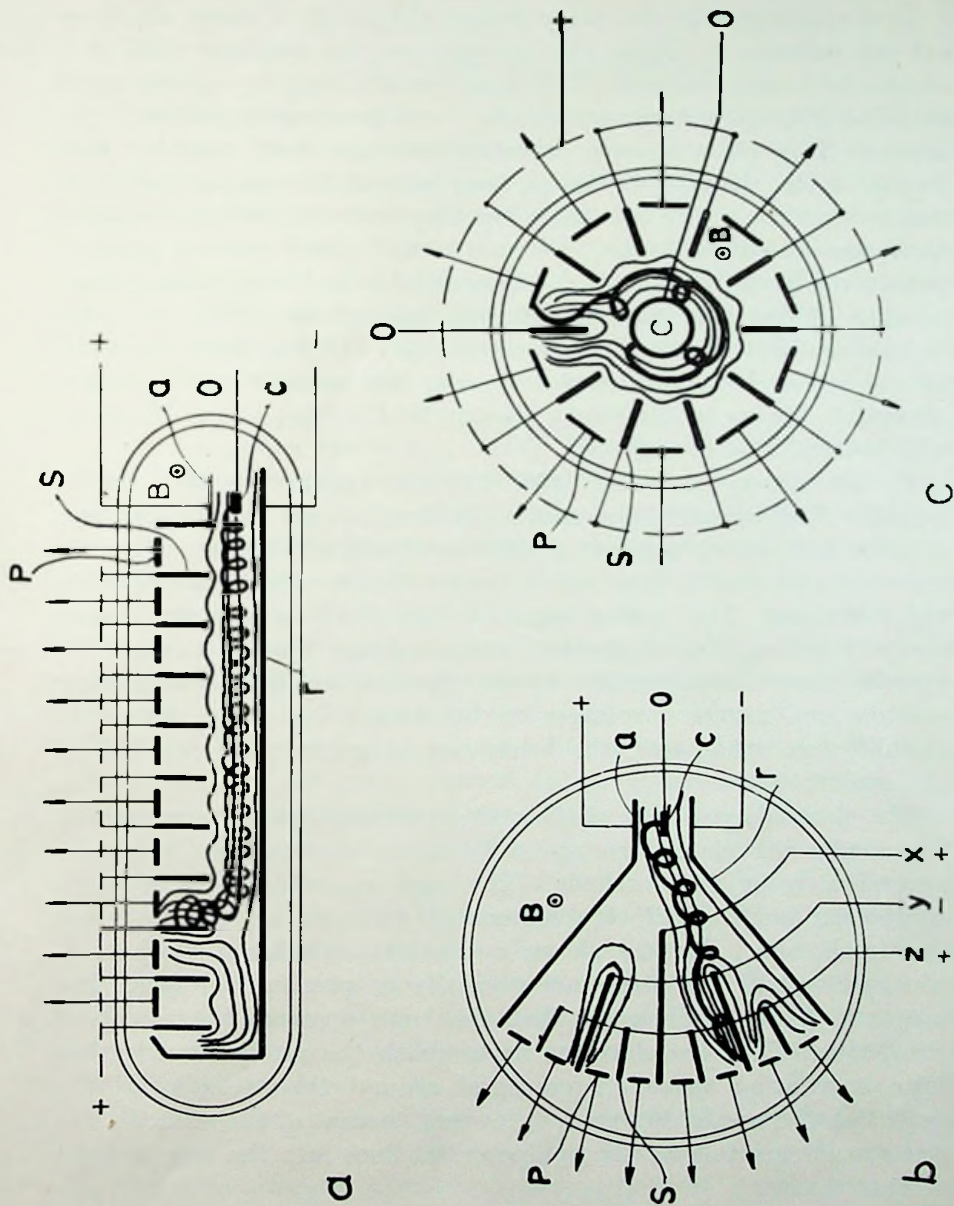


Fig. 1.2. Schematic cross-sections of trochotrons: *a*, the plane, *b*, the binary and *c*, the cylindrical type.

The thin lines indicate electrical equipotential surfaces and the heavy trochoidal-shaped curves illustrate electron paths.

In a trochotron of the plane design the anode a draws electrons off the cathode c . Under the influence of the magnetic field B a trochoidal beam is formed. This beam travels along the equipotential lines into the space between a «rail», r and an array of positive «spades», s . The rail is at zero potential or a few volts negative with respect to the cathode. In the spacings between the spades, electrodes named «plates», p , are inserted. Together with the spades the plates form the electrode boxes. Normally the plates are at positive potential. If the potential of a spade is lowered and brought near to that of the rail, the equipotential lines along which the beam travels are bent up into the corresponding box. The beam is guided to the corner between the plate of the box and the spade at low potential. Owing to the strong electric field in that corner the plate will collect the electrons.

In the binary trochotron (fig. 2 *b*) the spades are of different lengths. The largest of the spades divides the tube in an upper and a lower half, two somewhat smaller spades divide these halves into quarters and finally four small spades divide these quarters into eight sections. The spades together with the plates constitute an array of boxes. The trochoidal beam emerging from the cathode c , travels above a negative and below a positive spade. By combining positive and negative voltages on the terminals x , y , z , joined to the different spade sets, the beam can be guided into any one of the eight boxes.

The electrode structure of the cylindrical trochotron is very simple. The spades and plates forming the boxes are arranged symmetrically around a cylindrical cathode. The tube resembles a split-anode magnetron but instead of a segmented anode it has the boxes of the trochotron. Fig. 2 *c* shows a ten box cylindrical trochotron. The spades and the plates are normally at positive voltages. The magnetic field is so strong that the tube operates above cut-off conditions. Thus the electrons never reach the positive spades but form a rotating space charge cloud around the cathode. If the potential of a spade, however, is lowered to that of the cathode, the electron stream follows the equipotential lines into the box in front of that spade.

The «breadth» of the beam, *i. e.* the extension in the direction of the magnetic field, is limited either by metal side plates or by mica

sheets. The former method is preferred in tubes where the length of the beam is large in comparison with the breadth.

1.3. Tube characteristics

The main characteristics of a trochotron are shown by the diagrams of fig. 1.3. In these the current to an arbitrary spade s and its neighboring electrodes are plotted as functions of the voltage V_{sn} of that spade. The electrodes are numbered in the direction opposite to the electron flow. Thus seen in the latter direction the spade s_{n-1} is the spade behind s_n and s_{n+1} that in front of it as illustrated in fig. 1.4. The plate p_{n-1} is the neighboring plate behind s_n and p_n is the plate adjacent to the spade on the front side. When the beam goes to the box $n-1$ it passes between s_{n-1} and s_n and lands on p_{n-1} .

Assuming the spade s_{n-1} being initially at zero potential, the beam will, following the equipotential lines, go to the box $n-1$ behind s_n . If the voltage of s_n then is decreased from the supply voltage V_{s0} , the equipotential lines are bent upwards in front of s_n and the beam brought to the plate p_n . The current distribution is illustrated in fig. 1.3 *a*. At high values of V_{sn} the whole beam current appears as $I_{p_{n-1}}$, current to the plate p_{n-1} . At lower values of V_{sn} this current drops and current begins flowing to p_n , indicating that the beam is shifting over to that plate. When the spade s_n has about the same potential as the beam it takes current from it. As shown in fig. 1.3 *a* the current to s_n , I_{sn} , increases when V_{sn} is decreased. After passing a maximum this current will decrease again when V_{sn} is lowered still more.

The current to s_n at high V_{sn} is zero or negligible, however, only if the plate p_{n-1} is at a high positive potential. Then, as shown in Fig. 1.4 *a* the beam goes to the slit between s_{n-1} and p_{n-1} leaving s_n practically currentless. In the case shown in Fig. 1.4 *b* p_{n-1} is at zero potential. Here the equipotential lines are bent over to the slit between p_{n-1} and the rear side of s_n , causing the current to flow to the positive spade.

Fig. 1.3 *b* shows a family of spade characteristics with the voltage of p_{n-1} , $V_{p_{n-1}}$, as a parameter. The full line curve $V_{p_{n-1}} = V_{p0}$ is the characteristic obtained when p_{n-1} is at its positive supply voltage. When p_{n-1} is at zero potential, the dashed characteristic is obtained, and the dot-dashed curve $V_{p_{n-1}} = V_{st}$ is the characte-

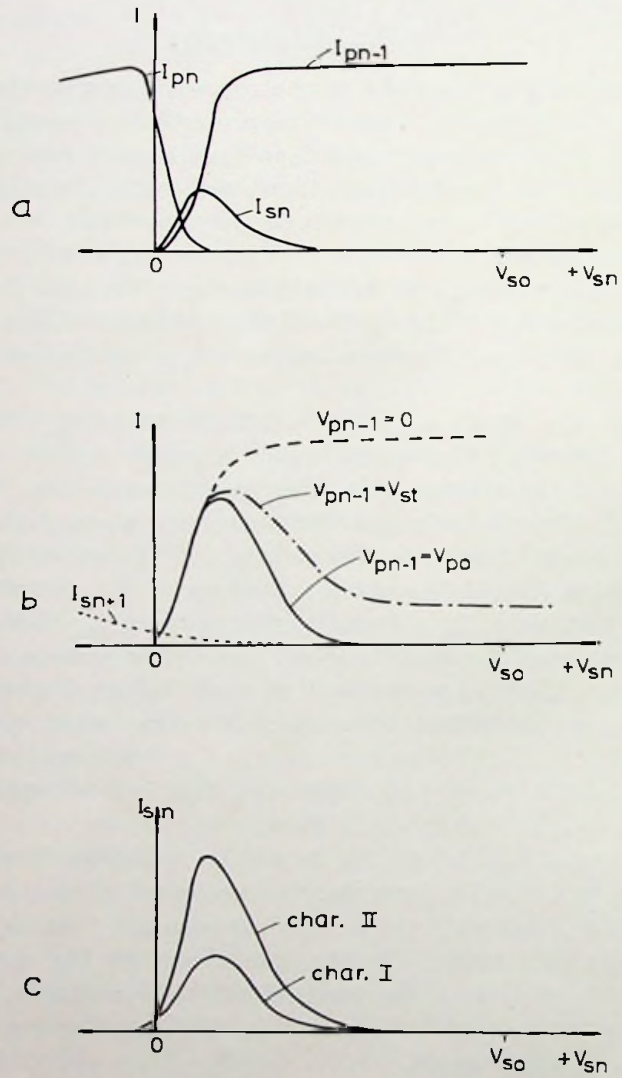


Fig. 1.3. Main characteristics of a trochotron.

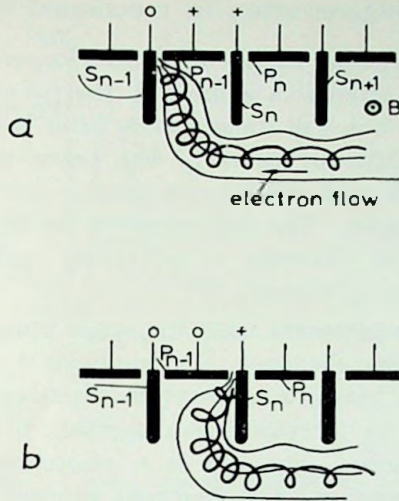


Fig. 1.4. Beam switch-over.

ristic for a critical plate voltage, the «stepping voltage» V_{st} . The significance of the stepping voltage will be explained in 1.6.

The spade characteristic is generally dependent on the potential of the spade behind it. When the voltage of the spade s_n is varied, the voltage of s_{n-1} being positive, the first order spade characteristic, or briefly characteristic I, is obtained. The second order characteristic, characteristic II, appears when s_{n-1} is at zero voltage. Still higher order characteristics are obtained when two or more spades behind s_n are at zero potential. The spade characteristics in fig. 1.3 *a* and *b* are consequently of second order. As illustrated in fig. 1.3 *c* the characteristic II generally is higher than characteristic I. These two characteristics determine the conditions for stable locking of the beam as will be evident in 1.6. The higher order characteristics are important in high speed operation.

The dotted curve $I_{s_{n+1}}$ in fig. 1.3 *b* is the current to the spade s_{n+1} when the beam goes to the box n . It is called the «leak current». When s_n goes negative the beam is pushed against the spade s_{n+1} and current will flow to it. But even when s_n is at zero or slightly positive potential the leak current will not disappear completely in most cases. Leak currents to other positive electrodes appear in some cases. These are however generally much smaller and of any importance only in special applications.

1.4. Degeneration in trochoidal beams

There is a phenomenon in the trochoidal beam which impairs the characteristics and often sets a limit to the tube performance. The beam is not stable but will »degenerate» after travelling a distance. The electrons in different parts of the beam interchange energy, some of them gain and other loose energy, causing a more or less high degree of disorder. The degeneration has been investigated by MALMFORS, ÅSTRÖM [ALFVÉN *et al.* 1948] and STRANDELL [yet unpublished laboratory report].

The degeneration increases with the space charge density and the time of flight of the electrons. It manifests itself in three ways: 1. widening of the beam, 2. current to negative electrodes (N-current) accompanied by increased leak currents to positive electrodes and 3. excessive noise. Fig. 1.5 is a photograph by STRANDELL showing the degeneration. The electrons proceed from right to left. Near the cathode the beam shows clear trochoidal structure but due to the degeneration it grows diffuse before it arrives at the receiving electrode. The beam is visible because of fluorescence when the electrons exite residual gas molecules. The gas pressure is quite low, however, (molecular mean free path about ten times the total length of the beam) and disordering of the trochoidal paths due to electron collisions with the gas molecules is negligible.

Fig. 1.6 illustrates the influence of the degeneration on the spade characteristics. Curve *a* shows a characteristic obtained with an undegenerate beam. The current drops to zero at a positive spade

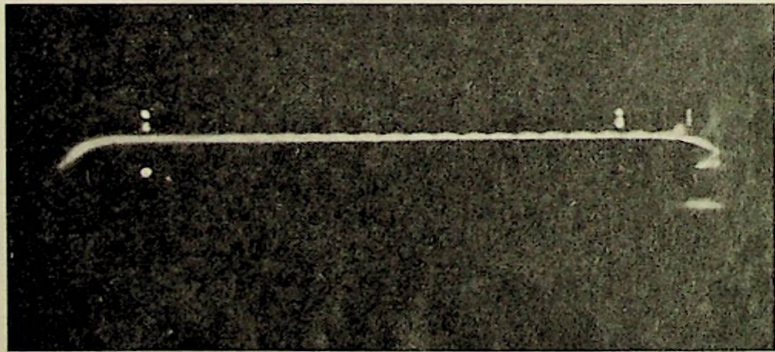


Fig. 1.5. Photograph of a trochoidal beam degenerating in homogeneous fields. (STRANDELL).

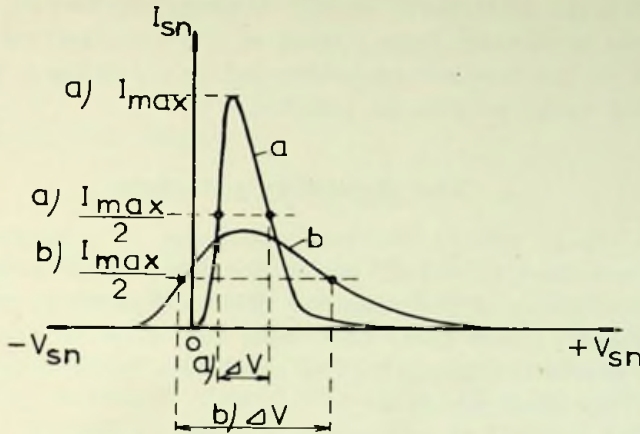


Fig. 1.6. Effect of beam degeneration on the characteristics.

potential indicating that no electrons have gained energy during their journey from the cathode. Further the characteristic is narrow and steep especially on its low voltage side. Curve *b* is a degenerated characteristic. It is much lower and broader and even extends over negative voltages of the spade. As will be evident later this shape of the characteristics is very unfavorable to circuit design.

As a figure of merit of a characteristic the ratio of the maximum spade current and the voltage width of the characteristic at a level equal to half of the maximum may be used:

$$S = \frac{I_{max}}{\Delta V} \quad (1.1)$$

Fig. 1.6 shows how this is to be measured. The ratio *S* will here be called the «steepness» of a characteristic.

The steepness of a characteristic is of course some function of the geometrical shape of the tube and of the space charge effects including the degeneration. Due to the complicated discharge conditions in the trochotrons, however, this function is known only qualitatively. In technical applications the trochotrons commonly operate in a constant magnetic field. If then the supply voltage is varied upwards from a low value, *S* will at first increase owing to decreasing degeneration. At a certain point *S* will be a maximum and after this decrease again because of increasing height of the

beam. Before the optimum is reached, however, the leak current may have become intolerably large. Much of the experimental development work on the trochotrons is devoted to obtaining a high S in an operating range as wide as possible.

1.5. The similarity principle

A space charge limited electronic discharge in a magnetic field obeys the common three-half power law for voltage and current, provided the square of the magnetic field is changed in proportion to the voltage. Under these conditions the shape of the electron paths will remain unchanged. The conditions for similar electron paths in a trochtron are thus

$$\frac{I_2}{I_1} = \left(\frac{V_2}{V_1} \right)^{3/2} \quad (1.2)$$

$$\frac{V_2}{V_1} = \left(\frac{B_2}{B_1} \right)^2$$

when the supply voltage is altered from V_1 to V_2 , the ratios of the various electrode voltages being constant. I_1 and I_2 are corresponding currents obtained at V_1 and V_2 if the intensity of the magnetic field at the same time is changed from B_1 to B_2 .

The degeneration in a trochoidal beam seems to be unaltered during such similarity transformations. According to ÅSTRÖM [ALFVÉN *et al.* 1948, p. 72] a manifestation of the degeneration is the »N-current», *i. e.* current to electrodes negative with respect to the cathode. A constant ratio of N-current to cathode current then would indicate a constant degree of degeneration. For low values of such a constant ratio ÅSTRÖM [ALFVÉN *et al.* 1948, p. 85] has obtained the empirical formula:

$$I_e \cdot B^2 \cdot V^{-2.5} \cdot l^{0.7} = \text{const.}_1 \quad (1.3)$$

Here I_e denotes the cathode current and l the beam length. For the same box in the same tube l is constant and can be included in the constant on the right side. Eq. (1.3) may then be written

$$\frac{I_e \cdot B^2}{V^{5/2}} = \text{const.}_2 \quad (1.4)$$

If then the concept «perveance» defined as

$$P = \frac{I_c}{V^{3/2}} \quad (1.5)$$

is introduced, one obtains

$$P \cdot \frac{B^2}{V} = \text{const.}_2 \quad (1.6)$$

But when B^2/V is kept constant, according to (1.2), P will also be constant, indicating an unchanged degree of degeneration. As the principle of similarity thus applies even to the degeneration at least at moderate degrees, the shape of a spade characteristic will remain unchanged during a transformation in correspondence with (1.2). In many cases it is permissible to perform such a transformation merely by multiplying the voltage and current scales with appropriate scale factors.

When the supply voltage is altered from V_1 to V_2 , ΔV in eq. (1.1) will become $\frac{V_2}{V_1} \Delta V$, and I_{max} will change to $\left(\frac{V_2}{V_1}\right)^{3/2} I_{max}$. If S_1 denotes the steepness of a spade characteristic at V_1 and S_2 that at V_2 one thus obtains

$$\frac{S_2}{S_1} = \left(\frac{V_2}{V_1}\right)^{1/2} \quad (1.7)$$

in addition to both of the similarity equations (1.2).

Experimental investigations by ÅSTRÖM [ALFVÉN *et al.* 1948, p. 79] show that the similarity principle holds for tubes of different size, provided the shape of the electron paths is unchanged. Thus, if the magnetic field is varied in inverse proportion to the geometrical dimensions,

$$\frac{l_2}{l_1} = \frac{B_1}{B_2} \quad (1.8)$$

but all voltages are kept constant, both the current and the degree of degeneration will be unchanged. Except for the electrode capacitances no properties of a tube are altered if the mechanical dimensions are scaled up or down by some factor. If, however, the dimensions perpendicular to the magnetic field are reduced but the extension of the electrode system along the magnetic field is kept unchanged, an increase in current is obtained.

1.6. Trochotron circuits

By means of resistors in series with the spades the electron beam can be locked to any one of the boxes. When a spade is slightly positive with respect to the cathode it takes current from the beam. This current gives a voltage drop in the loading resistor and the spade is kept at low potential.

Fig. 1.7 *a* illustrates the locking action diagrammatically. On the spade characteristic in fig. 1.7 *a* a load line corresponding to the spade resistor is drawn. The load line intersects the characteristic in three points A, B, and C, giving three possible states of voltage and current in the spade circuit. Of these, however, B is an instable state. The stable operating points are given by A and C. A represents the currentless state when the spade is at its supply voltage V_{so} . At point C the spade locks the beam. The current flowing in the circuit is I_{sl} , and the voltage of the spade is V_{sl} , the locking voltage.

In the plane and the cylindrical trochotron a self-locking beam can be shifted from box to box with the aid of negative voltage pulses applied to the plates. When the plate voltage is decreased below a certain critical value, called the stepping voltage, V_{st} , the beam cannot remain stable in the box any longer. The equipotential lines along which the beam travels are changed over to the other side of the plate, to the spacing between the plate and the next positive spade (see fig. 1.4). Hence current begins flowing to that spade, the voltage of which drops and a switch-over occurs.

As evident from fig. 1.7 *b* the stepping voltage depends on the spade load resistor. It is the plate voltage for which the spade characteristic just grazes the load line (point A' in fig. 1.7 *b*).

If the plate voltage suddenly drops from the supply voltage V_{po} to zero, the operating point is shifted from A to A". From this intermediate state the current and voltage of the spade follow the dashed characteristic $V_p = 0$ down to the locking position C, discharging the spade capacitance.

The stepping technique is described in some detail by LINDBERG [ALFVÉN *et al.* 1948, p. 43] and in chapter 6. In order to get dependable switching, a mechanism preventing the beam from stepping twice or more for one switch pulse is necessary. This is achieved by one of two methods: 1. RC-coupled plate-pulsed circuit or 2. push-pull-coupled plates.

According to the first method a resistor bridged by a capacitor is inserted in series with every plate. The switch pulses are simul-

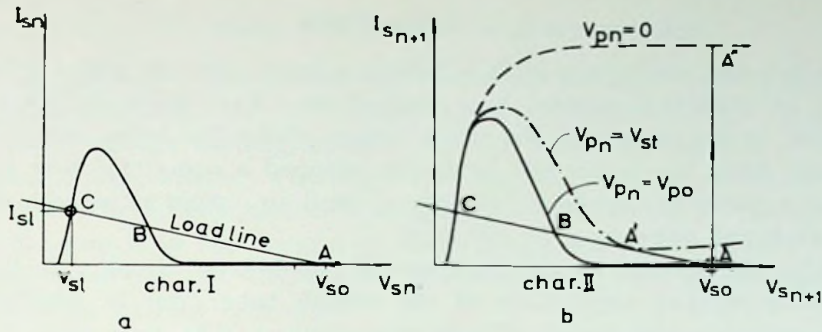


Fig. 1.7. *a.* Locking of the beam to a spade by means of a resistor.
b. The switch-over to the next box.

taneously applied to all plates across the RC-combinations. If the time constant of the plate RC-circuits are sufficiently great the voltage of the plate to which the beam is switched cannot drop below the stepping voltage during the switch pulse.

In the other method the plates are connected into two groups, odds and evens. The groups are joined to the anodes of a bistable multivibrator (scale-of-two). The circuit parameters are so chosen that the two stable anode voltages of the driving multivibrator are above and below the stepping voltage, respectively. Thus the beam can remain only in such a box, the plate of which has the higher voltage. A pulse on the input of the scale-of-two shifts the voltages of the plate groups to the opposite condition and the beam will step to the next box.

Combining these methods, the plates can be connected to two groups, each supplied with an RC-circuit and pulsed.

In a trochotron of the plane type the beam is shifted from box to box toward the anode. Ultimately it arrives at the last box immediately in front of the anode. From this position it has to be returned to the first box in the far end of the tube. This resetting of the beam can be achieved by suppressing the cathode current for a moment. Meanwhile all electrodes return to their supply voltages and when the beam is turned on again it will go to the first box. The beam can be made self-returning if a load resistor is inserted in the anode circuit. When the beam is in the last box a switch pulse will shift the beam over to the anode. Then the anode voltage drops and the emission decreases allowing the last spade to gain voltage after which the beam resets.

1.7. Scale-of-ten

A ten-box trochotron with self-locking beam and the plates either RC- or push-pull coupled is a scale-of-ten. Each pulse fed to the plates or the input of the driver stage shifts the beam one step each. After ten pulses the beam has stepped a complete cycle and from a particular spade (arbitrarily chosen) an output pulse at every tenth input pulse may be obtained.

The scale-of-ten is the fundamental trochotron circuit. It is a very important application of the switch tube, and in addition, a convenient test circuit of new tube designs. The properties of a scale-of-ten are easily studied. The conditions for correct operation are readily determined, and figures of merit — used in comparing different tube designs — can be expressed in terms of speed and stability of the device.

Fig. 1.8 shows schematically an experimental arrangement in testing a trochotron as a scaler. In the case shown the plates are RC-coupled and pulses of negative polarity are fed to the plates over a capacitor C_1 . The operation of the circuit is studied with the aid of a cathode ray oscilloscope. A capacitive probe picks up the voltage variations of the electrode to be studied. Through a screened lead these voltage variations are brought to the vertical deflection amplifier of the oscillograph. The capacitor C_2 of the probe is very small, about 1 pF, and thus the electrode under test is left almost unloaded.

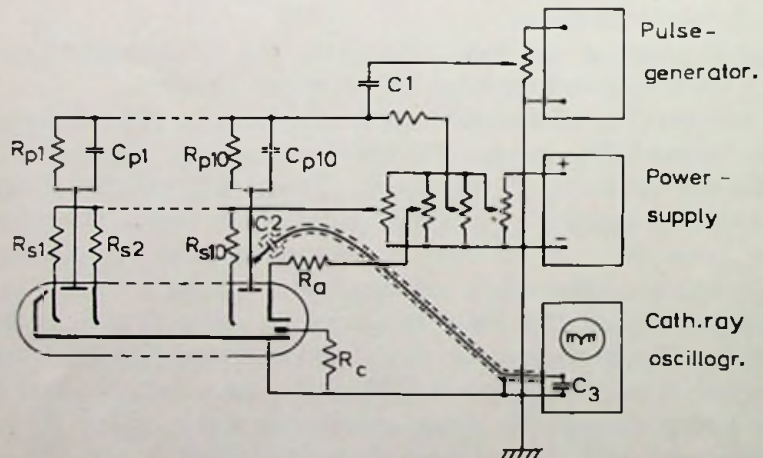


Fig. 1.8. Test circuit for a trochotron as a counter.

1.8. The plane trochotron as a scale-of-ten

Fig. 1.9 shows two oscillograph recordings obtained from stepping experiments with an RC-coupled plane trochotron. Fig. 1.9 *a* is a plate voltage oscillogram and fig. 1.9 *b* the oscillogram of the corresponding spade. The repetition frequency of the pulses fed to the plates is 50 kc/s and their amplitude about 100 volts. The spade oscillogram is in the same time and voltage scale. The supply voltages are about 200 volts for the plates and 150 volts for the spades. The beam current is 1 mA.

It is seen how the plate voltage drops exponentially owing to charging of the plate capacitor when the beam arrives to the box. The time constant of the plate circuit sets an upper limit to the stepping frequency. If this frequency is too high the plate voltage has no time drop sufficiently low to reach the stepping voltage at the following pulse. As mentioned before, however, the time constant has to be large in comparison with the duration of the pulses, or the plate RC-circuit will not safely prevent the beam from stepping twice or more.

The beam switch-over is best studied from the spade voltage oscillograms. In fig. 1.9 *b* the beam shift is very rapid and almost completed during the duration of the plate pulse, as it has to be for safe operation. Due to interelectrode capacitances pulses from the plates leak over to the spades. These capacitive pulses must not be large or they cause erroneous stepping. Because of the voltage dip the beam will go near the spade edges during a pulse and it may hit a spade several boxes away from the right one. The capacitive leakage pulses can be kept within permissible values either by loading the spades capacitively or by making the fronts of the driving plate pulses smooth.

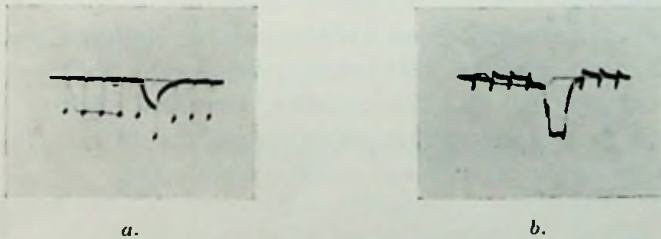


Fig. 1.9. Waveforms of a plate and a spade of an RC-coupled trochotron stepping at 50 kc/s.

A number of factors combine to make the stepping speed of the RC-scale low. The upper limit of speed reached in laboratory experiments with trochotrons of the plane type is the vicinity of 50—60 kc/s. In order to get a safety margin the practical limit has to be set lower, about 10—15 kc/s.

Much greater speeds are achieved by the push-pull scales. The switch-over process is the same here as in the RC-case, but no waiting time is necessary before the beam can step again. Further, the disturbing capacitive leakover pulses from the plates to the spades are much smaller than in the RC-circuit.

The speed limit for push-pull scales is usually set by the beam re-set and not by the switch-over action. A scale counting random pulses has a greater resolving power than what may be concluded from tests with pulses of continuous rate. A push-pull scale can count about 300 kc/s pulses continuously when properly adjusted. For practical purposes the limit has to be set to 100 kc/s.

The stability is about the same for both types of scales. Variations of $\pm 15\%$ of the supply voltages are permissible.

In order to investigate the reliability a long time test has been performed. Two scale-of-100 pulse counters, each consisting of two trochotron stages were supplied from the same pulse generator. The frequency was quite low, 1 kc/s.

One counter had RC- and the other push-pull coupled plates. Synchronism or difference between the output pulses were observed on an oscilloscope screen.

In the best cases the counters stepped synchronously 8 and 9 days, corresponding to $7 \text{ à } 8 \cdot 10^8$ pulses. Voltage surges on the a.c. mains could cause erroneous stepping and were probably never screened off completely. Another error source was traced to a particular tube where leak current sometimes caused disturbances in the operation.

The trochotrons were of an early tentative design manufactured by Aktiebolaget Svenska Elektronrör, Stockholm. They were run totally about 2000 hours. The emission decreased slightly and some vaporization from the cathode deteriorated the cathode insulation, but no other aging phenomena could be detected.

CHAPTER 2.

THE CYLINDRICAL TROCHOTRON

BY

J. BJÖRKMAN

2.1. Comparison of the plane and the cylindrical trochotron designs

As pointed out in chapt. 1 the degeneration of the trochoidal beam frequently sets a limit to the performance of a trochotron. This is true especially in trochotrons of the plane type. The long distance between the cathode and the first box in the far end of the tube makes the beam disposed to degeneration. Generally the degeneration will be considerable at fairly small current densities where other limiting effects are insignificant. To meet the demand for larger current capacities of the trochotrons the cylindrical design was suggested by ROMELL.

A cylindrical trochotron has the following advantages over the plane tube type: 1. simpler and symmetrical electrode structure, 2. equal characteristics of all boxes, 3. much higher perveance ($P = I/V^{3/2}$) and larger current densities, 4. no beam re-set needed in stepping circuits. These advantages are partly counteracted by the following disadvantages: 1. some control possibilities of the beam are lost because of the lack of anode and rail, 2. oscillations are difficult to suppress, 3. the beam can unintentionally be split into two or more separate beams.

2.2. Electrode arrangement

The cylindrical trochotron is constructed on the basis of rotational symmetry. A cylindrical cathode is surrounded by a ring of spades arranged co-axially with the cathode. Between the spades plates and possibly other electrodes are inserted constituting a set of boxes.

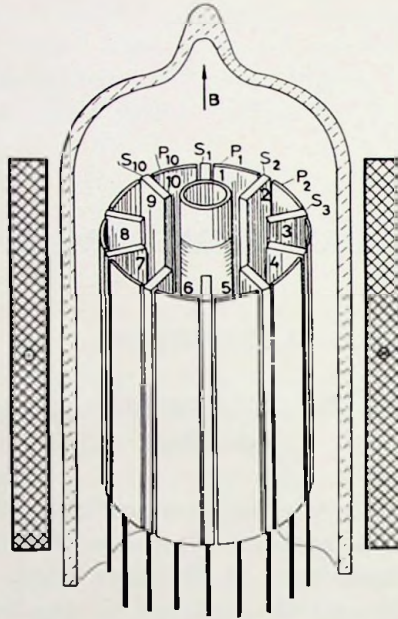


Fig. 2.1. The electrode system of a cylindrical trochotron

Generally the boxes are all like each other and have identical characteristics. In some particular cases there can be a need to give the boxes or some of them unequal internal structure *e. g.* by inserting special electrodes, but to the main electron discharge between the cathode and the boxes such a dissymmetry is insignificant.

Fig. 2.1 is a schematic perspective sketch of a ten-box cylindrical trochotron. The cathode *c* is a circular nickel tubing, coated with a common oxide mixture and heated by a tungsten filament (not shown in the figure). The spades and the plates are made of some non-magnetic metal. The shape and the mutual location of these electrodes can be very different in different tube designs, but as a rule, only the spades will have any real influence on the electric field near the cathode, the plates being more or less screened off by the spades. In fig. 2.1 showing only the principle, the spades are pictured as radially directed plane sheets and the plates as sheets covering the space between the outer edges of the spades. The electrode boxes thus formed are from an arbitrary one numbered 1, 2, 3 . . . The spades and plates are in a corresponding manner denoted s_1, p_1 for box 1, s_2, p_2 for box 2 and so on.

The magnetic field, symbolized by the arrow B , is homogeneous and parallel to the axis of symmetry of the electrode system. In experimental work the magnetic field is produced by a coil, the strength of the magnetic field being varied by controlling the coil current.

2.3. The discharge mechanism

The state of the electronic discharge in the cylindrical trochotron is not known in its details. The conditions are complicated due to the curved electron paths, the space charge and the degeneration. Nothing is known with certainty about the electron paths, and yet it is impossible to give an accurate account of the behaviour of the tube based on the equations of motion of the electrons. The most adequate concept of the discharge is obtained when the electrons are regarded as constituting a cloud in which a translational motion perpendicular to the electric and magnetic fields is superimposed by a random diffusion of the electrons.

When all spades are at a positive potential a mainly radial electric field is produced around the cathode perpendicular to the axial magnetic field. Due to the action of the magnetic field the paths of the electrons emitted from the cathode become curved. At a certain critical strength of the magnetic field the electrons will just graze the innermost spade edges and at higher values form a rotating cloud around the cathode. This is the well known magnetron cut-off. If in a cylindrical trochotron at cut-off one of the spades is brought to a potential near to that of the cathode, the rotating electron cloud will be bent out off the cathode and guided to the box in front of this spade at low potential. Then the ordinary trochotron discharge is established of which fig. 2.2. is an illustration.

Fig. 2.2 is a cross-section of a cylindrical trochotron perpendicular to the axis of symmetry of the electrode system. The magnetic field is directed out of the plane of the paper. All spades and plates, except one spade, s_1 , are at a positive voltage with respect to the cathode. The electric field thus produced is represented by a network of thin lines symbolizing lines of force and equipotential lines. In the combined electric and magnetic fields the electrons will drift in a counter clock-wise direction around the cathode.

The electrons originate at an area of the cathode facing the few first positive spades following the spade at low potential in the direction of the electron flow. In fig. 2.2. where s_1 is at cathode

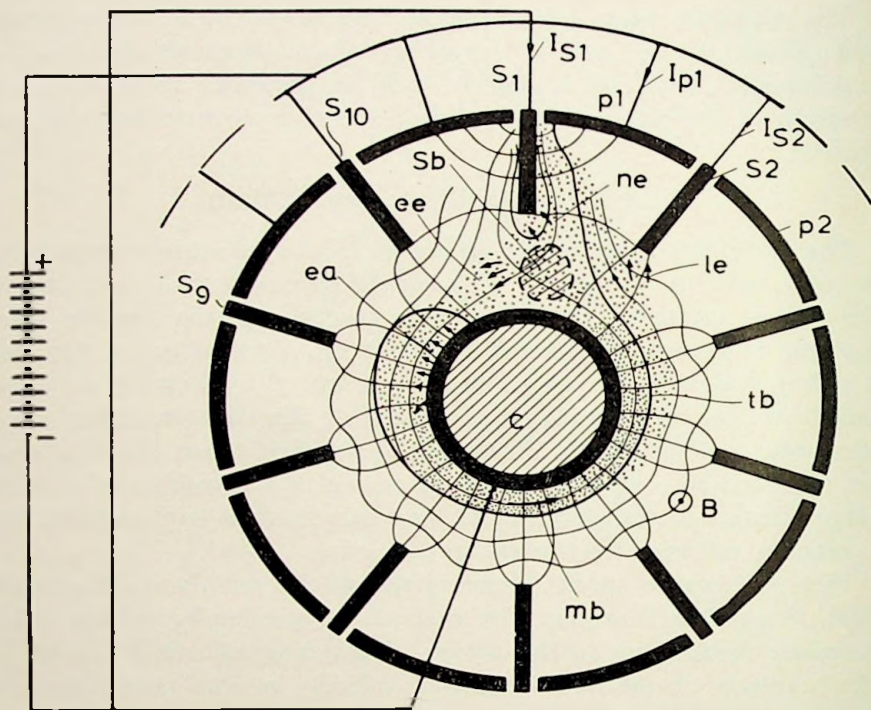


Fig. 2.2. Illustrative sketch of the electron discharge.

voltage this «emitting area», ea , is below the spades s_{10} , s_9 and perhaps s_8 . The liberated electrons produce a heavy space charge, which will suppress the emission from other parts of the cathode. After leaving the space above the emitting area the electrons will form the «main beam», mb , and go nearly one turn around the cathode to box 1, s_1 , p_1 .

Below the spade s_1 a region exists, where the electric field is weak and the electrons will have very low drift velocities. The space charge will press down the electric potential in this region even more, and a kind of potential barrier, the «space charge barrier» sb is obtained. The space charge barrier aids to guide the beam into the box.

With somewhat simplified assumptions it is possible to calculate theoretically the current density and the height of the main beam. The calculations dictate a sharp outer boundary of the beam. This theoretical boundary is in fig. 10 denoted tb . Due to the degeneration, however, the electrons will not be confined to the calculated space, but diffuse out from it.

The electrons which by the degeneration process have lost energy will be found in the space between the beam and the spades. These »leak electrons», le , cause leak currents to those spades which in the direction of the electron stream precede the spade at low potential. In fig. 2.2 I_{s_2} is the leak current produced in this way to the spade s_2 . The leak electrons will have their counterparts in electrons, which have gained energy due to the degeneration. A large portion of these electrons go to the cathode, but some of them, ne , give rise to N-current (see 1.4) to s_1 , and others, the »escaping electrons», ee , penetrate the space charge barrier.

The picture of the electron discharge outlined above, gives quite a good account of the properties of the cylindrical trochotron. Only a portion of the cathode surface is used for electron emission. Several spades in succession can be brought to a low potential without decrease of the current. As the beam then becomes shorter the degeneration will decrease, a case which manifests itself in increasing steepness of the spade characteristics and decreasing noise and leak currents in the tube. Oscillations and a certain type of noise are further easily explained with the aid of a feedback mechanism offered by this conception of the discharge conditions.

When only one spade is at low voltage the distance is short between the part of the cathode where the electrons are emitted and the region in which they are deflected into the box. Both the voltage of the spade at low potential and the potential of the space charge barrier will have a considerable influence on the electric field which determines the cathode current. Any disturbance in either the voltage of the deflecting spade or the potential of the space charge barrier will cause a corresponding change in the emitted current. The changes are then propagated with the main beam around the cathode and will after a certain elapse of time give rise to a new disturbance. Oscillations, partly of noise character may be produced in this way.

The probability for oscillations should be greatest at a frequency corresponding to the transit time of the electrons. The transit time is, however, different in different parts of the main beam, being shortest for the outermost electrons and increasing to — theoretically — infinity at the cathode surface. The slow electrons carry, however, only little current, the majority of the beam current being supplied by electrons with times of flight equal to and a little longer than the minimum. In accordance with these presumptions experi-

ments show a marked increase and high peaks of the noise spectrum at the expected frequencies.

Besides the electrostatic coupling an electronic coupling between the emission and deflection regions does exist. The escaping electrons penetrating the space charge barrier will cause disturbances in the emission. These disturbances are of more clear noise character than those caused by the electrostatic feedback. The escaping electrons are degenerated giving much noise to electrodes on which they fall. This noise is now impressed on the emitted current and maybe real amplification of the noise in the main beam occurs.

Experimentally the electrostatic and the electronic feedbacks cannot be completely distinguished from each other. But when a spade is made more negative than the cathode, certain alterations of the noise spectrum can be explained in such a manner that the escaping electrons are barred while an appreciable electrostatic coupling still remains. When two or more adjacent spades are brought to a low voltage the feedback is wholly interrupted and the noise and the oscillations described above disappear. The discharge behaves now as a short trochoidal beam in a plane trochotron and shows only the noise of the intrinsic degeneration.

In designing cylindrical trochotrons one thus meets a problem resembling that arising in the design of *e. g.* reflex klystrons and some types of multigrid tubes: the emitting parts of the cathode have to be protected from influence of reflected electrons or the tube will be noisy and unstable in operation.

2.4. Characteristics and circuits

The characteristics of a cylindrical trochotron are essentially those described in 1.3. When a spade is held at cathode potential and the voltage of the following one varied (numeration opposite to the electron flow), the characteristic curves of fig. 1.3 *a* are obtained. The spade characteristics depend on the plate voltage in a manner illustrated in fig. 1.3 *b* and the characteristics I and II are in principle those showed in fig. 1.3 *c*. The difference between the characteristics I and II can be very great in a cylindrical trochotron because the noise due to feedback is interrupted when characteristic II is measured.

In the cylindrical trochotron characteristics of higher order than II are of interest. If an array of spades behind a particular one

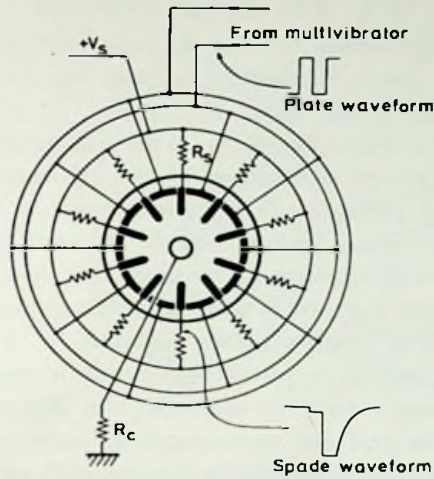


Fig. 2.3. Circuit diagram of a push-pull coupled cylindrical trochotron.

sequentially are set to cathode potential and the characteristic observed, the prime effect is an increase of the steepness. When finally only a few spades are at positive potential the height (maximum current) of the characteristic is substantially lowered due to decreased beam current.

The circuit technique is principally the same as that for the plane trochotron described in 1.6. Fig. 2.3 shows a basic scale-of-ten arrangement. By means of spade resistors the current can be locked to any one of the boxes, and negative pulses on the plates shift the beam from box to box in a direction opposite to the circulating electron stream. Either RC- or push-pull-coupled plates can be used.

When the beam is at rest in a box for a long time the characteristic I determines the locking action. Characteristic II governs the stepping, the spade which has locked the beam being at a low potential during the switch-over. At high stepping speeds of continuous rate the higher order characteristics control the performance, several spades behind the instantaneous beam-catcher being at low potential because of the time constants of the spade circuits.

The operating point can be automatically stabilized by means of a cathode resistor (R_c in fig. 2.3.). The voltage drop in this resistor equalizes the current to the different boxes and compensates both for variations of the supply voltage and decrease of the current at high counting speeds when many spades are at low potential.

2.5. The design problem

The design of cylindrical trochotron tubes will be treated in chapter 5, but before going to details, a brief survey of the questions encountered will be given here.

The trochotron is intended to be a decade counter or switch and thus the design problem is confined to the arrangement of ten boxes around a cylindric cathode. The tube should be an astatic device capable of performing random counts or switch-overs from zero up to a maximum frequency. This requires that the tube is non-oscillating and that the static and dynamic characteristics do not differ too much. The beam must be lockable to the boxes by means of spade resistors, which requires that when a spade is a few volts positive with respect to the cathode the beam current divides between this spade and its corresponding plate only, the currents to other electrodes (leak currents) being negligible or not exceeding certain tolerable limits. Further simple construction, low noise, and small and symmetrically distributed interelectrode capacitances are desirable.

The most important part of the tube is the discharge space between the cathode and the spades, the structure of this determining principally the properties of the tube. Fig. 2.3 presents its main measures, the cathode radius r_c , the spade radius r_s and the box opening r_o . Depending on the ratio r_s/r_c three classes of tubes can be distinguished: 1. large size cathode tubes with $r_s/r_c \leq 2$, 2. medium size cathode tubes with $2 \leq r_s/r_c \leq 2,5$ and 3. small size cathode tubes with $r_s/r_c \geq 2,5$. Commonly small size cathode tubes have r_s/r_c ratios of about 5 to 8. As will be evident below and in chapt. 5 tubes belonging to the different classes have quite different properties.

During operation of the tube the main beam occupies the largest part of the discharge space. The main beam is subject to conditions closely resembling those existing in a non-oscillating magnetron. It might then be supposed that the height of the main beam and the current density in it could be obtained from the theory of the static magnetron. According to this the cut-off radius r_h is determined assuming the spades replaced by a cylindric anode of radius r_s held at the spade supply voltage. No quantitative agreement between such a simple theory and experiments can be expected, however. The conditions at the start and the end of the beam are neglected and as previously mentioned, because of the degeneration, the electrons will diffuse out off the theoretically predicted space. The validity of the theory is discussed in chapt. 5.

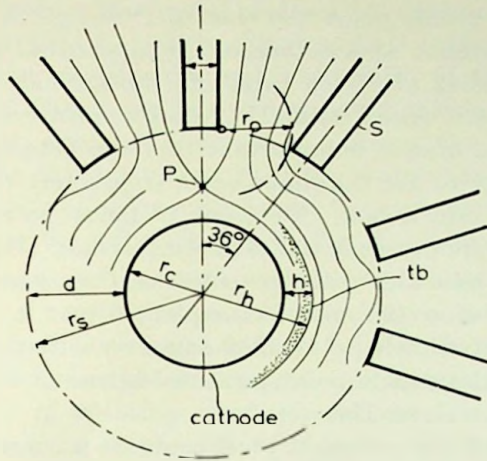


Fig. 2.4. The discharge space of a cylindrical trochotron.

Just at the cut-off state, *i. e.* when r_h equals r_s , the largest circulating current at a given spade voltage or a given magnetic field is obtained. The current decreases rapidly if either the magnetic field is increased or the spade voltage lowered. At cut-off the perveance of the tube is high and the time of flight of the electrons low, in consequence of which degeneration and noise are small. It is impossible to operate the tube at cut-off, however, mainly because large leak currents will then appear, but an operating point as near the cut-off state as possible is — with certain exceptions — always desired.

The electric field has to be of cylindrical shape in the space occupied by the main beam, tangential components of the field tending to disperse the beam. However, the spade edges alternating with the box openings give the electric field a wavy shape. In order to get a large r_h , and thus a high perveance, this wave structure should be smoothed out in the largest possible part of the discharge space. This requires that the distance d ($d = r_s - r_c$) between the spade edges and the cathode surface is not too small and that the box openings are not too wide. The openings of the boxes have, however, to be wider than the beam height h ($h = r_h - r_c$), or the beam does not find room there.

To both these requirements a third is added, the ability of a spade to deflect the beam. When a spade is at cathode potential or a few

volts positive a saddle point like that of P in fig. 2.4 appears in the electric field without space charge. Equipotential lines of higher potential than that of P are bent off the cathode whilst lines of lower potential are closed around it. As the electrons tend to follow the equipotential lines it is important that the potential of the point P is low in order to get the main beam completely or almost completely deflected into a box. Electrons of lower potential than that of the saddle point by-pass the deflecting spade. When sufficiently many electrons pass above the potential of P a space charge barrier can be formed below the spade as explained in 2.3. The configuration of the electric field is then changed substantially, but a low value of the initial saddle point potential is one of the requirements for a stable space charge barrier.

A low value of the potential at P requires a considerable electrostatic penetration of the individual spades to the cathode sector below them. This is favored by great thickness t of the spades and small distance d to the cathode. A large t will moreover aid to separate the emission and deflection regions thus reducing the disturbing feedback described in the section above.

These considerations lead to a tube construction with a large cathode, the distance d being equal to or smaller than the cathode radius ($r_s/r_c \leq 2$), a great thickness t of the spades and small box-openings r_o . In such a tube the beam will be completely deflected, the internal feedback is rather small and the characteristics of a spade differ only little whether the spade behind is at positive or zero potential. The perveance and current capacity of the tube are quite low, however. The height h of the beam is necessarily small and the transit time of the electrons long. At arrival to the deflection region the beam is considerably degenerated, a consequence of which is low and flat spade characteristics.

A higher perveance is achieved if the spade-cathode distance d is made greater than the cathode radius. If d is between one and one and a half times the cathode radius one has a medium size cathode tube. Here the individual electrostatic penetration of the spades to the cathode is smaller and the potential in the saddle point P higher, but the beam can be completely deflected with the aid of a space charge barrier. The formation of an effective space-charge barrier requires, however, the degree of degeneration to be low and, in order to get a considerable part of the electrons above the initial saddle point potential, the height h of the beam to be

comparatively large. The main problem in designing medium size cathode tubes is thus to get the box-openings sufficiently wide and at the same time confine the wave structure of the electric field to certain limits. For a ten box arrangement satisfactorily solutions can be obtained when d is about 1,5 times the cathode radius ($r_s/r_c = 2,5$). For smaller values of d the wave shape of the electric field tends to be too pronounced and for greater values the box-openings will not be sufficiently wide for the beam height.

If the spade radius is made still larger, some 5–8 times the cathode radius, a small size cathode trochotron is obtained. This operates in a mode somewhat different to both the other types. The magnetic field is rather strong and if all spades are at a positive potential a core of rotating electrons will be formed around the cathode. When r_s is much greater than r_c all electrons have the same angular velocity, the core thus rotating as a rigid body.

Fig. 2.5 illustrates the operation of the tube schematically. The spade at zero potential does not deflect the electrons off the cathode, but owing to the tangential electric force introduced, the core ec , is displaced eccentric with respect to the cathode and partially dispersed. The dispersed electrons de are deflected into the box in front of the zero potential spade. The circulating electrons can be regarded as constituting a virtual cathode supplying electrons to a main beam in the de region. As only a part of the rotating electron cloud is deflected to a box, the small cathode trochotron is a low-perveance tube. Trochotrons of this type, constructed and

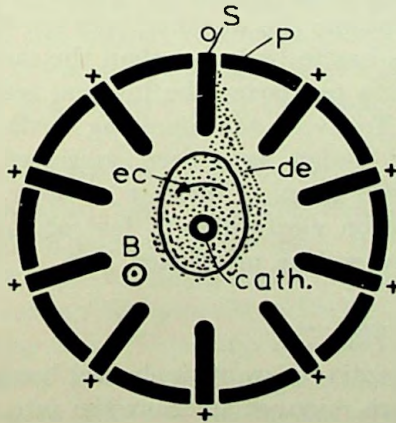


Fig. 2.5. The discharge mechanism in a small-size cathode tube.

investigated by STERNBECK and collaborators (Telefonaktiebolaget L. M. Ericsson, Stockholm) will be described in a publication elsewhere.

Both the large cathode and the small cathode cylindrical trochotrons comprise reliable counting devices. They are stable in operation and noncritical to the operating point and running conditions. Their electrical data are about equivalent, but the small cathode design has the advantage of having greater mechanical tolerances and smaller heater power consumption. The perveance of the both tube types is however low and the noise level high. The most interesting constructions are to be found among the medium size cathode tubes. There it is possible to realize a tube having high perveance and practically no degeneration and noise.

The perveance of a medium cathode tube is about 3 and 4 times that of the large and small cathode tubes and more than 10 times the perveance of a planar trochotron of equivalent breadth, *i. e.* extension of the electrode system in the direction of the magnetic field. Considering the counting speeds a plane trochotron is, as mentioned in 1.8, capable of counting about $3 \cdot 10^5$ pulses/sec. The large and small cathode cylindrical trochotrons can count about $2 \cdot 10^6$ pulses/sec. but the maximum counting rate for a medium cathode tube is well above 10^7 .

2.6. Hybrid tube types

In some respects the simple cylindrical tube is not an ideal solution of the trochotron problem. To obtain a high perveance and a reasonable low heater power the distance between the cathode surface and the spade edges has to be larger than the radius of the cathode. But being confined to ten boxes the internal feedback then affords severe difficulties. To avoid the annoying feedback hybrids of the principal cylindrical design have been suggested. All of them are of comparatively little practical interest however, but as an illustration to the «trochotron electronics» a few of the innumerable construction possibilities will be mentioned here.

The helical beam trochotron.

Fig. 2.6 is a perspective view of the helical beam trochotron. Some spades and plates are removed to show the internal structure. The spades and the plates are arranged coaxial to a central rod r , this

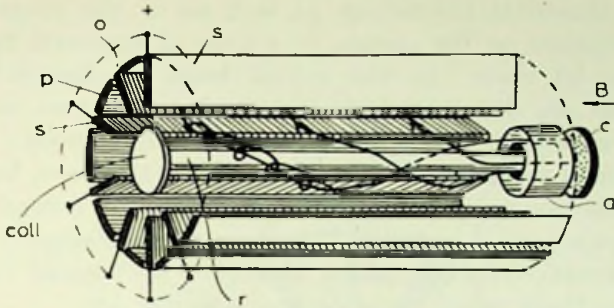


Fig. 2.6. The helical beam trochotron.

rod corresponding to the rail in the plane trochotron. A disk or ring shaped cathode *c* and an anode *a* consisting of two coaxial cylinders are located at one end of the spade-plate system and at the opposite end a collector disk is arranged. In a direction parallel to the magnetic field *B*, an annular electron beam is injected into the space between the rod and the spades. The rod is negative with respect to the spades, in consequence of which the electrons encounter crossed electric and magnetic fields. Owing to this the electrons begin spiraling around the rod. If one of the spades is brought to a low potential, the electrons will be guided along the equipotential surfaces into the corresponding box.

The tube is free from internal feedback as no reflected electrons disturb the emission process. By varying the cathode potential the time of flight of the electrons can be controlled and the degeneration kept at low values. The current can be modulated by means of the anode voltage, and if the anode current is zero, as it easily can be by proper design of the electron gun, the modulation consumes no power.

The current density, referred to the extension of the boxes in the direction of the magnetic field, is a function of the transit time of the electrons and in general quite low. If a low degeneration is desired the transit time of the electrons has to be short and then a large part of the current flows to the collector. At the expense of a low noise level the current density can be increased by giving the collector a negative potential. The electrons are then reflected back through the space between the spades and the rod and the current density about doubled.

In the cylindrical trochotron as well as in the magnetron the electrons originate at the surface of a tube of magnetic flux, giving a single cut-off state. In the helical beam trochotron, however, the electrons are distributed in a space between two coaxial flux tubes determined by the ring shaped slit in the anode. Hence no sharply defined magnetic cut-off does exist in this case, but in their circulating motion the electrons return toward the central rod from different equipotential surfaces. This state of the discharge influences the spade characteristics, making them low and broad (low steepness) with a fairly tardy slope on the positive side.

The tube is symmetrical in principle, but according to experience, it is difficult to get the characteristics of all boxes identical. The cathode has to emit uniformly over its entire surface and the magnetic field has to be adjusted very carefully parallel to the axis of symmetry of the electrode system.

The «auxiliary spade» trochotron.

In this construction the feedback is avoided by holding two or more spades at low potential simultaneously. In the example shown in fig. 2.7 the beam locks down three spades in every position. Due to increased height and steepness of the spade characteristics the spade resistors can be reduced and a considerable gain in stability at rest is achieved.

In front of the original spades, sets of special electrodes, «auxiliary spades», s' and s'' , are located. These spades, like the plates, do not have any noticeable influence on the electrostatic field in the discharge space, their action thus being restricted to the box into which the beam is going. The auxiliary spades are connected to the other spades according to the pattern shown in fig. 2.7: every s' is joined to the spade behind its own box and the corresponding s'' to the spade one step further backwards.

When the beam is deflected into a box it encounters at first the slit between the original spade and s' . The latter electrode takes current from the beam until its voltage is pressed down. After this the beam climbs over s' to the slit between s' and s'' , now pulling down the voltage of s'' . Ultimately the beam goes to the slit between s'' and the plate. The two spades connected to the auxiliary spades are thus at low potential together with the beam deflecting spade. The emitting and deflecting regions are thus effectively separated from each other.

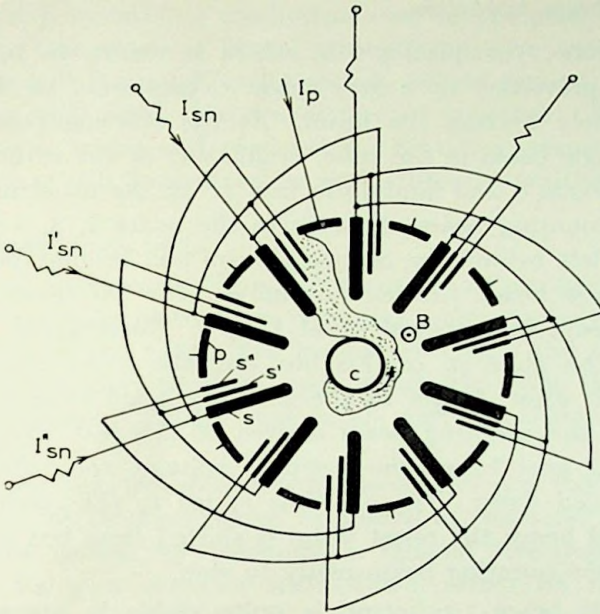


Fig. 2.7. The auxiliary spade trochotron.

The tube can be built with only one auxiliary spade in each box or, if desired, with more than two. In the latter case, the beam of course becomes shorter and less degenerated, but the electrode system will be more complicated.

In the auxiliary spade trochotron several spade resistors load the beam at a time, reducing the plate current. The auxiliary spades cover an appreciable part of the surface of the original spades. This increases the spade-to-spade capacitance and lowers the spade characteristics. The feedback is not entirely annihilated. If a disturbance in the beam causes a voltage variation of the auxiliary spades, this variation is transmitted to the emitting region over the spades connected to the auxiliary electrodes. This type of feedback can, however, be suppressed by proper design of the tube and damping of the spade circuits.

NETTELBLADT (L. M. Ericsson) has invented this arrangement independently.

The double beam trochotron.

In this tube, the principle of which is shown in fig. 2.8, the feedback is prevented by a long spade s_0 connected to the cathode and completely barring the beam. At the starting position there is only a single beam in the tube, originating at the cathode section facing the anode a and landing in box 1. In the usual manner this beam, the counting beam cb , steps to the boxes 2, 3, 4 and so on. The spades left behind the counting beam will become positive and produce a new beam, the re-set beam rb . The bar spade s_0 deflects the re-set beam to a special re-set box, 0. No stepping pulses are applied to the plate p_0 of this box and the re-set beam remains there, only it grows longer as the counting beam steps toward box 10. Finally the counting beam arrives at this last box and when the plate p_{10} goes below the stepping voltage, the voltage of the anode is pulled down. The anode is joined to the spade s_1 of the first box and hence the re-set beam is shifted from box 0 to box 1, forming a new counting beam ready to step.

The double beam trochotron is quite stable in operation. The tube is non-symmetrical, however, and the various boxes may have unequal characteristics.

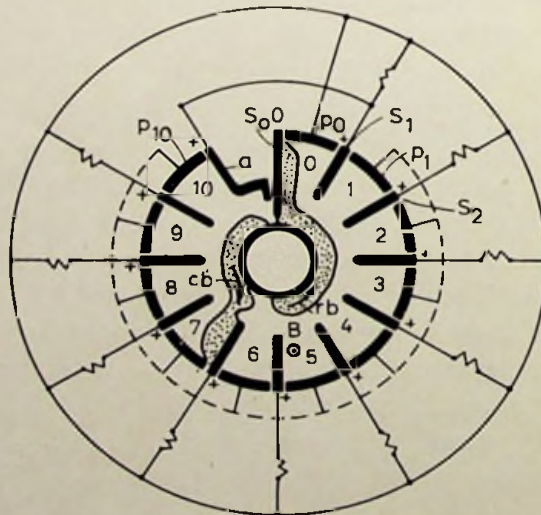


Fig. 2.8. The double beam trochotron.

An ordinary cylindrical trochotron can be operated as a double beam tube. One spade is biased strongly negative with respect to the cathode and the neighboring spades, one or two on the one side and one on the other side are connected together. These spades will operate as anode and spade of the first box, respectively. The counting beam will have seven or eight different positions.

The twin beam trochotron.

When two diametrically opposite spades in an ordinary cylindrical trochotron are brought to a low potential simultaneously, two beams are produced in the tube. The beams are short, and if the spades are properly de-coupled from each other, the tube is completely free from feedback. Thus a very stable sort of trochotron discharge is obtained.

If in a ten-box trochotron opposite spades are joined together, either by direct short-circuit or by means of resistors, and the five groups then loaded by resistors, a reliable five-step counter is obtained. Using a common scale-of-two, either on the input or output side, a ten-step device is obtained, capable of very fast operating.

The rising-sun trochotron.

If the number of boxes is decreased below ten better stability and higher perveance is obtained. Because the boxes get more angular space the spades can — without decrease in perveance — have a larger thickness and a greater electrostatic penetrating power on their adjacent cathode sectors. A five-box trochotron will thus have much better characteristics than a ten-box tube of equal perveance.

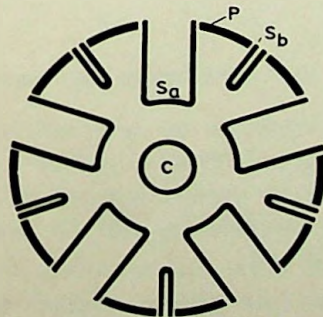


Fig. 2.9. The rising sun trochotron.

If the boxes in a five-box trochotron are divided into two parts by spades not protruding to the cathode region one obtains the ten-step tube shown in fig. 2.9. This tube has a set of five large spades s_a , another set of five small spades s_b and ten plates p .

Because the beam in every second position locks down two spades the tube is slightly unsymmetrical with respect to the plate currents. Another case of asymmetry is the difference between the characteristics of the large and the small spades. Finally the characteristics of the large spades are lowered when the corresponding small spades are brought to zero voltage.

Although not very well suited to ordinary counting purposes, the rising-sun trochotron may find special applications, *e. g.* as modulator and detector in pulse time modulation systems. The designation «rising-sun trochotron» is chosen by analogy to the rising-sun magnetron.

CHAPTER 3

THEORETICAL CONSIDERATIONS

BY

L. LINDBERG

An exact theoretical treatment of the electron motion in trochotrons offers like that of the magnetrons unconquerable difficulties. Firstly, the electric field has a very complicated structure and is lacking symmetry. Secondly, it is strongly reacted upon by the space charge, and thirdly, the streaming of electrons is not stationary owing to the perpetual interchange of energy between groups of electrons. Only some very special and strongly idealized cases can be treated exactly.

It has, therefore, been necessary to base the development on rather crude assumptions from these idealized cases in conjunction with experiments. Some general principles applying to trochotrons can be found in magnetron theory. The plane case is preferred since the mathematical treatment is simpler than that in the cylindrical case, and it seems to be a tolerable approximation as far as only qualitative effects are studied. (Many references to the extensive magnetron literature are given by HARVEY [1943], SPANGENBERG [1948] and COLLINS *et al.* [1948].)

3.1. General differential equations for a plane magnetron

The magnetic Lorentz force on an electron in motion is always perpendicular to its velocity; thus the magnetic field when constant in time can never change the energy of an electron. The kinetic energy is only related to the electrostatic potential.

Using a coordinate system x, y, z with the z -axis parallel to the magnetic field B , the energy equation and force equations in MKSA-units become:

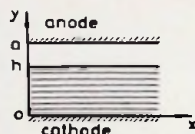


Fig. 3.1. Plane magnetron.

$$\dot{x}^2 + \dot{y}^2 + \dot{z}^2 = \frac{2e}{m} (V + V_e) \quad (3.1)$$

$$\ddot{x} = \frac{e}{m} \frac{\partial V}{\partial x} - \frac{e}{m} y B_z \quad (3.2)$$

$$\ddot{y} = \frac{e}{m} \frac{\partial V}{\partial y} + \frac{e}{m} \dot{x} B_z \quad (3.3)$$

$$\ddot{z} = \frac{e}{m} \frac{\partial V}{\partial z} \quad (3.4)$$

where e is the absolute value of charge, and m the mass of the electron. V denotes the electrostatic potential, which is a function of the coordinates, V_e is any excess in kinetic energy over that gained from the electric field, e. g. initial velocity, and will in most cases be neglected. The motion in the z -direction is independent of the magnetic field, and will not be considered since it is governed by very small forces.

In a plane electrode system (see fig. 3.1) consisting of two planes $y = a$ and $y = 0$ representing anode and cathode, a stream of electrons extending from the cathode up to a height $y = h$, and moving in the $-x$ -direction, is assumed. An infinite number of electron paths are possible, depending on the choice of initial conditions, each path connected with its definite potential distribution within the space charge region.

3.2. A simple special case; laminar streaming

To derive the potential distribution and space charge density let us assume that all the electrons move in linear horizontal paths. Neglecting the initial energy, eq. (3.1) gives:

$$\dot{x}^2 = 2 \frac{e}{m} \cdot V$$

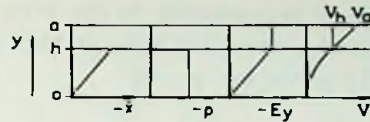


Fig. 3.2. Electron velocity, space charge, field strength and potential.

The vertical electric and magnetic forces must be equal in magnitude but opposite in sign, thus eq. (3.3) gives

$$0 = \frac{e}{m} \frac{\partial V}{\partial y} + \frac{e}{m} \dot{x} B$$

Eliminating \dot{x} a differential equation for the potential is obtained. If we assume $V = 0$ at the cathode the solutions for potential, V , electric field strength, E_y , space charge density, ρ , and electron velocity, \dot{x} , are:

$$V = \frac{e}{m} B^2 \frac{y^2}{2} \quad (3.5)$$

$$E_y = -\frac{e}{m} B^2 y \quad (3.6)$$

$$\rho = -\epsilon_0 \frac{e}{m} B^2 \quad (3.7)$$

$$\dot{x} = -\frac{e}{m} B y \quad (3.8)$$

The space charge density is constant throughout the electron filled region. The potential rises quadratically to the boundary h , after which it continues linearly to the anode voltage V_a .

These functions are illustrated by fig. 3.2.

3.3. The general cut-off relation

In spite of the many possible solutions there exists a general definite relation between the height h and the potential V_h of the upper boundary surface. When the electric field has no x -component, eq. (3.2) can be directly integrated to give

$$\dot{x} = -\frac{e}{m} B y + v$$

If the initial velocity v is assumed to be zero, and it is observed that the vertical velocity must be zero at the upper boundary, the energy equation (3.1) gives for $y = h$

$$\left(-\frac{e}{m} B h\right)^2 = 2 \frac{e}{m} \cdot V_h$$

or

$$V_h = \frac{1}{2} \frac{e}{m} B^2 h^2 \quad (3.9)$$

To make $h = a$ the anode must have the voltage

$$V_0 = \frac{1}{2} \frac{e}{m} B_0^2 a^2 \quad (3.10)$$

the anode cut-off voltage.

Combination of eq. (3.9) and (3.10) then gives

$$\frac{V_h}{V_0} = \frac{h^2}{a^2} \quad (3.11)$$

These expressions are valid both for the space charge free case and for any type of space charge and potential distribution. Of course, they are only a special case of the well-known Hull cut-off parabola.

3.4. The translation current

We confine ourselves to cases where the space charge density has a plane of symmetry at $y = h/2$ and assume it being so strongly developed that it just catches the whole electrostatic D -flux from the anode. Then both potential and electric field strength become zero at the cathode, which is the usual criterion for space charge limitation of emission. Under these assumptions it is possible to get definite expressions for the height and the translation current as function of the applied anode voltage and magnetic field without knowing the exact space charge and potential distributions. These may for example be of the type shown in fig. (3.3).

From the symmetry with respect to $y = h/2$ follows that

$$E(y_1) + E(h - y_1) = E_h, \text{ so that}$$

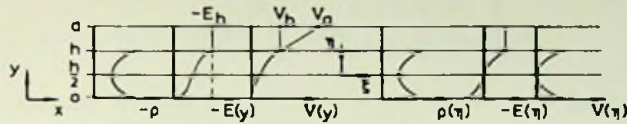


Fig. 3.3. Space charge, field strength and potential in electron stream, referred to stationary and moving coordinate systems.

$$E_{h/2} = \frac{1}{2} E_h \quad (3.12)$$

$$V_h = \frac{1}{2} E_h \cdot h \quad (3.13)$$

To get an expression for the current, a moving coordinate system ξ, η, ζ , is used,¹⁾ having a constant velocity u in the $-x$ -direction, so that

$$\xi = x + ut \quad \eta = y - \frac{h}{2} \quad \zeta = z$$

By the motion an induced electric field in the η -direction $E_i = uB$ is superimposed on the original one, and by choosing $uB = -\frac{1}{2} E_h$ the electric field strength can be made zero on the ξ -axis. Then complete symmetry prevails in the ξ, η, ζ -system, so that

$$\rho(\eta) = \rho(-\eta) \quad E(\eta) = -E(-\eta), \quad V(\eta) = V(-\eta)$$

which is also illustrated in fig. 3.3. Electrons crossing the ξ -axis perpendicularly will then move in paths symmetrical about this axis, so if they constitute a current to the left above this axis, they will give an equal current to the right below it. Electrons that never cross the ξ -axis must be assumed to exist in equal quantities on both sides in order to fulfill the assumed space charge symmetry. Under this assumption the net translation current is zero in the moving system, so that the current in the resting system can be simply computed as

$$I = ub \int_0^h \rho dy$$

where b is the extension in the direction of the magnetic field.

¹⁾ This method was kindly pointed out by mr E. ÅSTRÖM.

As
$$u = -\frac{1}{2} \frac{E_h}{B} \quad \text{and} \quad \int_0^h \rho \, dy = \epsilon_0 E_h$$

it follows that

$$I = \frac{\epsilon_0 E_h^2}{2} \frac{b}{B} \quad (3.14)$$

If E_h , B and V_h are eliminated with the aid of eqs. (3.13) (3.9) and (3.11) there results

$$I = \sqrt{2} \epsilon_0 \left[\frac{e}{m} \frac{b}{a} \frac{h^2}{a^2} V_0^{3.2} \right] \quad (3.15)$$

which is the three-halves power relation between current and voltage, valid under similarity conditions. The maximum current at cut-off is

$$I_0 = \sqrt{2} \epsilon_0 \left[\frac{e}{m} \frac{b}{a} V_0^{3.2} \right] \quad (3.16)$$

The potential increases linearly above the space charge region so that

$$V_a = V_h - E_h (a - h) \quad (3.17)$$

With the aid of this equation analytical expressions for h and I in terms of the applied voltage and magnetic field strength are obtained:

$$\frac{h}{a} = 1 - \sqrt{1 - \frac{2 m V_a}{e B^2 a^2}}$$

Elimination of B gives

$$\frac{h}{a} = 1 - \sqrt{1 - \frac{V_a}{V_0}} \quad (3.18)$$

$$\frac{I}{I_0} = \left[1 - \sqrt{1 - \frac{V_a}{V_0}} \right]^2 \quad (3.19)$$

valid for constant B corresponding to cut-off at $V_a = V_0$.

Elimination of V gives

$$\frac{h}{a} = 1 - \sqrt{1 - \frac{B_0^2}{B^2}} \quad (3.20)$$

$$\frac{I}{I_0} = \left[\frac{B}{B_0} \right]^3 \left[1 - \sqrt{1 - \frac{B_0^2}{B^2}} \right]^2 \quad (3.21)$$

valid for constant voltage $V_a = V_0$

3.5. Graphic representation for a plane magnetron

The results just obtained may be summed up in the diagrams of fig. 3.4 and 3.5.

Fig. 3.4 is valid when the magnetic field is kept constant at a value B_0 corresponding to cut-off at the anode voltage V_0 . The

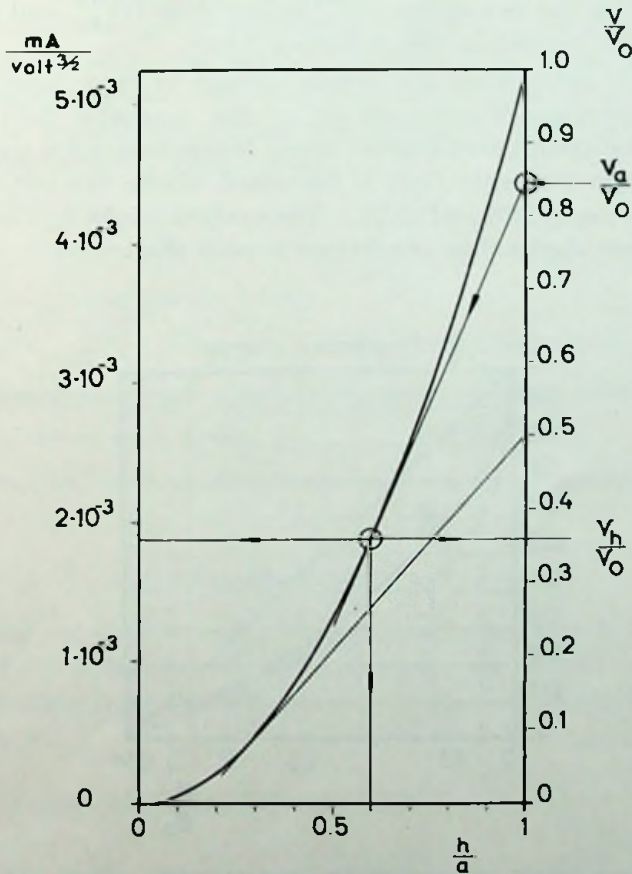


Fig. 3.4. Cut-off parabola for plane trochotron.

parabola illustrates the relative potential V_h/V_0 in the upper boundary of the space charge as function of its relative height extension h/a according to eq. (3.11). Above the space charge the potential increases linearly according to the tangent. The current is also a quadratic function of h/a according to eq. (3.15) and may be represented by the same parabola using the left scale, valid for $b = a$.

When the anode voltage V_a is decreased below the cut-off value V_0 it is observed that the point of tangency rapidly slides downwards. The height decreases slowly, the current rapidly.

For the laminar case, the parabola is also valid within the space charge region. The decrease in current is, of course, very unfavorable. For practical use as a figure of merit, the concept perveance will be reserved for the expression $I/V_a^{3/2}$ rather than $I/V_0^{3/2}$, and its variation is better studied in the following figure.

Fig. 3.5 is valid when the anode voltage is kept constant at a value V_0 corresponding to cut-off at the magnetic field B_0 and illustrates the variation of relative space charge height h/a and current I/I_0 when the magnetic field is increased above the cut-off value according to eq. (3.20) and (3.21.) The cycloid height h_c/a corresponding to space charge free conditions is also illustrated.

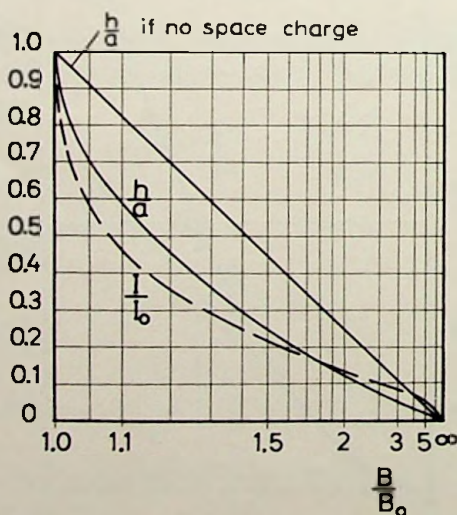


Fig. 3.5. Beam height and current for constant anode voltage and varying magnetic field.

3.6. Space charge influence on electron paths

Just at cut-off the height of the electron path is independent of space charge. Above cut-off space charge makes it decrease faster than it would without, as is obvious from fig. 3.5. In the limiting case, when B is very great or the anode very distant, the electric field strength above the space charge tends to the same value and the height tends to half the space-charge-free value. This is also illustrated in fig. 3.6. The electron paths here shown for the space charge saturated case are obtained from a paper by MOULLIN [1940], who has treated the case in which all orbits are similar to cycloids, all congruent and reaching the cathode once every period. Beyond expressions for height and potential in full agreement with our results he has also given parametric expressions for the orbit and the time of a period. The period is twice as long as for the cycloid. The x -extension of one orbit now is $2\pi h$ as compared to πh for the cycloid. As h tends to half the cycloid value, the x -extension tends to the same value in both cases.

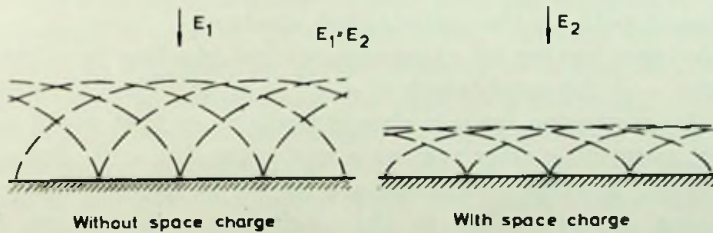


Fig. 3.6. Decrease of the beam height due to space charge.

3.7. Disturbed electron paths

Supposing an electric field distribution corresponding to the case of laminar streaming we are going to study the path of a disturbed electron starting from a certain point $x = 0$, $y = y_1$, with the velocity $x = v$, $y = w$.

Eq. (3.6) gives the electric field

$$E_y = -\frac{e}{m} B^2 y \quad (3.6)$$

Eq. (3.2) is integrated and gives:

$$\dot{x} = -\omega_0 (y - y_1) + v$$

where $\frac{eB}{m} = \omega_0$, the gyro frequency, is introduced.

Inserted in eq. (3.3) this gives:

$$\ddot{y} = \omega_0 (\omega_0 y_1 + v)$$

which has the solution:

$$\frac{y - y_1}{y_1} = \frac{w}{\omega_0 y_1} \omega_0 t + \left[1 + \frac{v}{\omega_0 y_1} \right] \frac{\omega_0^2 t^2}{2}$$

$$\frac{x}{y_1} = \frac{v}{\omega_0 y_1} \omega_0 t - \frac{w}{\omega_0 y_1} \cdot \frac{\omega_0^2 t^2}{2} - \left[1 + \frac{v}{\omega_0 y_1} \right] \frac{\omega_0^3 t^3}{6}$$

If $v = -\omega_0 y_1$, and $w = 0$ the solution is $y = y_1$, $x = -\omega_0 t$ which is the linear path of the undisturbed electron.

For electrons having no excess energy but starting in other directions than $-x$ the condition is $v^2 + w^2 = \omega_0^2 y_1^2$. Then the quadratic term in the expression for y is always positive, so that y will increase infinitely, eventually after passing a minimum if $w < 0$. Some paths corresponding to these conditions are drawn in fig. 3.7. Only electrons having excess energy in the $-x$ -direction can return to the cathode. Periodic paths within the space charge are impossible, but electrons emerging through the upper boundary of the space charge can turn there and thus move in periodic paths.

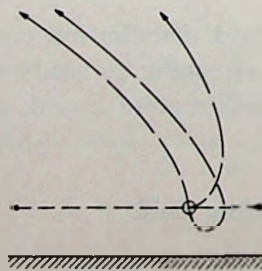


Fig. 3.7. Equilibrium and disturbed electron paths in laminar stream.

Another case in which the differential equations are easily solved is when the space charge density is somewhat reduced but still constant. Let us assume:

$$V = \frac{1}{2} \frac{e}{m} B^2 y^2 (1 - \alpha^2) + E_0 y$$

$$E_y = - \frac{e}{m} B^2 y (1 - \alpha^2) - E_0$$

$$\rho = - \epsilon_0 \frac{e}{m} B^2 (1 - \alpha^2)$$

$$\alpha \ll 1$$

The solution of the differential equations is then:

$$y = y_1 + A \sin \alpha \omega_0 t$$

$$x = v t + \frac{A}{\alpha} \cos \alpha \omega_0 t$$

Seen from a moving coordinate system with the translation velocity v the electron moves in an elliptic orbit, the axis of which are proportional to the vertical initial velocity $w = \alpha \omega_0 A$. If $\alpha = 1$ the ellipse turns to a circle and the path to a trochoid.

Consequently periodic paths may occur when the space charge is reduced below saturation, at first with a very long period, but approaching the gyro frequency when the space charge vanishes.

These results are of very little value, and are included here mainly to show the extreme sensitivity of the solutions to small changes in the field distribution. It may be concluded that periodic electron paths of lower frequencies than the gyro-frequency are likely to be found. When space charge effects are taken into consideration the gyro frequency seems only to play the role of a mathematical shorthand without any direct physical meaning.

3.8. Influence of nonhomogenous electric field

In the real trochotrons the positive electrode is not a plane surface but constituted of a set of spades with more or less thin edges, giving the electric field a wavy structure. The electrons translating through the tube then experience a pulsating or rotating component of electric field strength, and for those having a translation velocity

of such a magnitude that the frequency of this pulsating field component corresponds to their own circling frequency a strong interaction may be expected. The rotation energy will be increased or decreased depending on the initial phase between motion and force. An exact treatment of the space-charge-free case is very difficult. An approximate solution for an assumed sinusoidal variation of the potential as function of x appears to be very sensitive for changes in this assumed potential distribution. In this case the variable component of the electric field rotates in a direction opposite to the electron, and the energy gained by the electron is the difference between that supplied by the vertical component and that supplied by the horizontal one. In reality they are not equal in magnitude, and then a remarkable effect may be expected. This effect is also considered in 4.5.

3.9. Field distribution and circulating current in a cylindrical magnetron

An expression for the current under the assumption that the electrons move in circular paths around the cathode can easily be derived. This current may be considered representative of the beam current in a cylindrical trochotron, as in such a tube the electrons under the main part of the circumference move undisturbed by the spade having zero potential and the beam current becomes space charge saturated.

The differential equations for the static cylindrical magnetron are: [SPANGENBERG 1948.]

$$\dot{r} - r \dot{\theta}^2 = -\frac{e}{m} r \dot{\theta} B_z - \frac{e}{m} E_r \quad (3.22)$$

$$\frac{1}{r} \frac{d}{dt} (r^2 \dot{\theta}) = \frac{e}{m} \dot{r} B_z \quad (3.23)$$

The z -components are neglected. The cathode and anode radii are denoted r_c and r_a and it is assumed that the space charge extends to the radius r_h .

Eq. (3.23) can be integrated under the assumption that $\dot{\theta} = 0$ at the cathode

$$\dot{\theta} = \frac{1}{2} \frac{e}{m} B \left(1 - \frac{r_c^2}{r^2} \right) \quad (3.24)$$

Inserting this into eq. (3.22) and assuming no radial motion, that is $\dot{r} = 0$, an expression for the field strength is obtained:

$$E_r = \frac{1}{4} \frac{e}{m} B^2 r \left(\frac{r_c^4}{r^4} - 1 \right) \quad (3.25)$$

From this the space charge density and potential distribution are obtained:

$$\rho = -\frac{1}{2} \epsilon_0 \frac{e}{m} B^2 \left(1 + \frac{r_c^4}{r^4} \right) \quad (3.26)$$

$$V = \frac{1}{8} \frac{e}{m} B^2 r_c^2 \left(\frac{r}{r_c} - \frac{r_c}{r} \right)^2 \quad (3.27)$$

The latter equation gives also the cut-off voltage:

$$V_0 = \frac{1}{8} \frac{e}{m} B_0^2 r_c^2 \left(\frac{r_a}{r_c} - \frac{r_c}{r_a} \right)^2 \quad (3.28)$$

The tangential current between the cathode and the boundary of the space charge at r_h is given by the integral:

$$I = \int_{r_c}^{r_h} b \rho r \dot{\theta} dr$$

which has the solution:

$$I \cdot \frac{r_c}{b} = \frac{1}{8} \epsilon_0 \left(\frac{e}{m} \right)^2 B^2 r_c^3 \left[\frac{r_h^2}{r_c^2} - \frac{r_c^2}{r_h^2} - 2 \ln \frac{r_h}{r_c} - \frac{1}{2} \left(1 - \frac{r_c^4}{r_h^4} \right) \right] \quad (3.29)$$

3.10. Graphic representation

Potential and current obey different functions and are best illustrated in separate diagrams. There are two independent variables r_a/r_c and r_h/r_c replacing h/a in the plane case.

The potential within and at the boundary of the space charge is illustrated by the curves of fig. 3.8 according to eq. (3.27). Outside the space charge the potential increases logarithmically. Now by drawing the diagram with logarithmic abscissa the potential can be extrapolated by a straight line. Starting for instance with given values of r_a/r_c and V_a a point in the diagram is obtained, from

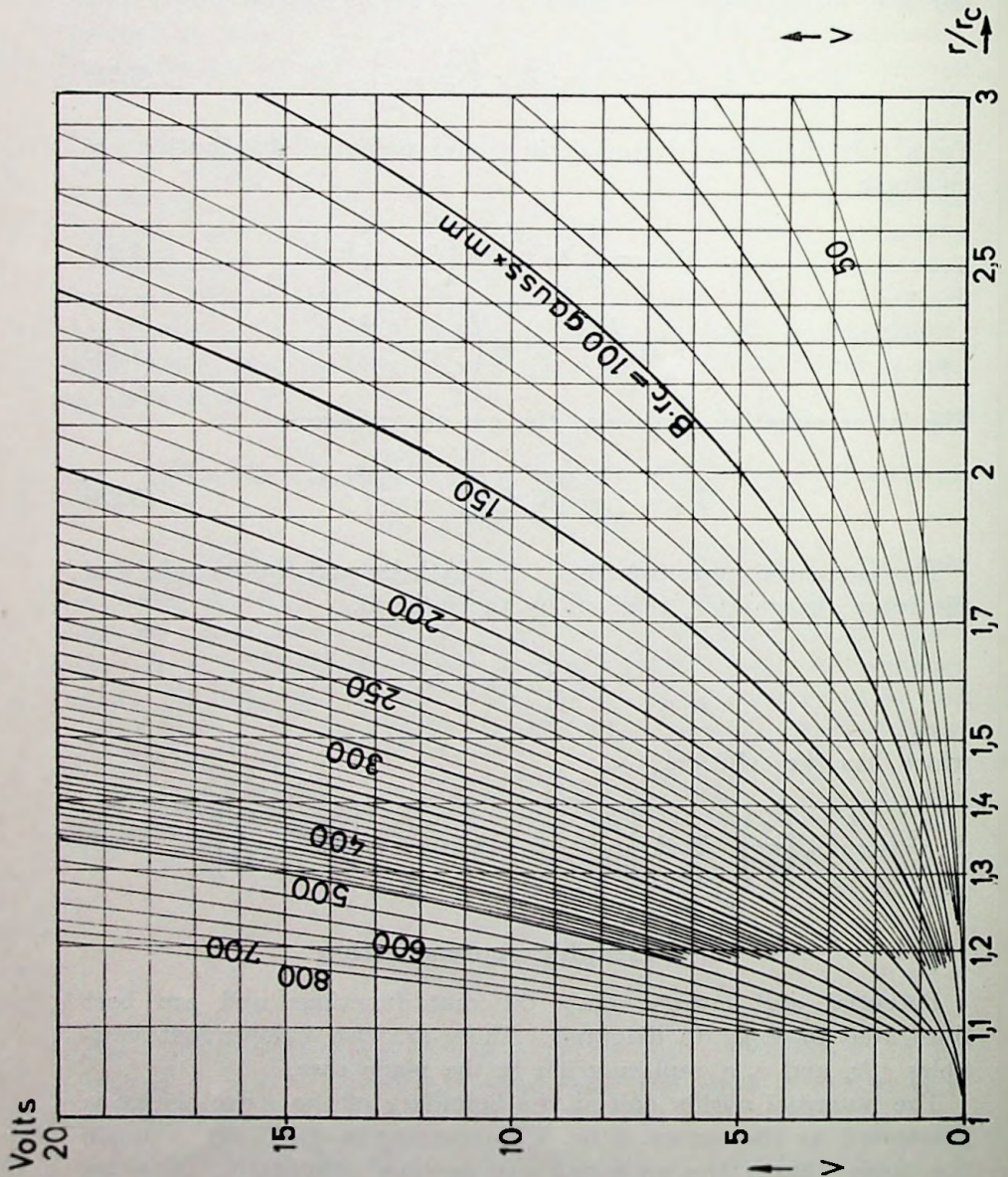


Fig. 3.8. Diagram for determination of the beam cut-off radius in a cylindrical trochotron.

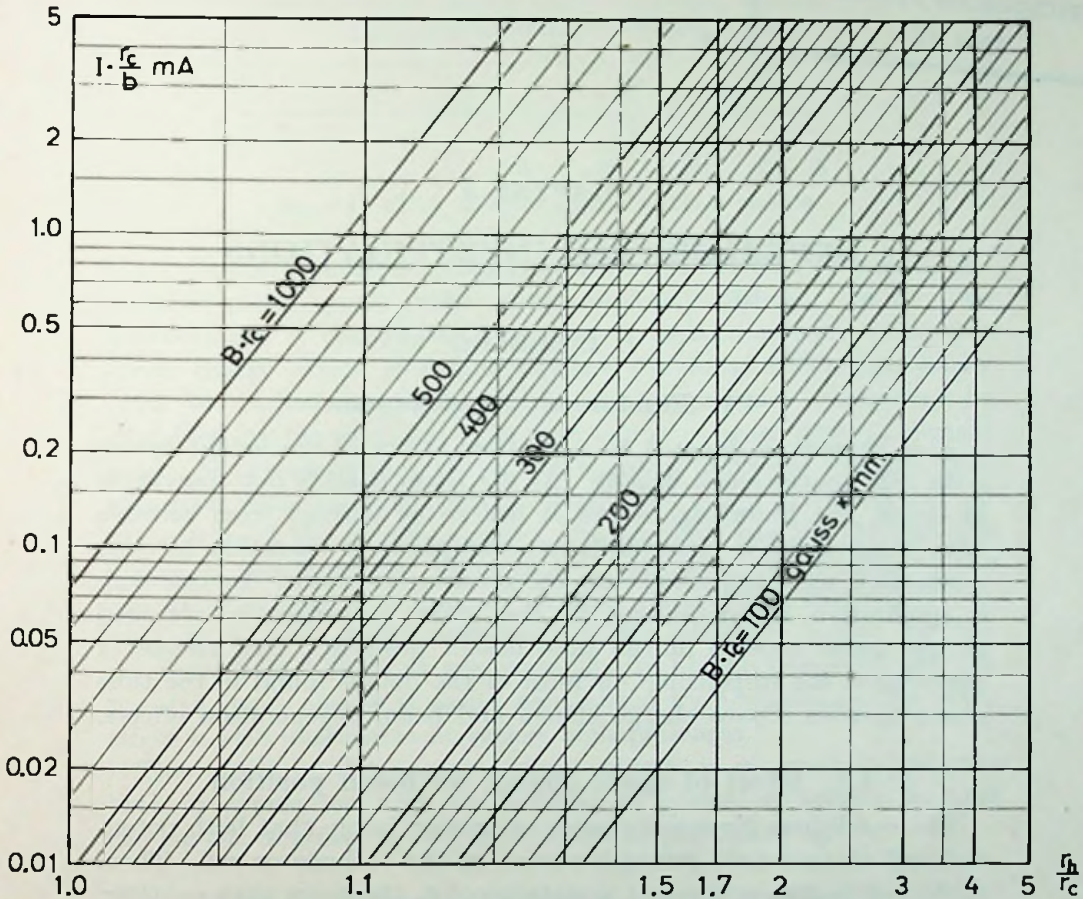


Fig. 3.9. Diagram for determination of the beam current in a cylindrical trochotron.

which a tangent to the curve is drawn corresponding to the actual product of B and r_c . The point of tangency indicates the radial extension r_a/r_c of the space charge and the potential at its boundary.

The circulating current is in a similar way illustrated by fig. 3.9, corresponding to eq. (3.29). The curves are here transformed to straight lines by suitable choice of scale for the abscissa.

These diagrams are derived for the very specialized case of single-stream (no radial current) neglecting the effect of beam degeneration and initial velocity. They should, therefore, be regarded as rough approximations and are included only to indicate the order of magnitude and the nature of the considered relations.

BIBLIOTHEEK
LABORATORIUM VOOR
TECHNISCHE FYSIKA
DELFT

CHAPTER 4.

EXPERIMENTAL INVESTIGATIONS

BY

L. LINDBERG

4.1. Fundamental phenomena

This chapter is devoted to a detailed study of trochoidal beams with high space charge density. As the beam itself is not observable in detail, the knowledge about it has to be derived from suitable tube characteristics under different conditions of operation in close connection with hypotheses on the electron behavior. In this way a qualitative understanding of the main properties is obtained giving useful aspects of the tube design problem. Two classes of phenomena are responsible for most of the details found in the tube characteristics: Space charge effects and beam degeneration effects.

4.2. Effect of space charge on beam position

The conditions for space charge saturation imply that both potential and electric field strength vanish at the cathode or rail. Then, if the rail is discontinued at a certain point, the beam may continue following the the positive electrode without »noticing» the break. In any case it is clear that it is very loosely coupled to the negative electrodes, but strongly to the positive, so it has a strong tendency to form its own rail by space charge and follow the shape of the positive electrodes.

To investigate this effect a tube with cross-section according to fig. 4.1. was built. Electrons are shot from the simple electron gun C, R, A, into a space where the field strength without space charge is of the same magnitude as in the electron gun. The beam is made visible by residual gas of about 10^{-4} mm Hg pressure. If the emission is temperature limited, the beam proceeds like a in fig. 4.1 along an equipotential line corresponding to the mean potential of the gun. It is very thin and shows clear trochoidal structure. At full

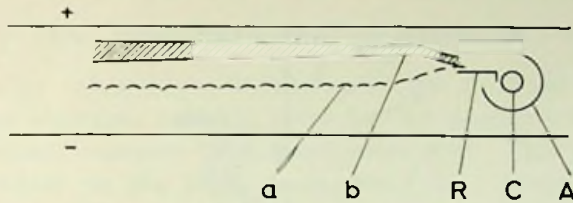


Fig. 4.1. Effect of space charge on beam position.

space charge saturated emission however, it drives up beneath the positive plate, grows wider and completely diffuse, like *b*. The degeneration is remarkable. At first it seems confusing that this space charge effect is not neutralized by ions, which necessarily must be created in large quantity at this pressure. This may be explained by the fact that ionization can only occur above a certain potential surface where the electrons have sufficient energy. The ions start with negligible initial velocity and move in slightly curved paths toward the negative plate. During their passage through the region of zero potential they reach a velocity corresponding to the ionization potential or greater, whereas electrons in this region can only have very small energies and are strongly bound by the magnetic field. The ions are consequently quickly removed and the positive space charge is easily neutralized by electrons so the main effect is still observable at rather high pressures.

This effect of the negative space charge is of great importance both in connection with the guiding of beams by spades and for the cut-off relation, as will be evident in the following.

4.3. Deflection by space charge barrier

When a trochoidal beam is deflected by a spade of low potential, some electrons are able to continue through the region of low potential below it as pointed out in 2.3.

In a binary trochotron it is possible to measure the current escaping under a spade of zero potential. This was done in a tube according to fig. 4.2 with spade *a* and bottom plate at cathode potential, spades *b* positive. The beam then should go to the upper half of the tube and the eventually penetrating electrons to the lower half. The curves in fig. 4.3 illustrate total emission and penetrating current as functions of the magnetic field. The solid curves refer to full space charge saturated current, the dashed curves to a temperature limited emission about 10 % of the normal value and the dot-dashed

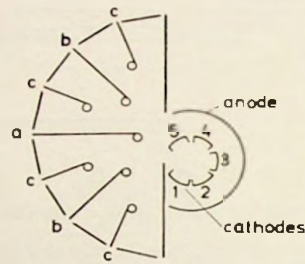


Fig. 4.2. Binary trochotron with sectionized cathode.

curves to a still smaller value, 2 %. It is evident that with temperature limitation not only the percentage of emission passing below *a* is greater but also the absolute value. Even at 10 % emission space charge effects are clear. The sudden rise in penetrating current at about 300 gauss for the space charge saturated case seems to correspond with the appearance of considerable beam degeneration. This is reasonable since by the degeneration some electrons gain much energy and become able to penetrate even the barrier. Similar phenomena also occur in cylindrical trochotrons and contribute to the complexity of their characteristics, as will be discussed in the following.

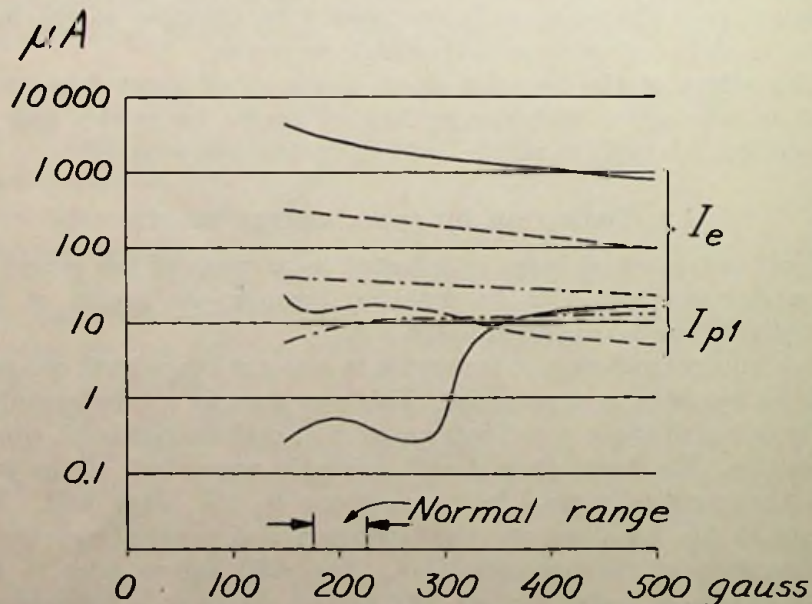


Fig. 4.3. Effect of space charge barrier on penetrating current.

4.4. Distribution of the emission

The emission takes place mainly from the farthest part of the cathode. The electrons emitted there form a negative space charge which suppresses emission from the former part. This phenomenon was also studied on the large scale model of a binary trochotron just mentioned. The cathode was here composed of five separate segments, as shown in fig. 4.2. The distribution of emission from different cathodes is shown by rectangles in fig. 4.4 for different magnetic field strengths. The curves are drawn to indicate the

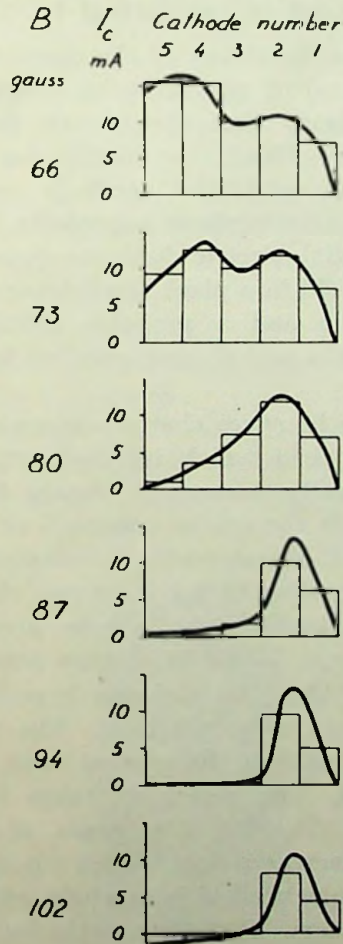


Fig. 4.4. Distribution of the emission for varying magnetic field.

specific emission density. Below cut-off all parts emit, but with increased magnetic field the emission from the parts 5, 4, 3 is successively decreased and finally N-current appears to them. (The emission from part 1 is small because the electric field from the anode is partially screened by the bottom plate.)

The fact that only part of the cathode is emitting may be of some value for the reliability and the life time of trochotrons. The characteristics of the model tube were only slightly altered if any one or two segments were let to cool.

4.5. Cut-off in cylindrical trochotrons

As well known from the theory of the magnetron the general cut-off relation is independent of the radial distribution of potential, the only condition being that the electric field should have no tangential components. This is not exactly the case in a cylindrical trochotron, where the cylindrical anode is replaced by a set of spades. The equipotential surfaces necessarily become more or less wavelike and tangential electric field components are introduced. The effect of such a field in a plane trochotron without space charge was considered in 3.8 and a probable influence was found on electrons moving with a period corresponding to the wave structure of the field.

Now there will also be space charge accumulations in the regions of the weak electric field which increase cumulatively when the degree of nonhomogeneity exceeds a certain limit. They tend to press the beam towards the spades causing leak currents to such an extent that the cut-off-characteristic is completely ruined. A tube with cross section according to fig. 5.5 *a* (see chap. 5), for instance, has practically no cut-off, whilst a tube according to fig. 5.5 *d* (U 17), with a ratio $r_s/r_c = 2,4$ has a very good cut-off, illustrated by fig. 4.5, in which the total emission is recorded as function of the voltage at constant magnetic field. The voltage ranges from -30 to $+30$ volts and in the current scale one coarse division corresponds to $10 \mu\text{A}$. The curves are taken for five values of the magnetic field, 150, 175, 200, 250 gauss, and become displaced towards the right for increased field.¹⁾ Such a good cut-off can only be obtained when the magnetic field is carefully adjusted to parallelism with the electrode system. If the magnetic field is slightly inclined

¹⁾ An explanation of the photographic recording of characteristics is given in 8.1.

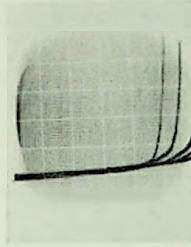


Fig. 4.5. Cut-off curves for U 17.

a maximum appears in the cut-off characteristic at a voltage lower than the cut-off voltage. This is shown by the two pictures in fig. 4.6, which refer to the same tube but with $0,5^\circ$ and 1° inclination of the field. A comparison of the curves shows that after passing the maximum the curves approach the original ones, so that the real cut-off voltage is rather unaffected by a slight inclination of the field. The voltage at which the maximum occurs varies with the magnetic field and is approximately half the cut-off voltage. We have not found any explanation for this effect.

The cut-off curve is the most sensitive indication of misalignment between the electrode system and the magnetic field and has therefore been used for alignment purposes before making other measurements every time a new tube was set up.

Neither the characteristics nor the leak currents are so sensitive to inclination as the cut-off curve, and in practical counter circuits an inclination of the field does not matter until it becomes much greater.

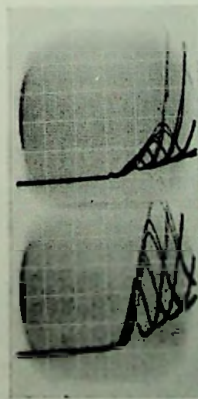


Fig. 4.6. Cut-off curves for U 17 at inclined magnetic field.

4.6. Deflection characteristics and noise

A fundamental requirement is that a spade that is slightly positive, as it usually will be under locking conditions is able to deflect the beam of circulating electrons completely into a box. This property is best illustrated by a «deflection characteristic» showing the total beam current irrespective of where it goes, and is obtained by recording the cathode current as function of the voltage of one spade, all others being positive. In fig. 4.7 *a* a set of such curves are shown for different magnetic fields, 150, 162, 175, 200, 225, 250 gauss. (Current scale 1 mA/div.) When the actual spade has the same voltage as the others, the tube is cut off and the current is negligible, but when it approaches zero voltage, a beam is deflected, and for voltages below a certain value the current becomes constant, indicating complete deflection. A jump often occurs in the curve, corresponding to the sudden formation of a space charge barrier. The critical voltage necessary for complete deflection grows lower when the magnetic field is increased, and in the fourth picture is seen that the current continues to increase when the spade goes negative.

The degeneration has now grown intense and the coupling around the cathode cannot be broken. A simultaneous record of the noise level at the cathode is shown in fig 4.7 *b*. As long as the magnetic field is weak, a high peak appears just before the beam is completely deflected, but in the stronger field of the fourth picture from the top, this level remains also when the spade goes negative.

Two spades of low voltage have greater power to deflect a beam than a single spade. This is shown in fig 4.7 *c* and *d* which show deflection characteristic and noise, respectively, when the voltage of two adjacent spades is simultaneously varied. Generally the deflection occurs at higher spade voltage, and is still complete in the fourth picture, but not in the fifth and sixth although the deflected current is greater than for a single spade.

The characteristics here shown are representative for a tube of bad construction, just to point out its bad properties. The electrode system is similar to that shown by fig. 5.5 *d* (U 17), but the spades had accidentally got thinner and less curved edges against the cathode. In tubes of more successful construction these phenomena hardly occur or are less pronounced. If the emission is temperature limited, the noise may also vanish before the space charge barrier, as will be described in 4.8 and 5.5.

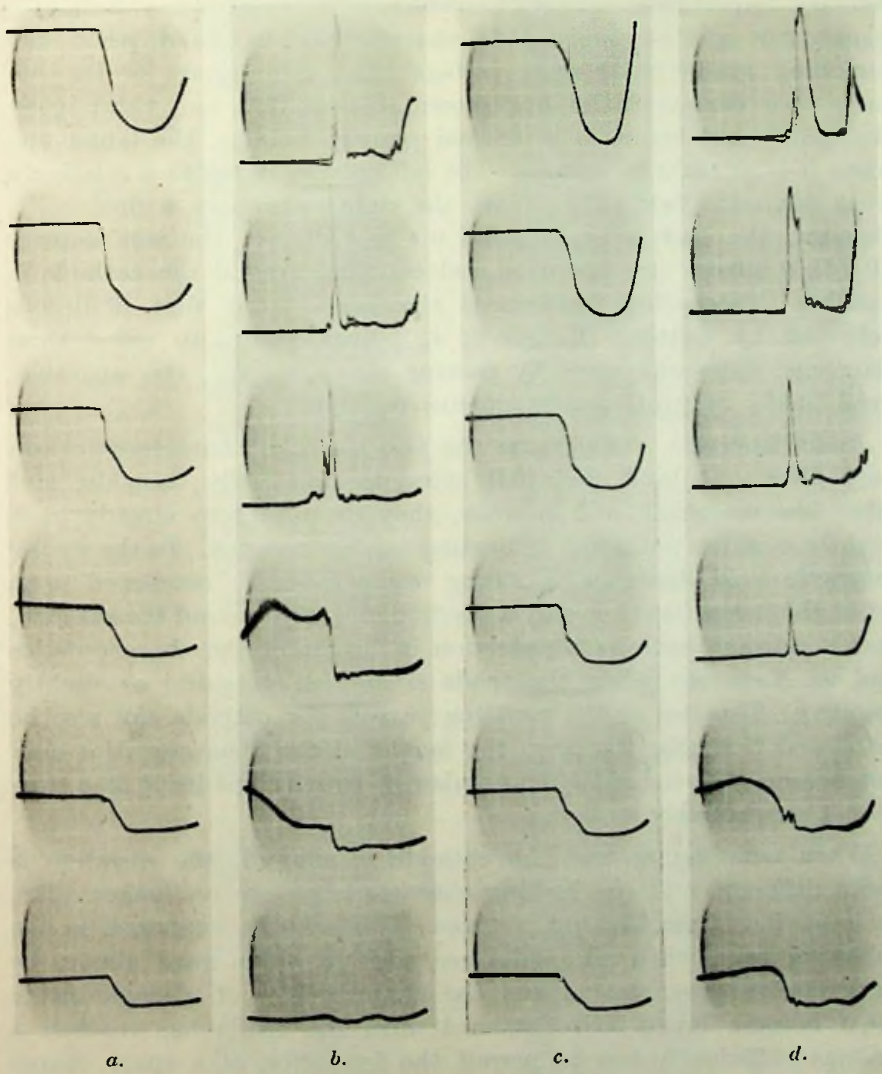


Fig. 4.7. Deflection characteristics and noise.

4.7. Spade characteristics and the beam length

As mentioned in 1.3 two kinds of spade characteristics are of primary importance: spade characteristic I, valid when all other spades are positive and spade characteristic II valid when the preceding spade is at zero voltage. In each picture of fig. 4.8 these two characteristics are shown, the smaller one valid when the spade next before is at normal positive voltage, the larger one when it is at cathode voltage. The left column refers to a relatively weak magnetic field (170 gauss), the right column to a field 50 % stronger, the current scale being 0,4 mA/div. In the top pictures all other spades are positive, and coupling around the cathode is possible. Proceeding downwards the beam is at first definitely deflected by putting the spade s_{n-2} negative (-10 volts) then shortened more and more by putting also s_{n-3} , s_{n-4} etc. negative, until finally only one spade remains positive.

Apart from the top pictures the two kinds of characteristics are very alike. At least their left sides do practically coincide, and when the magnetic field is weak, they drop to zero already at a slightly positive potential, indicating no degeneration. In the strong magnetic field, however, a strong degeneration is developed even when the beam length is only a fraction of a turn around the cathode, and it appears both as a reduction in height of the characteristics and as N-current when the spade is at zero potential or slightly negative. The size of the emitting part of the cathode can also be estimated from fig. 4.8 since the height of the characteristics does not become reduced until the number of positive spades is less than 6 or 4, respectively.

When coupling around the cathode is allowed, the situation is quite different and the locking characteristics are no longer alike, as is obvious from the top pictures. This may be explained in the following way: when all spades are positive, there must always be an excessive degeneration and the characteristic of a single spade must become broad and flattened until the spade has reached a voltage sufficiently low to permit the formation of a space charge barrier. When this happens, the state of degeneration is suddenly changed, and for lower voltages the characteristic is higher and narrower corresponding to a lower degree of degeneration. The sudden change appears as a discontinuity in the left top picture. In spite of this, the two characteristics do not coincide at low vol-

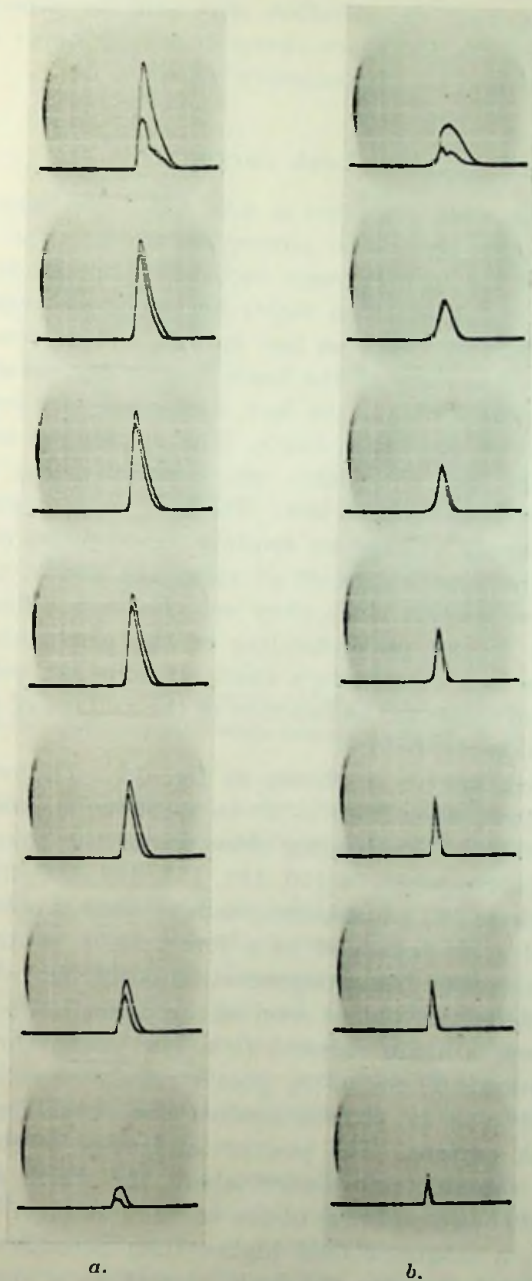


Fig. 4.8. Influence of beam length on spade characteristics.

tages, indicating that degeneration may still be present. In the strong magnetic field, the space charge barrier is never able to stop the degeneration and no discontinuity occurs.

4.8. Leak currents

The expression «leak currents» is used for those currents flowing to electrodes which should be currentless if the tube did operate ideally. Even if the leak currents outside the electrode system are prevented by careful «electron tight» design, there remains several causes inside the tube, such as bad cut-off, too narrow opening to the box, diffuse boundary of the beam due to degeneration or oscillations, beam spread within the box, and secondary emission from the plate on which the beam lands. The spades are more exposed to such currents than the plates, and especially that spade under which the beam bends into a box. The leak current gives rise to a tail near the supply voltage on spade characteristics of the second order. From the practical point of view, the use of those characteristics is most correct since they set the upper limit for spade resistance, but for an understanding of the electronic phenomena in the tube the leak current to a spade at constant voltage is more instructive when measured as function of the voltage of the preceding spade or the magnetic field.

A set of such curves is shown in fig. 4.9. The voltage of the preceding spade s_n runs from -30 to $+30$ volts, and the current scale is $100 \mu\text{A/div}$. Proceeding downwards the magnetic field is increased, and corresponds to 150, 162, 175, 188, 200, 225, 250 gauss, respectively, where 162 gauss corresponds to normal operation. When the voltage of s_n is decreased to a few volts a maximum appears owing to the excessive beam degeneration occurring before the beam is completely deflected, but as soon as the deflection has taken place the leak current is again reduced to a low value, corresponding to normal operation. Then, as s_n goes strongly negative, the beam entering the box n is pressed against the actual spade s_{n+1} and gives high leak current. The position and slope of this part of the curve affords valuable information about the width of the opening to the box and the smoothness of the beam boundary. If the opening is too narrow, a magnetic field higher than necessary for good cut off must be used to keep the leak current to a reasonable value under normal conditions ($V_{s_n} = 0$). This is undesirable since it

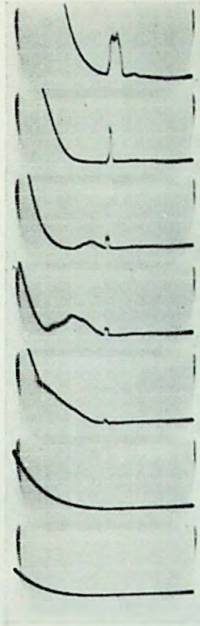


Fig. 4.9.

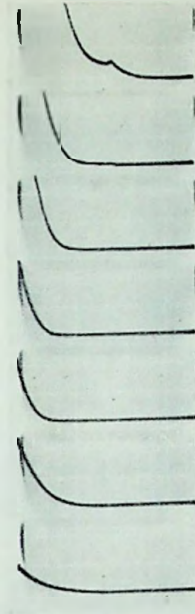


Fig. 4.10.

Fig. 4.9. Leak currents under normal conditions.

Fig. 4.10. Leak currents when internal feedback is interrupted.

means decreased current and increased risk for beam degeneration. In the third, fourth, and fifth pictures some other kind of oscillation disturbs the curves.

If the beam is deflected completely by keeping s_{n-1} negative (-10 volts), the next set of curves, fig. 4.10, is obtained. The peak of leak current then disappears, as well as the annoying oscillations. The rising left part of the curve is displaced to the left when the magnetic field is increased as is to be expected when the beam grows thinner. In the last two pictures, however, the slope of the curve changes, indicating a diffuse beam boundary caused by degeneration.

The plate voltage also has great influence on the leak current, as shown in fig. 4.11, with normal magnetic field strength and $V_{pn} = +10, +20$ and $+30$ volts, respectively.

The leak current under temperature limited conditions is also of great interest, since the beam structure is then quite different.

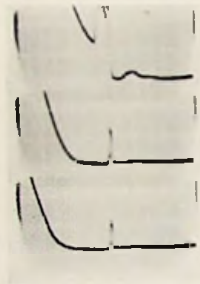


Fig. 4.11.

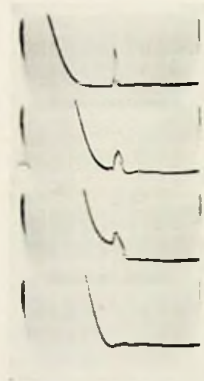


Fig. 4.12.

Fig. 4.11. Influence of plate voltage on the leak current.

Fig. 4.12. Leak current under temperature limited conditions.

This is recorded in fig. 4.12 for normal magnetic field. The top picture shows the case with full space-charge limited emission of 2,8 mA. The temperature is then decreased so the emission becomes 2,7, 2,5 and 1,8 mA for the following pictures. It is clear that the height of the electron paths increases in good agreement with the theory in 3.6, and that the degeneration or oscillations producing the peak near zero spade voltage vanish. A higher magnetic field displaces the curve to the left (Not shown).

In some cases the leak currents have been measured as a function of the magnetic field, and the measurements extended to very low currents. For a good tube, curves like those in fig. 4.13 are obtained. The emission, I_e , and the height of spade characteristic I, I_{char} , are plotted as well. The beam is deflected by spade 2, which is at zero voltage. When the beam is completely deflected by putting spade 1 to -10 volts, the dotted lines are valid. In most practical cases only the ratio between leak current and useful current is of importance as a figure of merit. If no degeneration is present, this ratio increases with the magnetic field in a monotonic manner, but when degeneration becomes excessive, this is not the case until the magnetic field is extraordinarily strong.

In some tubes does the leak current to the most exposed spade drop still more rapidly than shown here.

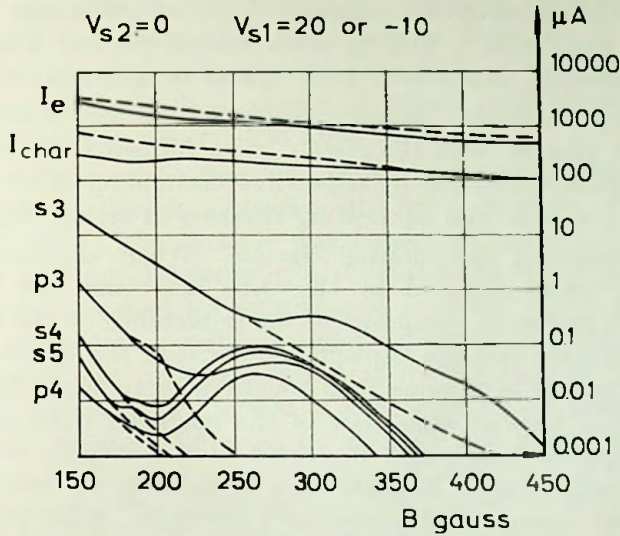


Fig. 4.13. Beam-current, I_e , height of spade characteristic I_{char} , and leak currents as function of the magnetic field strength. (Dotted curves refer to interrupted internal feedback).

4.9. Oscillations and noise

Parasitic oscillations were already observed in the plane trochotrons, but could usually be suppressed during measurements by damping resistors and decoupling capacitors as described by ÅSTRÖM, [ALFVÉN et al. 1948, p. 72].

Owing to the high currents in cylindrical trochotrons, disturbing h. f. oscillations are much more difficult to suppress, but they must be suppressed if the true static characteristics are to be measured. The same types of oscillation mechanisms as encountered in magnetrons may be expected, i. e. negative resistance oscillations, cyclotron frequency oscillations and travelling-wave mode oscillations, but also other types seem to exist.

Generally oscillations in electron tubes are most easily set up when the electrons can interact with some kind of resonant circuit. At moderate frequencies circuits may be provided by the wiring and measuring instruments, and at very high frequencies by the leads inside the tube and the interelectrode capacitances. Two methods of preventing oscillations in a circuit have been tried:

At first the characteristic reactance $\sqrt{L/C}$ of the circuit is reduced so that it even with a high Q-value cannot present a sufficiently high antiresonant impedance, then the Q is decreased to about 1 by inserting a suitable damping resistance of the order $\sqrt{L/C}$ in series or in parallel with the circuit. The influence of the external circuits is thus eliminated by capacitive decoupling of all electrodes near the tube base and connecting resistors in series with all leads.

Now considering the internal circuits. When all electrodes are capacitively short-circuited at the tube base any two electrodes may form a resonator composed of the inductance of the leads from base to electrode and the capacitance between the electrodes. The leads have usually been some 5 cm long in order to bring the electrode system into a homogeneous part of the magnetic field undisturbed by the magnetic base pins. Regarded as a two wire transmission line, they will have a characteristic impedance of 50–200 ohms and a lowest resonant frequency of 1 500 Mc/s. Now, when loaded by an interelectrode capacitance which for adjacent electrodes amounts to 2–6 pF the leads act as an inductance of 0,02–0,06 μ H giving a circuit which resonates somewhere between 800 and 270 Mc/s and has a characteristic impedance $\sqrt{L/C}$ of the order of 60–180 ohms. In reality things are of course much more complicated since all leads and electrode capacitances form a complicated network of coupled resonant circuits but their resonant frequencies and characteristic impedances must be of the order of magnitude mentioned. Searching resonances with the aid of a grid-dip-meter on a cold tube placed in a short circuited socket also indicated a number of resonance frequencies, e.g. 185, 240, 245, 275, 285, 290, 305 Mc/s. Below 185 Mc/s no resonance was found.

In use as a scale the spades are not decoupled at the tube base but connected to rather high resistances, which for these high frequencies may be regarded as open circuits. Two spades may then oscillate in a way similar to a half-wave-length line, the circuit being composed of the lead inductance, loaded in one end by the spade-to-spade capacitance and in the other by the socket capacitance. The resonant frequency would then be about $\sqrt{2}$ times that of the quarter wavelength circuit.

All these circuits will become effectively damped if resistors are inserted in series with all leads near the base, and oscillations will be prevented in most cases unless the equivalent negative conductance

offered by the tube is extremely high. Resistors of 80Ω decoupled with 100 pF capacitors have been used as described in chapter 8. Even if the circuits are completely damped, so that all electrodes are at constant potential, purely electronic oscillations may still occur, as have been observed in some cases.

A video detector also described in 8.3 has usually been connected to the cathode during measurements for indication of noise and h. f. oscillations. The cathode was chosen as being the most symmetrically positioned electrode in the tube. In some cases a radio receiver was also used for searching oscillation frequencies. Several types of oscillations occurring under different operating conditions were observed but only one type was investigated by plotting the frequency spectrum. This type of oscillation takes place when the beam is incompletely deflected by a spade and gives rise to a high leak current to the next spade (see fig. 4.9 in 4.8) and is consequently of great interest. The spectrum measured between 38 and 350 Mc/s is shown in fig. 4.14. It exhibits certain characteristic peaks of high level, but although of a noisy character. The following pictures show the spectrum when all operating data are changed according to the similarity laws, *i. e.* all voltages in the same scale and the magnetic field in proportion to the square root thereof. Then those frequencies at which the highest peaks occur also increase accurately

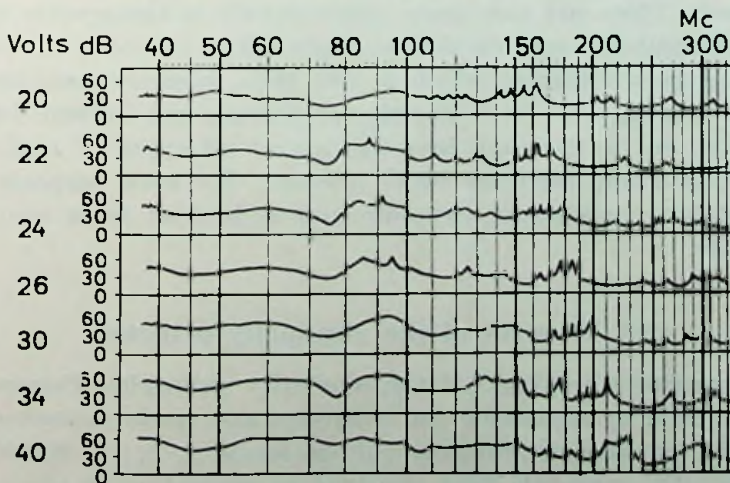


Fig. 4.14. Noise spectra. Voltage and magnetic field changed according to similarity laws.

in proportion to the square root of the voltage. Consequently there must be a type of purely electronic oscillations which are independent of resonant circuits for their existence, since the frequency would otherwise remain more constant. If the circulation frequency around the cathode for the lowest voltage, 20 volts, corresponding to the top picture, is computed with the aid of equation (3.24) in 3.9, $f < 185$ Mc/s is found which corresponds well to the peaks found below 165 Mc/s. A feedback mechanism like that described in 2.3, by which the noisy beam reacts back on the emission range or part of the beam travels more than one turn around the cathode and thereby constitutes a feedback of noise is likely to be the explanation of these oscillations.

A peak is also observed at half the circulation frequency, probably caused by electrons travelling twice around the cathode. The spectra of fig. 4.14 are not drawn in correct scale, since the variation in sensitivity of the receiver is not corrected for, and it may be responsible for the slow changes in the curves. The dB scale is also approximate. However, for frequencies below and above the high peaks there are marked minima in the noise level, possibly indicating that electrons which would travel with higher or lower velocities than the main stream are caught by the bunches and forced to circulate with their frequency. In an other measurement such a minimum showed practically complete extinction of noise just above the main frequency. There are also many other details in the spectra which show no regularity and cannot be explained.

At the gyrofrequency, which is 450 Mc/s, however, nothing noticeable was found. The investigations were not carried further than this, but a thorough investigation of all types of oscillation phenomena would certainly be of interest. For such purposes new tubes of less complicated structure and with short leads would be preferable.

4.10. Control of the similarity principle

An experimental check of the similarity principles discussed in 1.5 was made by measuring the deflection and spade characteristics of a tube operated at different voltage levels, 2, 5, 10, 20, 40 and 80 volts. The magnetic field was kept in proportion to the square root of the voltage. The curves obtained were then transformed to the same scale by dividing with the appropriate scale factors, and

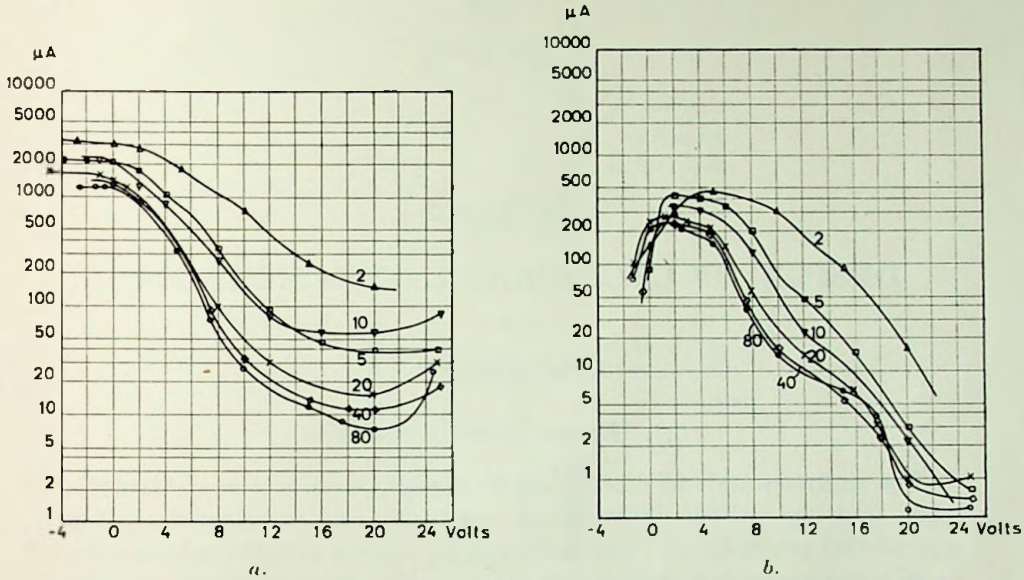


Fig. 4.15. Control of the similarity principle, a. Deflection characteristics.
b. Spade characteristics.

plotted in the same diagram, fig. 4.15 *a* and *b*, respectively. The agreement is quite good except for the lowest voltage levels, at which the emission energies play a considerable rôle, as expected since the potential within the beam is usually lower than a fourth of the spade voltage. The use of a standardized operating voltage level of 20 volts is consequently justifiable.

CHAPTER 5

DESIGN OF CYLINDRICAL TROCHOTRONS

BY

J. BJÖRKMAN

5.1. Experimental tubes

The ordinary aids to electron tube design, such as the electrolytic tank and the rubber sheet model are quite useless when designing cylindrical trochotrons. The only way to obtain reliable information is to build operating models and measure the characteristics. In this work many models have been built and from these experiments the picture of the electronic discharge mechanism is pieced together.

When models are used, it is desirable to keep the scale rather large to avoid difficulties in mechanical design. In the case of the cylindrical trochotron, however, a large scale requires a large cathode and the very great heater power then needed introduces practical difficulties. Some models having cathode diameters of 10–12 mm have been built, but the major part of the work has been carried out with tube models equipped with standard vacuum tube cathodes of diameters in the range of 3 to 1 mm. Of these latter models some selected types will be described in this chapter. The examples are chosen to give an illustration of the design problem and thus tubes having both bad and good characteristics are included.

5.2. Mechanical construction

All experimental tubes were made by hand in the tube workshop of the laboratory. The technique used is illustrated by fig. 5.1, showing the electrode system of the tube type U 10. The electrodes are welded to metal wires, 0,5 mm in diameter. The wires are brought through holes in drilled mica sheets and the electrodes held in position by means of mica spacers. In tubes having the spades bent

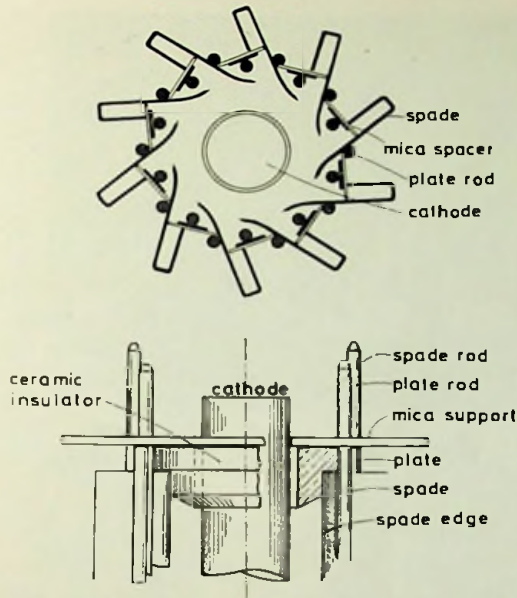


Fig. 5.1. The electrode arrangement of the cylindrical trochotron U 10.

tangentially to the cathode as the U 10 type, the spade edges are supported by ceramic insulators at each end of the electrode system. Fig. 5.2 is a photograph of the electrode assembly of the U 17 type, the electrode structure of which is similar to that of U 10. In the electrode system to the left of the picture some spades and plates are removed to show the cathode and the ceramic rings. In tubes where the spades are directed radially no ceramic rings are used. An example of this construction is shown in Fig. 5.3, a photograph of the U 20 electrode system.

Fig. 5.4 *a* and *b* shows two completed experimental tubes. The tube in fig. 5.4 *a* has separate leads to all electrodes through a 27-pin base. Because the chrome-iron of the base pins disturb the magnetic field the electrode system is mounted on a long stem of non-magnetic leads. Fig. 5.4 *b* shows a tube mounted on a standard 7-pin miniature tube base. The tube has spade resistors inside the vacuum shell and the plates are internally connected to two groups.

Only non-magnetic materials are used for the electrode systems, the nickel cathode being above its Curie-point when operating. As electrode metals molybdenum, tantalum, nichrome and constantan have been used.

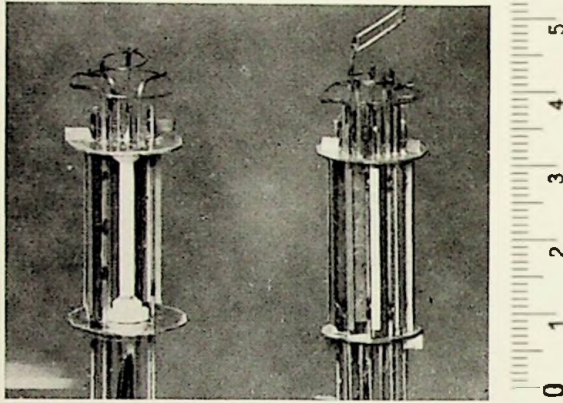


Fig. 5.2. The electrode system of U 17.

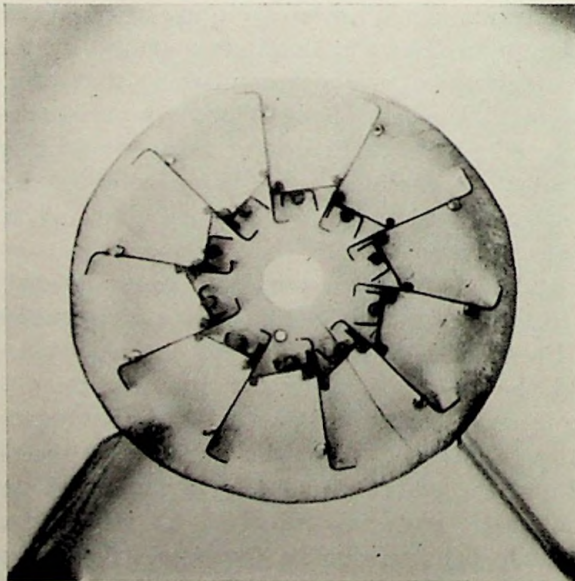


Fig. 5.3. The electrode system of U 20.

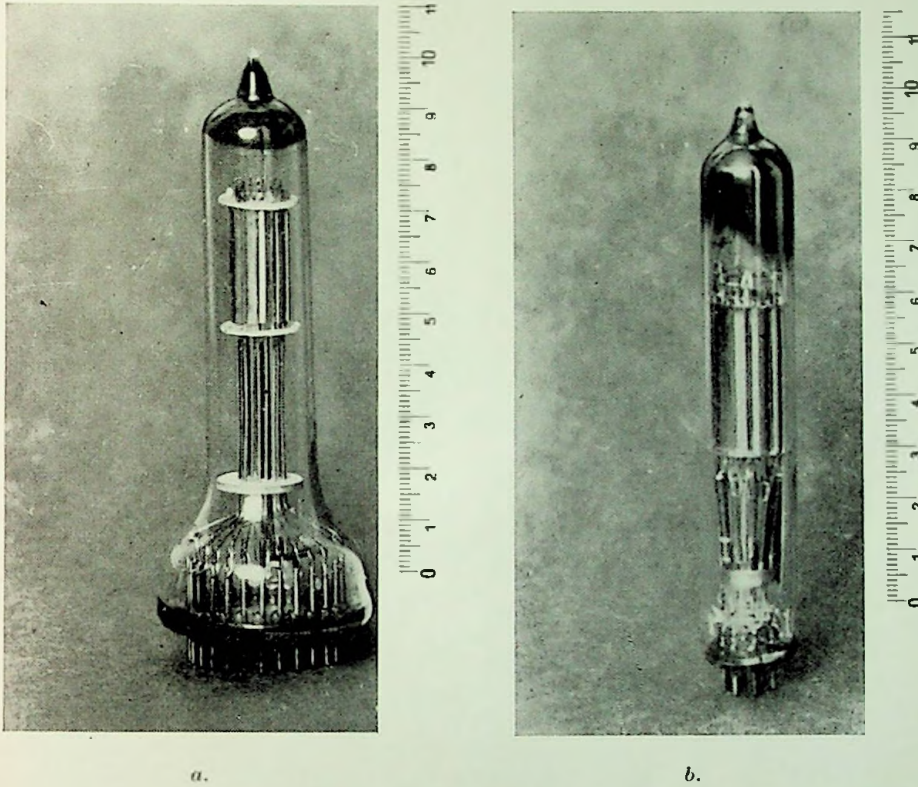


Fig. 5.4. Two experimental tubes.

5.3. Data and characteristics of the experimental tubes

The crosssections of the tubes to be described are shown in fig. 5.5 together with their main mechanical and electrical data. The electrical data given for optimum characteristics are V_s/B^2 , where V_s denotes the spade voltage in volts and B the magnetic field strength in voltseconds per m^2 , and the preveance P at this operating condition, where the current is the cathode current and the voltage is the spade voltage. S_I and S_{II} give the steepness of spade characteristics I and II, respectively, at the optimum V_s/B^2 and a V_s of 20 volts. To get a correlation between the electrical and mechanical data the ratio r_h/r_c is introduced, where r_h is the theoretical cut-off radius (see 2.5) and r_c is the cathode radius. The thickness of the main beam $r_h/r_c - 1$ is to be compared with the box-openings r_0/r_c

Scale:

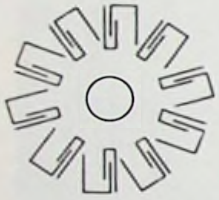
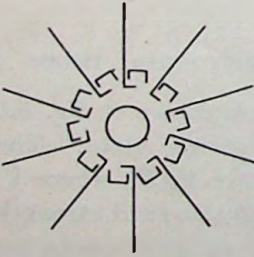
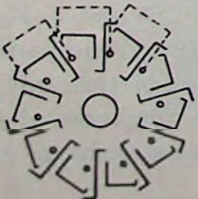

		DATA	
		Mechanical (Dimensions in mm)	Electrical (MKSA-units)
	a U5	$r_c = 1,65$ $b = 20$ $r_s/r_c = 1,52$ $r_o/r_c = 0,79$	No cut-off
	b U6	$r_c = 1,65$ $b = 2,0$ $r_s/r_c = 2,42$ $r_o/r_c = 0,97$	$\frac{V_s}{B^2} = 8,9 \cdot 10^4$ $P = 11,2 \cdot 10^{-6}$ $S_I = 3,44 \cdot 10^{-6}$ $S_{II} = 5,15 \cdot 10^{-6}$ $r_h/r_c = 1,25$
	c U10	$r_c = 1,65$ $b = 20$ $r_s/r_c = 1,70$ $r_o/r_c = 0,50$	$\frac{V_s}{B^2} = 3,2 \cdot 10^4$ $P = 20,0 \cdot 10^{-6}$ $S_I = 14,5 \cdot 10^{-6}$ $S_{II} = 30,0 \cdot 10^{-6}$ $r_h/r_c = 1,15$
	d U17	$r_c = 1,25$ $b = 25$ $r_s/r_c = 2,40$ $r_o/r_c = 0,80$	$\frac{V_s}{B^2} = 7,6 \cdot 10^4$ $P = 30,2 \cdot 10^{-6}$ $S_I = 100 \cdot 10^{-6}$ $S_{II} = 280 \cdot 10^{-6}$ $r_h/r_c = 1,45$
	e U20	$r_c = 1,50$ $b = 30$ $r_s/r_c = 2,00$ $r_o/r_c = 0,73$	$\frac{V_s}{B^2} = 6,5 \cdot 10^4$ $P = 40,3 \cdot 10^{-6}$ $S_I = 94,5 \cdot 10^{-6}$ $S_{II} = 375 \cdot 10^{-6}$ $r_h/r_c = 1,35$
	f U25	$r_c = 1,25$ $b = 25$ $r_s/r_c = 2,40$ $r_o/r_c = 1,00$	$\frac{V_s}{B^2} = 5,0 \cdot 10^4$ $P = 23,5 \cdot 10^{-6}$ $S_{II} = 167 \cdot 10^{-6}$

Fig. 5.5. Crosssections and main data of the experimental tubes described in text.

and the distance between the spades and the cathode $r_s/r_c - 1$. The former comparison in particular will give an idea of how much the beam is enlarged above its theoretical thickness. The extension of the electrode system in the direction of the magnetic field is given by b .

Of the examples shown, the U 5, U 6 and U 10 types are of early tentative design, U 17 and U 20 are advanced medium size cathode types and U 25 is an «auxiliary»-spade tube.

The U 5 type.

The U 5 type is included only to show a tube which does not operate due to lack of magnetic cut-off. The inhomogeneities of the electric field are enlarged by the space charge to such an extent that electrons diffuse to the boxes far above the theoretical cut-off condition (see 4.5).

The U 6 type.

The U 6 tube has a sharp magnetic cut-off. The uppermost oscillogram picture of fig. 5.6 shows the cathode current cut-off curves (see 4.5) at the magnetic field strengths 113, 125, 150, 200 and 250 gauss. All spades are connected together and the voltage varied from -30 to $+30$ volts. The cathode current along the vertical axis corresponds to $10 \mu\text{A}$ for one large division. The small humps on the curves just below the cut-off voltage are probably due to oscillations.

As seen from the spade characteristic records the U 6 tube is disposed to leak current. The fourth picture in fig. 5.6 shows the spade characteristics I and II at the magnetic field 113 gauss and the standard spade voltage 20 volts. (Current scale $0,2 \text{ mA/div.}$). Characteristic II, the larger one, decreases only slowly toward the $+20$ volts point. On such a characteristic it is impossible to find a stable upper locking point (point A in fig. 1.7) for a spade resistor. If the magnetic field is increased to 150 gauss the characteristic of the fifth picture in fig. 5.6 is obtained. Here the «tail» of characteristic II has disappeared, giving a stable operating point at the positive supply voltage but the height of characteristic I is substantially lowered. To get a stable locked-down position a very large spade resistor must be used.

The beam guiding action of the spades is shown by the deflection characteristics (see 4.6) in the second and third picture of fig. 5.6. The second picture shows the cathode current *versus* the voltage of one spade all other spades being at +20 V. The higher curve is valid for 113 gauss and the lower one for 150 gauss. (The current scale is 0,4 mA/div.). It is observed, especially on the curve for the stronger magnetic field, that the spade deflects the beam completely only when it is negative with respect to the cathode. The third

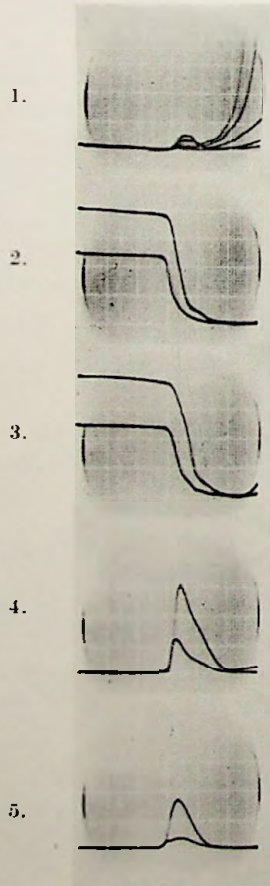


Fig. 5.6.

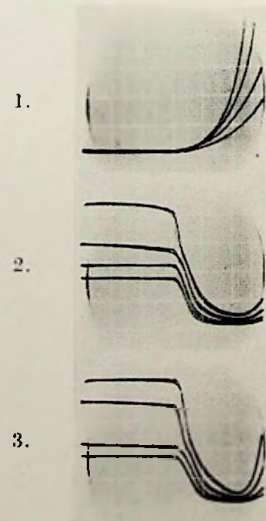


Fig. 5.7.

Fig. 5.6. Cut-off, deflection and spade characteristics of U 6.

Fig. 5.7. Cut-off and deflection characteristics of U 10.

picture shows the same curves when the voltage of two adjacent spades is varied simultaneously. Here the cathode current remains almost constant from zero voltage downwards.

The U 10 type.

To overcome the difficulties offered by the lack of cut-off in U 5 and the large leak currents in U 6 the U 10 tube was constructed. Here the spades are bent tangentially to the cathode to minimize the wave shaped nonhomogeneities of the electric field.

Due to the sharp spade edges the strength of the electric field is low in the major part of box openings. This reduces the tendency for the leak electrons to be pulled to the positive spade when the beam is guided to a box. The tube was intended to be run with the main beam going counter clock-wise in fig. 5.5 c, but at slightly increased magnetic field operation is possible in the reverse direction too.

The magnetic cut-off is not very sharp as seen from the top picture of fig. 5.7. The curves are the cathode current in a scale of 100 $\mu\text{A}/\text{div.}$ at the magnetic fields 225, 250, 300 and 375 gauss. The deflection characteristics at the same magnetic fields are shown, in the second picture for a single spade and in the third for two adjacent spades. (Current scale 0,5 mA/div.)

As observed the current curves become horizontal at zero potential even for a single spade at the strongest magnetic field indicating a great electrostatic penetration power to the cathode of the individual spades.

The U 10 type is a large cathode tube, however, and the main beam has a long way to go from the emitting to the deflecting region. Consequently the beam will degenerate. The beam degeneration effect is shown by two series of spade characteristics in fig. 5.8, series *a* for 250 gauss and *b* for 300 gauss. The current scale is 0,2 mA/div. in both cases. The series are obtained by shortening the beam in the manner explained in 4.7. On the full beam length characteristics of the top pictures large N-current portions are observed.

At the weaker magnetic field the N-current disappears in the fourth picture, where the beam extends below five positive spades. At the stronger magnetic field some N-current exists even in the sixth picture where only three spades are positive in front of the box receiving the current. The magnetic field cannot be reduced below

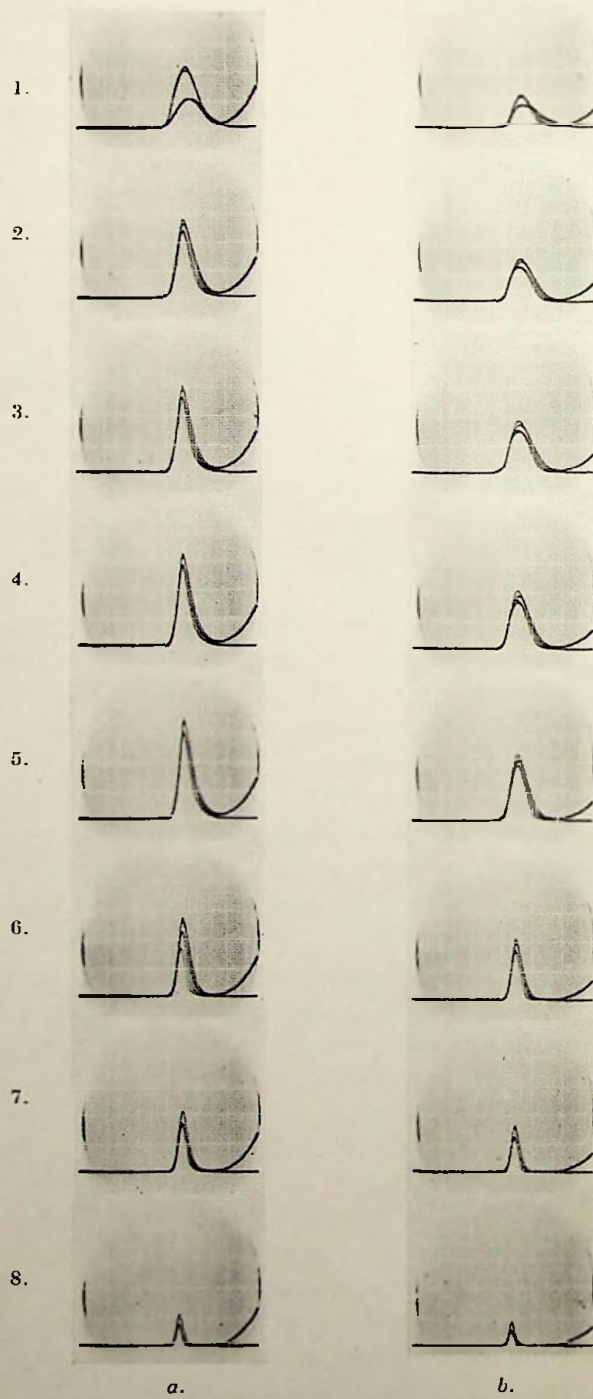


Fig. 5.8. Spade characteristics of U 10 at different beam lengths; *a.* magnetic field 250 gauss, *b.* 300 gauss.

250 gauss at 20 volts spade voltage since then the leak current would become too large owing to the quite narrow box openings. The narrow box openings cause the rising part of characteristic II above 20 volts. If the box openings were made wider, however, the magnetic cut-off would be destroyed as in the U 5 type.

Obviously nothing is gained by going to still larger relative cathode diameters. Experiments by ROMELL on this subject using a large scale model show only increased degeneration and lowered spade characteristics.

The U 17 type.

The U 17 type is a step in the opposite direction. Here the r_s/r_c ratio is increased to 2.40. This is about the same as that in U 6 but in U 17 the thin spade edges of U 10 are used. The U 17-tube can be operated in a much weaker magnetic field than U 6 without disturbing leak currents. Consequently the perveance will be higher and the degeneration lower.

The characteristics of U 17 are shown in fig. 5.9. The top picture shows the cut-off curves at 150, 162, 175 and 200 gauss in a scale of 10 μ A/div. (see also fig. 4.5). The second picture shows the deflection characteristics for a single spade at the same magnetic fields and the standard acceleration potential 20 volts. (Current scale 1 mA/div.) The third picture shows the same deflection characteristics for two spades. The four following pictures are the spade characteristics I and II for the magnetic fields listed above. (Current scale 0,5 mA/div.).

A very characteristic property of U 17 is the sudden formation of a space charge barrier. This occurs when a spade reaches about +5 volts with respect to the cathode. The formation of the barrier can be detected from the steep rise of the deflection characteristic or from the lowering of the noise level, but is most easily observed from the peak of characteristic I, as explained in 4.7.

The leak currents are very low as shown by the leak current oscillograms of fig. 5.10. These characteristics are recorded in the manner described in 4.9. Proceeding downwards the first and the second pictures in fig. 5.10 are the leak current characteristics for 162 and 175 gauss obtained with the main beam running in a counter clockwise direction when viewed as the electrode system in fig. 5.5. d.

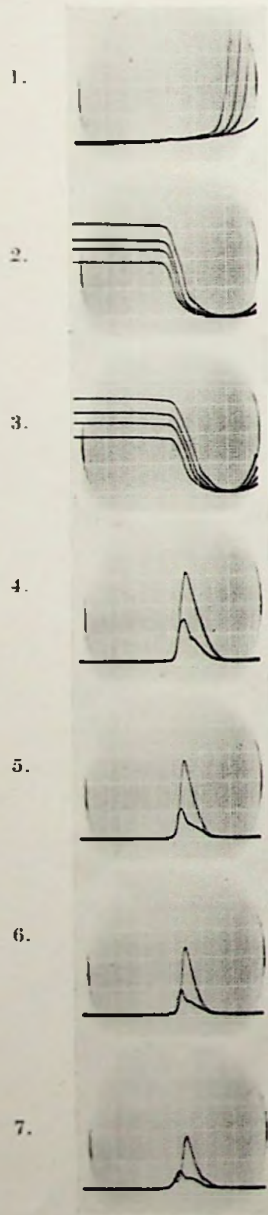


Fig. 5.9.

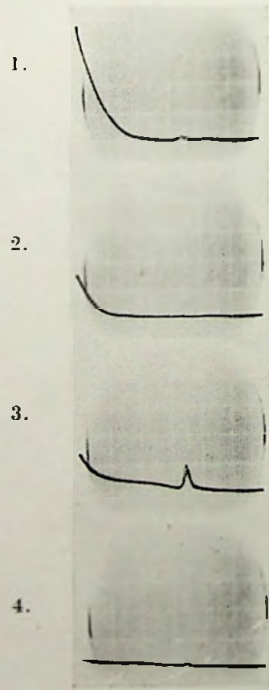


Fig. 5.10.

Fig. 5.9. Cut-off, deflection and spade characteristics of U 17.

Fig. 5.10. Leak current characteristics of U 17.

The third and fourth pictures are the leak currents at the same magnetic fields but with the direction of rotation of the beam reversed. In this latter case the leak current is greater, and especially the oscillation peak appearing just above zero is increased, but it is not large enough to jeopardize the proper operation of the tube. Thus, like U 10, the U 17 tube can step in either direction.

The U 20 type.

The U 17-type has a very low noise level, the lowest of the experimental tubes built during this development work. Because of the large r_s/r_c -ratio, however, the perveance of the tube is not very high. In an attempt to get a tube of still lower internal impedance the r_s/r_c -ratio is decreased to 2 in the U 20 type.

As the beam can be rotated in the »reverse» direction without serious leak current in the U 10 and U 17 types, it was concluded that the precise form of the spades plays only a minor rôle for the performance. To simplify the electrode construction, the spades in U 20 were then made plane radially directed sheets with right-angle bent flanges tangential to the cathode. The details of the electrode system can be studied from the photograph in fig. 5.3.

The main characteristics of the tube type are shown by the oscillograms of fig. 5.11. The cut-off curves in the top picture are for the magnetic fields 150, 175 and 200 gauss. The current scale is $100 \mu\text{A}/\text{div}$. In the second picture the spade characteristics at 175 gauss are shown in a scale of $0,5 \text{ mA}/\text{div}$.

As the cathode is quite large, the degeneration is not negligible, which can be observed from the N-current on especially characteristic I.

The characteristics of the third picture (in the same current scale) are obtained at the same voltages and magnetic field, but with the electron emission temperature limited. By lowering the cathode temperature the beam current is reduced from its full value 3,6 mA to 2,4 mA. Under these circumstances the emission distribution and the structure of the beam is altered as explained in 4.8. A degeneration reducing effect is clearly observable when comparing the two spade characteristic displays of fig. 5.11. The remarkable influence of temperature limitation on the discharge mechanism forms the basis for a cathode construction described in a section below (5.5).

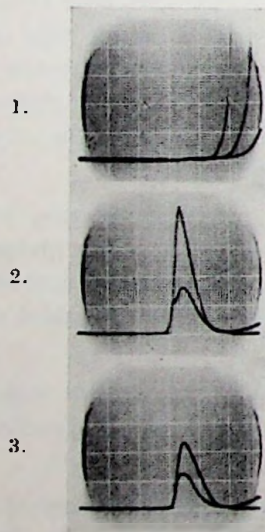


Fig. 5.11.

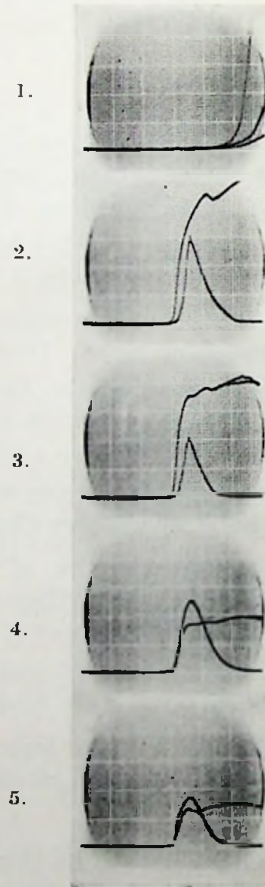


Fig. 5.12.

Fig. 5.11. Cut-off and spade characteristics of U 20.

Fig. 5.12. Cut-off and spade characteristics of U 25.

The U 25 type.

The U 25 type finally is included in this collection to show an embodiment of the «auxiliary» spade trochotron described in 2.6. The tube is constructed as a «reverse» U 17-tube with the right angle bent spades of U 20. Compared with the original U 17 the U 25 type requires a somewhat stronger magnetic field and consequently the perveance is lower. A wire 0,5 mm in diameter, constitutes an auxiliary spade in each box. Every auxiliary spade is to be connected to the spade behind its own box as indicated by dashed lines in fig. 5.5 f.

The characteristics of the auxiliary spade tube are shown in fig. 5.12. The top picture is the cut-off curves at the magnetic fields 150, 175 and 200 gauss in a scale of 100 μ A/div. In the following pictures the current scale is altered to 0,5 mA/div. The second and the third pictures show a spade characteristic and the auxiliary spade characteristic of the same box at 175 and 200 gauss respectively. The auxiliary spade characteristics show that such an electrode will lock its associated spade to about +2 or +3 volts with respect to the cathode. According to this the characteristics of the fourth and fifth pictures are recorded at the same magnetic fields (175 and 200 gauss) with the preceding spade at +3 volts.

5.4. Design of the boxes and influence of the plate voltage

As explained in chapt. 2 the discharge space between the cathode and the spades mainly determines the characteristics and the performance of the tubes. But the design of the boxes and the electrodes between the spades is far from being unimportant. An example of this is given by comparing the U 6 and the U 17 tubes. These tubes have about equivalent discharge spaces. They have about the same cut-off characteristics and beam currents when compared at corresponding magnetic fields. However, U 6 can never be operated at the favorable weak magnetic fields of U 17 due to large leak currents. The difference between U 6 and U 17 lies in the form of the box openings.

Apart from the box-openings the form and size of the box and the electrodes located therein have an important influence on the characteristics. It must be remembered that even after the deflection the beam is a trochoidal beam subject to the same laws as the main beam. It thus moves perpendicular to the electric field, disperses and degenerates in the same manner as in the discharge space.

As mentioned in chapt. 1 the spade characteristics are the result of the collection of electrons from a trochoidal beam by an electrode having about the same potential as the beam itself. Electrons having energies corresponding to the spade voltage or higher contribute to the spade current. Now, when the beam is guided to a box, the degeneration continues within the box generating more electrons having increased energy. With a certain probability, depending on the conditions, these electrons will be collected by the spade. Thus, the deeper the box and the greater the degeneration occurring within the box, the higher the spade characteristic will be. But, according to the general character of the degeneration, this increase in height is commonly accompanied by a still greater increase in voltage width, reducing the steepness.

In the experimental tubes, described in the foregoing section the plate voltage has a considerable influence on the spade characteristics. The boxes are of relatively little depth and the plates have flanges covering a large part of the spade area. Thus the plate voltage dominates the electric field within the boxes and acts upon the current distribution between spade and plate. This is illustrated in fig. 5.13 by two series of spade characteristics (scale 0,4 mA/div.) for an U 17 tube. Series *a* contains the first order characteristics and *b* the second order. The characteristics are recorded for different plate voltages: +30, +20, +10, 0 and -10 volts. At 30 volts in the top pictures the plate pulls a large part of the current away from the spade, diminishing the characteristic. At reduced plate voltage (the second pictures are for the tacitly assumed normal 20 volts plate voltage recorded in fig. 5.9) the characteristic grows higher until a maximum is reached after which it decreases again. In some cases it vanishes completely. The decrease is partly due to the fact that the low plate voltage deflects the beam away from the inside of the spade, but in the present case this effect is strongly influenced by the sudden formation of a space charge barrier within the box. This becomes evident when the beam is locked to the preceding box and the characteristics II recorded (series *b*). When the plate is at zero voltage or negative (fourth and fifth picture) the characteristics exhibit a sharp discontinuity. As soon as the spade voltage is sufficiently low to shift the beam into the box the current to the spade ceases. The effect is relatively independent of the strength of the magnetic field.

A problem of great technical interest is to make the boxes »electron

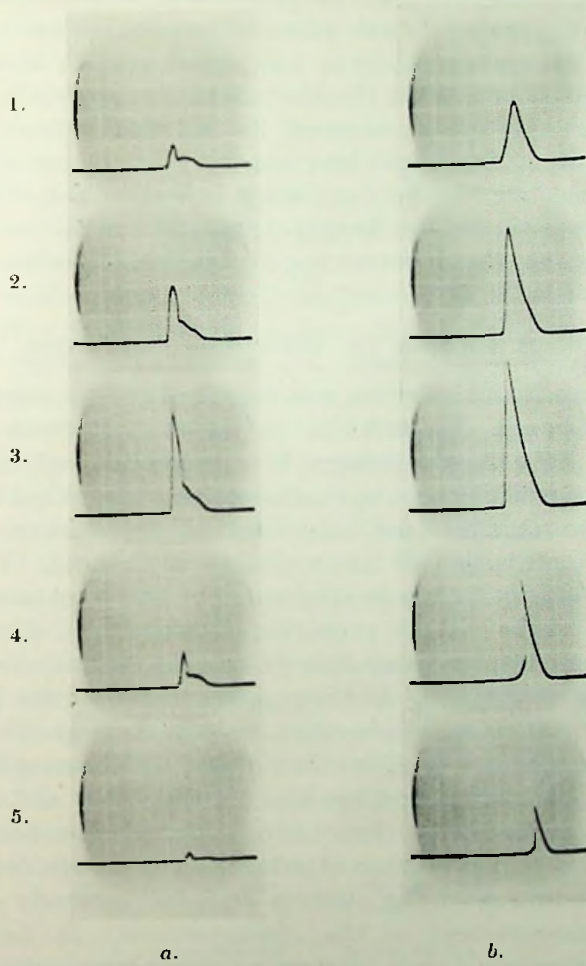


Fig. 5.13. Spade characteristics I (a) and II (b) of U 17 at different plate voltages.

tight». Electrons diverted to a box must not leak out to the outside of the electrode system causing stray currents. In the experimental tubes the electrons are simply stopped by mica sheets (see *e. g.* fig. 5.1). But from a technical point of view this is a bad solution. The micas increase the inter-electrode capacitances and reduce the power ratings. At high voltages (above 100 volts) surface charges and secondary emission can affect the characteristics, especially the leak currents, in an unpredictable manner. In technical tube designs the electrons thus are to be caught by means of slits not containing any insulator. The conditions for completely collecting the electrons in such slits are investigated by NETTELBLADT and several designs have been developed at the laboratories of Telefonaktiebolaget L. M. Ericsson.

5.5. A cathode for distributed emission

In 2.3 the emission distribution was described and the experimental evidence given in 4.4. The fact that only part of the cathode emits electrons may have its advantages but as pointed out in 2.3 the proximity of the emitting area to the deflection region is not desirable.

If the emission is temperature limited instead of space charge limited, however, the distribution of the emission is changed. The main beam does not emerge from a lumped area but builds up successively, the major part of the cathode supplying electrons to it. If the beam reaches full space charge saturation before the deflection the total beam current is unchanged. At temperature limitation the feed-back generating oscillations will be broken and the average transit time of the electrons decreased. The effect of the temperature limitation upon the leak current is considered in 4.8 (fig. 4.12) and upon the spade characteristics in 5.3 (fig. 5.11). Although the beam has a tendency to grow higher because of reduced space charge density, the temperature limitation of the electron emission generally creates a considerable improvement of the characteristics. In fact, many experimental tubes could only be operated under temperature limited conditions.

However, temperature limitation of the electron emission is an impractical solution. Several suggestions to achieve the desirable emission distribution by other methods have been tried. Most of these are based on the idea of a helical emission area. Electron emission is allowed only from a helical lamination going one or two turns around the cathode. Only very few electrons would then

originate at a point adjacent to the deflection region, most of the emitting helix being widely separated from the deflecting spade. In practice however, owing to the space charge, axial components of the electric field are set up in the vicinity of the helix. The electrons emitted near the borders acquire an axial component of velocity and are less accelerated perpendicular to the magnetic field than those originating at the middle of the emitting ribbon. The result is a great dispersion of the beam, and although the tubes are nonoscillating, no usable characteristics have been obtained.

A better result has been achieved by winding a non-emitting wire around the cathode. The arrangement is shown diagrammatically in fig. 5.14. The wire is wound on the emitting oxide coating and in direct metallic contact with the cathode. The wire reduces considerably the electric field strength above the emitting surface. Between the wire windings the emission is space charge limited, but in the strong electric field above the wire the space charge density is much diluted. Strictly speaking, the current from the cathode does not follow the Langmuir three-half power law because the thermal velocities of the electrons greatly influence the emission mechanism in the spacings between the wire windings. But for the present purpose this effect is of minor importance. As in the temperature limited case the main beam builds up around a large part of the circumference of the cathode.

The arrangement is tried by winding a nickel wire, 0,2 mm diameter, with 0,4 mm free space between the turns on the cathode of an U 25 electrode system. The characteristics of this new tube type, designated U 27, are then compared to those of an ordinary U 25 tube. In both electrode systems the auxiliary spades are omitted and the tubes are run in the «forward» direction (see. 5.3.).

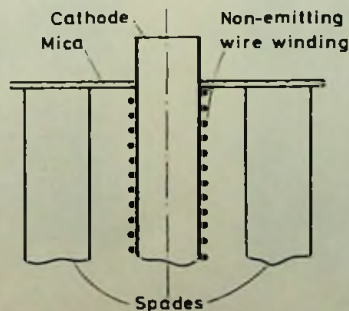


Fig. 5.14. Wire wound cathode.

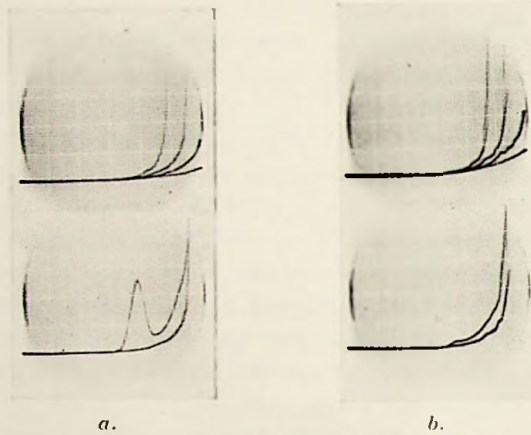


Fig. 5.15. Cut-off characteristics of *a.* U 25, *b.* U 27.

The cut-off characteristics are shown in fig. 5.15 *a* and *b*. The curves in *a* belong to the U 25 type and those in *b* to U 27. In the top pictures the characteristics are recorded for the magnetic fields 150, 175, 200 and 250 gauss, respectively, in a current scale of $10 \mu\text{A}/\text{div}$. The cut-off voltages are some 2 to 3 volts lower for U 27. The second pictures show the cut-off curves for 175 gauss with the magnetic field parallel to the cathode and with 1° inclination. The U 25 characteristic shows the hump of inclined field, mentioned in 4.5, but U 27 is without it.

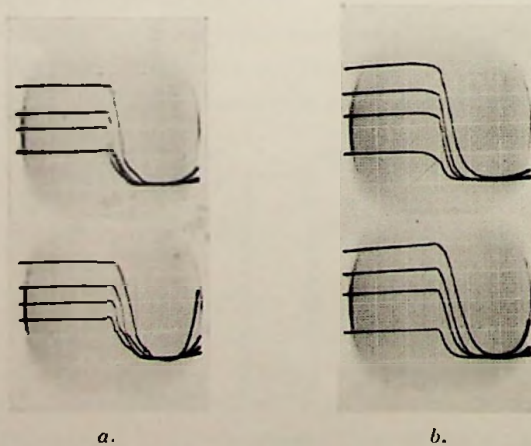


Fig. 5.16. Deflection characteristics of *a.* U 25, *b.* U 27.

Fig. 5.16 is the record of the deflection characteristics for a single and two adjacent spades at the same magnetic fields. The current scale is 1 mA/div. for U 25 (*a*) and 0,5 mA/div. for U 27 (*b*). As the beam current in U 27 is about 40 % lower than in U 25, the main beam in U 27 obviously does not become fully space charge saturated. From the deflection characteristics for a single spade in the top pictures one observes that a spade in U 25, aided by a space charge barrier, wholly deflects the beam at zero voltage. In U 27 a spade has to go down to between -3 and -5 volts for complete deflection.

The spade characteristics are compared in fig. 5.17, the series *a* being for U 25 and *b* for U 27. The records are, from the top downwards, the characteristics I and II for the magnetic field strengths 150, 175 and 200 gauss, respectively, all in a scale of 0,4 mA/div. The characteristics of U 27 are lower than the corresponding of U 25, but the decrease of the degeneration in U 27 is clearly observable. At 175 gauss for example, the characteristic I of U 25 has a large N-current tail and at 200 gauss both characteristics are much degenerated. In U 27 the *N*-current is negligible in all cases and the

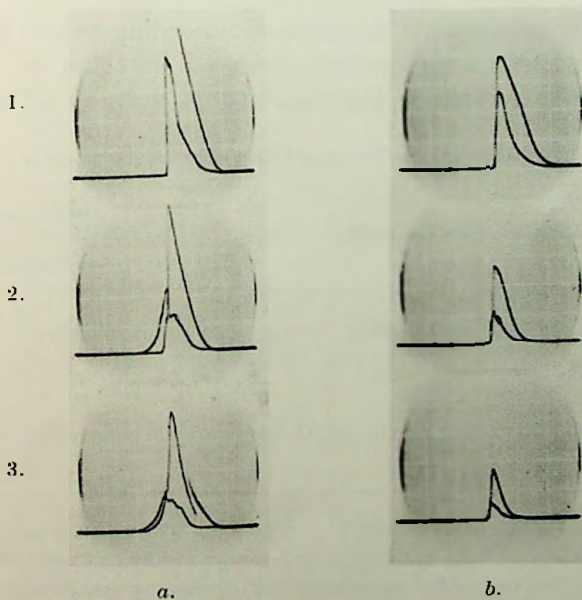


Fig. 5.17. Spade characteristics of *a*. U 25, *b*. U 27.

characteristics rise very steeply on their fronts just above zero voltage.¹⁾

The wire winding on the cathode of U 27 is quite coarse and a dispersion of the beam is probably present due to axial components of velocity of the electrons. A finer winding should possibly improve the characteristics making the slope toward the positive voltage steeper. As the degeneration obviously is depressed more than necessary, a larger cathode increasing the perveance seems to be of advantage. No such tubes have been built, however. Nothing further is known about the long-time reliability of the wire wound cathodes.

5.6. Theory and design

Although the electron stream in the main beam probably is not laminar, the theory developed in chapt. 3 gives approximately the correct result for the beam current. When calculating this current the most convenient way is to proceed as explained in 3.10: first the ratio r_h/r_c is determined from fig. 3.8, and with this ratio known, the current is obtained from fig. 3.9. Using the r_h/r_c ratio found from fig. 3.8 for trial in eq. (5.3) (given below) a better accuracy is obtained.

A couple of beam currents determined according to the theory are compared with the corresponding observed currents in table 5.1 below. The spade voltage is the standard 20 volts in all cases.

TABLE 5.1. Comparison of calculated and observed beam currents.

Tube	Magn.field	r_h/r_c	Beam current	
			Calc.	Obs.
U 6	113 gauss	1,55	1,75 mA	1,04 mA
	150	1,25	1,16	1,00
U 10	250	1,10	2,28	1,85
	300	1,10	1,50	1,10
U 17	102	1,45	2,88	2,70
U 20	175	1,35	3,80	3,60

¹⁾ The double trace of characteristic II for U 25 at 200 gauss is not readily explained. The tube is violently oscillating and jumps suddenly from one oscillation state to another. The jumps for increasing and decreasing spade voltages do not coincide and a hysteresis loop is obtained. The same effect is observed in some samples of U 17 at strong magnetic fields.

When estimating the beam currents the mechanical breadth of the electrode systems has been used. As end effects thus are not corrected for, possibly only two figures of the theoretical values are correct. The observed currents are throughout somewhat smaller than the calculated, but always of the right order of magnitude.

Maybe r_h , the beam height radius, does not have any physical significance but because the beam current can be calculated by means of it, it is used here to define the beam.

Using r_h different tube designs can be compared. If the «thickness» of the main beam, $r_h/r_c - 1$ is compared with the height of the discharge space, $r_s/r_c - 1$, in U 17 and U 20, the ratio is found to be about 1:3 in both cases. This leads to the assumption that the beam can fill a constant fraction of the discharge space despite different r_s/r_c ratios. At least in the medium size cathode range, $2 \leq r_s/r_c \leq 2,5$ this would be true.

If the fill fraction of the beam is denoted $1:n$, the ratios r_c/r_h and r_s/r_h can be expressed

$$\frac{r_c}{r_h} = \frac{n}{\frac{r_s}{r_c} + n - 1} \quad (5.1)$$

and

$$\frac{r_s}{r_h} = \frac{n}{1 + \frac{r_c}{r_s}(n - 1)} \quad (5.2)$$

Assuming circular electron paths (see 3.9) the potential distribution in the discharge space gives:

$$\frac{V_s}{B^2} \frac{1}{r_c^2} = \frac{e}{8m} \left(\frac{r_c}{r_h} \right)^2 \left[2 \left(1 - \frac{r_c^4}{r_h^4} \right) \ln \frac{r_s}{r_h} + \left(1 - \frac{r_c^2}{r_h^2} \right)^2 \right] \quad (5.3)$$

From the equations (3.27) and (5.3) an expression for the perveance is obtained:

$$P \frac{r_c}{b} = \varepsilon_0 \left(\frac{8e}{m} \right)^{1/2} \left(\frac{r_c}{r_h} \right)^3 \frac{\left[\frac{r_h^2}{r_c^2} - \frac{r_c^2}{r_h^2} - \frac{1}{2} \left(1 - \frac{r_c^4}{r_h^4} \right) - 2 \ln \frac{r_h}{r_c} \right]}{\left[2 \left(1 - \frac{r_c^4}{r_h^4} \right) \ln \frac{r_s}{r_h} + \left(1 - \frac{r_c^2}{r_h^2} \right)^2 \right]^{3/2}} \quad (5.4)$$

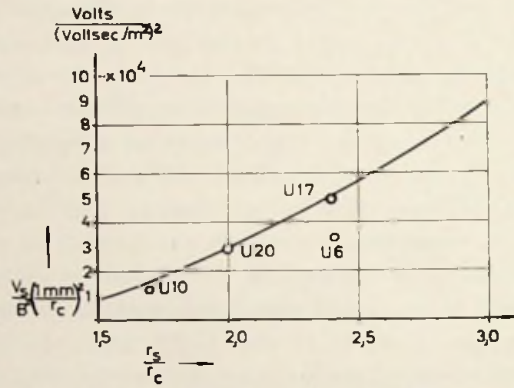


Fig. 5.18. Curve of V_s/B^2 as function of r_s/r_c for beam filling one third of the discharge space.

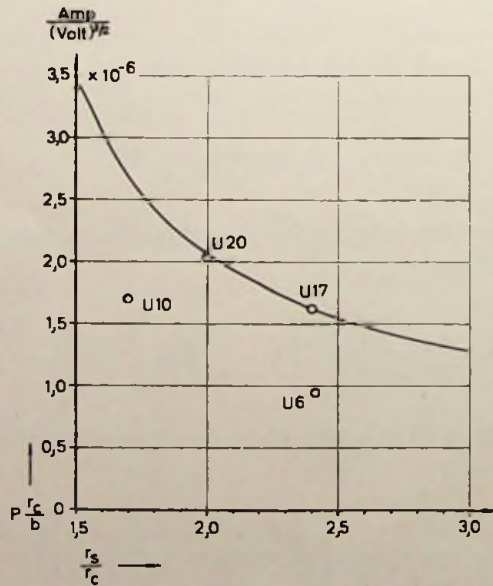


Fig. 5.19. The perveance as function of r_s/r_c for beam filling one third of the discharge space.

Substituting (5.1) and (5.2) into (5.3) the curve of fig. 5.18 is obtained for $n = 3$. The positions of the experimental tubes for their optimum working points are indicated by circles. In the same manner the curve in fig. 5.19 is obtained from eq. (5.4). As the U 17 and U 20 types are the best tubes developed during this work the curves in fig. 5.18 and 5.19 can be regarded as characteristics for good tubes.

There is nothing however, which claims improvements being impossible. The limiting factor is of course the leak current. Any arrangement protecting the following spade from leak current would push a tube, now being in the vicinity of U 17, well above the curves. U 10 is below the curves apparently because of great degeneration in its long beam. If, however, the degeneration could be decreased *e. g.* by means of a wire wound cathode (5.5), possibly a tube having a higher perveance than U 20 could be constructed.

5.7. Discussion

Measurements of the potential distribution in a simple cylindrical cut-off magnetron by ENGBERT [1938] and by REVERDIN [1951] indicate a space charge density gradually falling off toward the anode. The abrupt cut-off predicted by the theory is never observed. Fig. 5.20 shows two space charge density curves (1) and (2) observed by REVERDIN, together with two theoretical distributions (3) according to assumption of circular electron paths and (4) according to a double stream state calculated by PAGE and ADAMS. (References are found in the paper by REVERDIN). A distribution according to (1) is found only under certain circumstances, *i. e.*

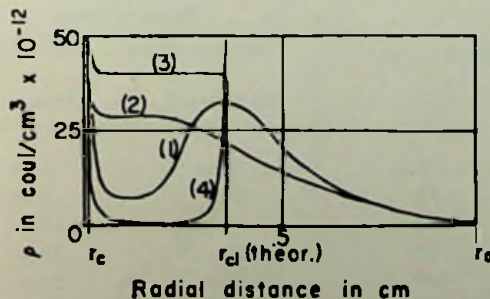


Fig. 5.20. Space charge distributions in cylindrical cut-off magnetron. (REVERDIN)

when the cathode is aligned very carefully co-axial with the anode and the emission near space charge limited, (2) being the »normal» state. The investigations by ENGBERT give a distribution similar to that of (2).

In these experiments the electrons can rotate many times around the cathode, the degeneration thus being much greater than in the trochotrons, where the beam is deflected to a box in less than one turn. Probably the space charge distribution in the trochotrons is more close to the theory than in the magnetrons. Investigations by NETTELBLADT on the space charge cloud above a plane cathode show, however, at least qualitatively, about the same space charge density distribution as that observed in the magnetrons.

With this knowledge of the diffuse character of the main beam the observed currents and those calculated according to the theory in chapt. 3 agree surprisingly well. It is not to be expected, however, that the agreement should be exact and the discrepancies in table 5.1 are merely due to experimental errors or to inaccurate determination of the conditions. NETTELBLADT has measured and calculated the ratio between the beam current for various beam heights and the space charge limited current without magnetic field. The trochotrons used had $r_s/r_c = 4,78$ ($r_c = 0,9$ mm, $b = 18$ mm). The results are listed in table 5.2 below. The beam height is expressed in percent of the discharge space height.

It is seen how the observed currents are smaller than the theoretical for low beams. When the beam grows higher the observed values

TABLE 5.2. Comparison of calculated and observed ratios of beam currents to radial space charge limited current. (NETTELBLADT)

Beam height	Beam current	
	Current without magn. field	
	Calculated	Observed
5 %	9,64 %	6,24 %
10	12,7	9,23
20	16,7	13,4
30	19,6	18,5
40	22,8	22,3
60	28,2	29,3
100	51,2	35,2

approach the calculated and at 60 % beam height the experimental beam current is the larger one. At 100 % beam height there is again a deficiency with respect to the theoretical value.

This result can be understood when assuming that at the beginning of the main beam, where the degeneration is low, about the right amount of current is obtained. From fig. 4.4 it is then seen how at strong magnetic fields a part of the current returns to the cathode, the observed current thus being smaller than the calculated. At weaker magnetic fields the cathode continues to emit beyond the original emitting area giving excess current. At 100 % beam height the cathode area is probably too small to establish a real main beam.

CHAPTER 6

DESIGN OF CIRCUITS

BY

J. BJÖRKMAN and L. LINDBERG¹⁾

This chapter is intended primarily for the circuit designer who wants to use trochotrons without penetrating into all the electronic phenomena occurring in the tubes. It may be read as a continuation of chapter 1. The trochotron as a counter will first be studied, since this is the most fundamental circuit. A trochotron capable of functioning as a counter will also be useful in most other applications, having less severe demands on the tube properties. The conditions for maximum reliability and for maximum counting speed are a little contradicting, and will be discussed in turn. Finally, some selfstepping and oscillating circuits are described.

6.1. Considerations for maximum reliability

The first demand on a counter is high reliability, *i. e.* it must function properly within as wide a range of operating conditions as possible.

The principles underlying the locking of the beam by spade resistors and stepping by negative voltage pulses on the plates is described in chapter I. The locking stability is set by the range within which the spade resistances can be chosen, giving proper operation. The lower limit of spade resistance is roughly proportional to the height of the first order spade characteristic, since the spade current must suffice well to keep the spade at a low voltage (the point C in fig. 1.7). The upper limit depends on the leak current to the next positive spade, which must remain at its positive supply voltage. More exactly it is determined by the shape of the second order spade

¹⁾ Sections 1—3 are written by LINDBERG, sections 4 and 5 by BJÖRKMAN.

characteristic, which must cross the load line near the supply voltage (the point A in fig. 1.7 *b*). As concerns the reliability, only the ratio between the highest and lowest value is of importance, and not the absolute value of spade resistance. Generally this ratio is increased for increased magnetic field strength, so it is preferable to operate well above cut-off and use relatively high spade resistances. Maximum reliability is then attained at some sacrifice in beam current and speed of response. Experiments have shown that the spade resistances should be chosen so, that the spade consumes 5 to 15 percent of the beam current.

In cylindrical trochotrons the switch-over time is very much shorter than that in the plane tubes, usually of the order of 0,1 μ s. In circuits using a multivibrator as driver, connected to the plates in push-pull, the plate voltage never rises as fast as it drops, and it may happen that the beam shifts over to the new box before the plate voltage there has risen sufficiently to prevent further stepping. This difficulty is easily overcome by increasing the plate voltage supply somewhat. The plate voltage swing should, however, extend down to the cathode voltage of the trochotron.

A cathode resistor, bridged by a small capacitor, increases the stability substantially and prevents the occurrence of two beams within the tube. It should be as great as possible preferably so that the voltage developed across it equals the cathode-spade voltage V_{sc} .

It must also be stressed that the spades are very sensitive to capacitive load, so that a high impedance probe of less than 1 or 2 pF input capacitance must be used when testing the circuits unless the operation of the trochotron will be disturbed. As the spade voltage waveform is of high amplitude, a capacitive voltage divider can be used when observing the spade voltage waveform on an oscilloscope having good amplification. A frequency-independent voltage divider as probe is still better, and it can be simply made in the following manner: A parallel circuit of about 1 pF and 20 M Ω is made by wrapping a piece of wire around a small 20 M Ω , 1/2 W resistor and connecting it to the screened test lead. The voltage divider is formed by this circuit and the input capacitance and resistance of the oscilloscope, which are adjusted until the the time constant is equal to that of the probe, by observation of a true square wave signal.

Scales designed and operated under these precautions are dependable and non-critical on magnetic field and supply voltage. For

one of the best cylindrical trochotrons, designed according to fig 5.5 *d* (U 17) tested at a moderate pulse frequency, 10 kc/s, with spade resistors of 100 k Ω and a cathode resistor of 10 k Ω , the following range of operation was obtained:

$$B = 135 - 170 - 290 \text{ gauss}$$

$$V_{sc} = 18,5 - 20 - 26 \text{ volts}$$

$$I_e = 1,85 - 1,70 - 1,15 \text{ mA}$$

$$\alpha = 0,10 - 0,12 - 0,23$$

α is the fraction of the beam current consumed by the spades. The figures in the middle are design values whilst the other figures are the limits obtained at maximum and minimum magnetic field, respectively. All supply voltages were kept constant during the experiment.

6.2. Considerations for maximum speed

High speed of response is favored by tubes having a high ratio of current-to-voltage, K^1). Trochotrons, especially of the cylindrical type, are therefore capable of very fast operation.

It is worth while to distinguish between high resolution power for pulses occurring at random, and capability of counting pulses at high constant frequency. Disregarding the driving circuits, the limitations inherent in the trochotron are set by the times required for discharging and charging of the spade-to-earth capacitances when the spade voltages fall and rise. Because the spade resistances must be relatively great to insure dependable operation, the spade voltages always drop much more rapidly than they rise when the beam has left a spade. The resolution time is set only by the fall time or switch-over time for a spade whilst the upper limit for constant frequency stepping is usually limited by the smallest cycling time of the circuit, which depends only on the rise time for the spades.

The switching time can be estimated approximately from the stepping characteristic, fig. 6.1 (earlier explained in 1.6). We assume that the beam initially is locked in a box and that the plate voltage in that box suddenly is decreased to zero. Then almost the whole beam current, I_{st} , is shifted to the next positive spade and goes mainly to discharge its earth capacitance, when its voltage falls.

¹⁾ The terms conductance or conductivity are avoided because they commonly are used for derivatives.

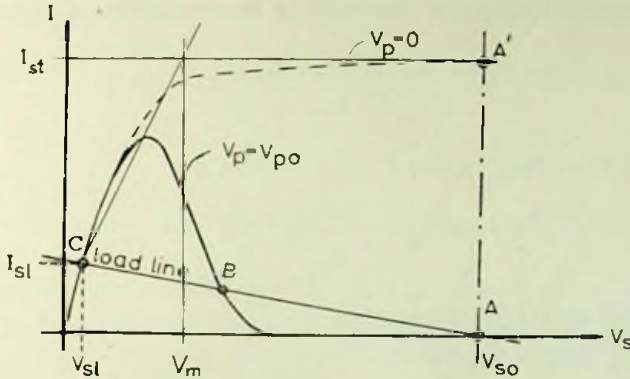


Fig. 6.1. Locking and stepping characteristics.

In the diagram this means that the characteristic of that spade is changed from the solid curve to the dashed curve and the operating point from A to A'. The dashed characteristic can be approximated with two straight lines implying a constant current to the spade from V_{so} down to a voltage V_m and then a linearly decreasing current down to the locking point C. The slope of the latter line is denoted by $1/r$. The discharging of the spade capacitance is thus divided into two phases. During the first phase, almost the whole current goes to the capacitance and the time to reach V_m is

$$t_{f1} = \frac{C \cdot (V_{so} - V_m)}{I_{st}} \quad (6.1)$$

where C is the total earth capacitance of the spade, including wiring capacitance.

During the second phase, the exponential decrease is pronounced, and the voltage approaches the final locking value according to

$$V - V_{sl} = (V_m - V_{sl}) \cdot e^{-\frac{t \cdot (r + R)}{r \cdot R \cdot C}} \quad (6.2)$$

As $R \gg r$ the time constant can be set to $r \cdot C$. The spade voltage is safely within the locking region of the characteristic for $t_{f2} = 2rC$, which can be regarded as the time for the second phase.

The total fall time t_f , is the sum of the times for the two phases:

$$t_f = \frac{C \cdot (V_{so} - V_m)}{I_{st}} + 2rC \quad (6.3)$$

If the current-voltage ratio

$$K = \frac{I_c}{V_{so}} \approx \frac{I_{st}}{V_{so}} \quad (6.4)$$

is introduced and V_m set equal to $\beta \cdot V_{so}$

then
$$r = \frac{\beta}{K}$$

and
$$t_f = C \cdot \frac{1 - \beta}{K} + C \cdot \frac{2\beta}{K}$$

$$t_f = (1 + \beta) \cdot \frac{C}{K} \quad (6.5)$$

β is about 0,25 and C of the order 5 pF both for plane and cylindrical trochotrons but K varies, being about $5 \cdot 10^{-6} \Omega^{-1}$ for plane tubes of early design, and $10^{-4} \Omega^{-1}$ for cylindrical tubes. The switching times become:

$$t_f = 1,25 \mu\text{s} \text{ for early plane tubes}$$

$$t_f = 0,06 \mu\text{s} \text{ for cylindrical tubes}$$

In reality the switching time becomes longer than these figures indicate, at least in the latter case, since it takes some time to decrease the plate voltages. $0,1 \mu\text{s}$ seems to be a reasonable limit for the resolution power of a cylindrical trochotron.

If the upper limit for constant frequency operation were set only by the switching time, it would consequently be 800 kc/s and 10 Mc/s for the early plane tubes and cylindrical tubes, respectively. However, these limits will be set lower when the cycling time is considered below. When the beam leaves a box, the current to the spade is interrupted and the spade voltage returns to the supply value exponentially with the time constant RC . The rise time can be set to

$$t_r = \gamma \cdot RC \quad \gamma = 1 - 5 \quad (6.7)$$

Since the spade resistance R is chosen so that a spade takes only a fraction $I_{st} = \alpha I_e$ of the beam current when locking, $R = \frac{1}{\alpha K}$

and

$$t_r = \frac{\gamma}{\alpha} \cdot \frac{C}{K} \quad (6.8)$$

As $\alpha = 0,05 - 0,2$, the rise time is always much longer than the fall time.

In plane trochotrons the cycling time is limited by the rise time of the last spade which can be estimated by setting $\gamma = 1$ and $\alpha = 0,2$, giving $t_r = 5 \mu s$. When a great anode resistance is used for resetting the beam the emission is also greatly reduced after re-set due to the low anode voltage and the fall time for the first spades becomes considerably increased. The theoretical upper limit for continuous stepping is thereby set about 200 kc/s when push-pull coupled plates are used, and about 50 kc/s when the plates are RC-coupled and pulsed, since the interval between pulses must be some 3-4 times the pulse duration. By using suitable means to reduce the rise time of the last spade and other re-setting methods, higher frequencies can be achieved.

In cylindrical trochotrons stepping at a high constant frequency, it may happen that the spades due to the long rise time do not return to the supply voltage sufficiently rapidly, so the emission cannot take place from the most distant part of the cathode as usual. The regulating mechanism of the space charge will, however, keep the emission unchanged still if only a few spades have returned to full voltage, the only and harmless effect being that the beam is shortened and that the tube operates on characteristics of higher order. It is sufficient that two or three spades have returned to full voltage in the cycling time, but full voltage now means within a few percent of the supply voltage, because the emission varies rapidly with the spade voltage when the magnetic field is constant. γ in eq. (6.8) must therefore be set to 4 or more, and the cycling time must exceed

$$t_r = \frac{4}{\alpha} \cdot \frac{C}{K} \quad (6.9)$$

For maximum reliability α should not exceed 0,1 and for the values $C = 5 \text{ pF}$, $K = 10^{-4} \Omega^{-1}$ ($R = 100 \text{ k}\Omega$), $t_r = 2 \mu s$. With some sacrifice of stability against changes in operating conditions the

spade resistances can be decreased to $50 \text{ k}\Omega$ ($\alpha = 0,2$) and then $t_r = 1 \mu\text{s}$ allowing the stepping frequency of 10 Mc/s to be reached. In such a design both fall time and rise time give the same limit, and the limit becomes rather sharp. The extent to which the spade resistances can be reduced or to be more exact, α increased, depends on the steepness of the first order spade characteristics which thus is a figure of merit for high cycling speed. Too small spade resistances may cause difficulties in several ways, as will be discussed in the next section, and it must be stressed that the resolution power is not favored by small spade resistances.

High current to voltage ratio is consequently favorable to fast operation, and it depends, besides on the design of the tube, on the choice of operating point, and on the voltage level of operation. Near cut-off this ratio is highest, and if all operating data are changed according to the similarity principle, the ratio increases in proportion to the square root of the voltage. Much speed cannot be gained in this way, however, since the power increases as $V^{5/2}$ and the tube becomes overloaded.

The fast driving waveforms on the plates required for high speed operation give rise to difficulties because they leak over to the spades capacitively, disturb the emission, and may cause erroneous stepping. Direct pulsing of all plates with sharp negative pulses must therefore be abandoned, since the main part of the spade-to-earth capacitance goes via the plates. When push-pull voltages are applied to the plate groups, the capacitive pulses can be balanced to a great extent, provided the partial capacitances of every spade are equal to both plate groups and that the plate voltages rise as fast as they fall.

Some experiments on high speed constant frequency counting have been made using sine wave voltages on the plates. The tubes tested were of the design shown in fig. 5.5 *f* (U 25 without the auxiliary spades). The oscillograms of fig. 6.2 show the voltages of a spade and one of the plate groups at a stepping frequency of 5 Mc/s . The operating data were:

$$\begin{aligned} V_{eo} &= 40 \text{ volts} \\ V_p &= 30 \text{ volts dc} + 30 \text{ volts ac amplitude} \\ R_s &= 50 \text{ k}\Omega \ (\alpha = 0,14) \\ B &= 210 - 270 \text{ gauss} \\ I_e &= 6,9 - 5,7 \text{ mA} \\ t_r &= 1,5 \mu\text{s} \end{aligned}$$

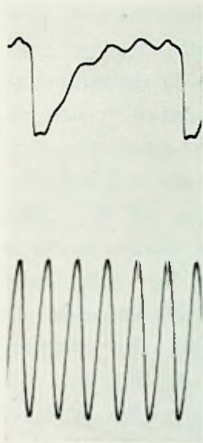


Fig. 6.2.

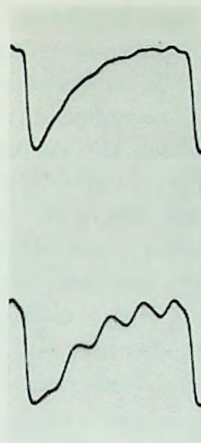


Fig. 6.3.

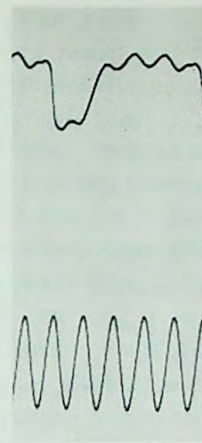


Fig. 6.4.

Fig. 6.2. Spade and plate voltage oscillograms at 5 Mc/s stepping frequency.

Fig. 6.3. Spade voltage oscillograms at 9 Mc/s.

Fig. 6.4. Spade and plate voltage oscillograms at 5 Mc/s for tube with built-in spade resistors.

The frequency could be increased to 9 Mc/s if a very large cathode resistance was used to stabilize the emission and fig. 6.3 refers to that frequency, the upper picture showing the voltage of a spade with balanced capacitances, the lower that of another spade with disturbing leakage from the plates. In this tube the capacitances were rather great and a test of another tube with built-in spade resistors (fig. 5.4 *b*) showed much faster rise time at 5 Mc/s, fig. 6.4. Due to the auxiliary spades used in this tube a spade is locked down twice.

6.3. Some details of the stepping process

The first and second order spade characteristics only tell us whether or not the beam can be locked to a box, and for what values of spade resistance this is possible. The dynamic stepping process sets other, more restrictive limits on the spade-resistances. These things are earlier considered for plane trochotrons [ALFVÉN *et al.* 1948, p. 43–50] and in principle the same discussion is valid also for cylindrical tubes. Here the results will be summed up briefly in connection with some actual characteristics.

To start with, we assume that the beam is locked to a box n , part of the beam going to s_n , keeping its voltage low, while the rest goes to p_n . When the voltage of p_n is decreased, current is deflected to s_{n+1} and its characteristic becomes higher at positive voltages, as evident from fig. 6.5 in which the pictures, counted from the top, correspond to $V_{pn} = 20, 15, 10, 0$ volts. The current scale is 1 mA/div. and the load line represents 100 k Ω . The decrease of V_{pn} also influences the characteristic of s_n , the height of which passes a maximum and finally becomes rather low, according to fig. 6.6, valid for $V_{pn} = 20, 10, 5, 0$ and $V_{sn+1} = 20$ volts. (Current scale 0,2 mA/div.). Furthermore, it shrinks still more when the voltage of s_{n+1} falls, as shown by fig. 6.7 measured for $V_{pn} = 0, V_{sn+1} = 20, 10$ and 5 volts, so it may happen that s_n returns to the positive

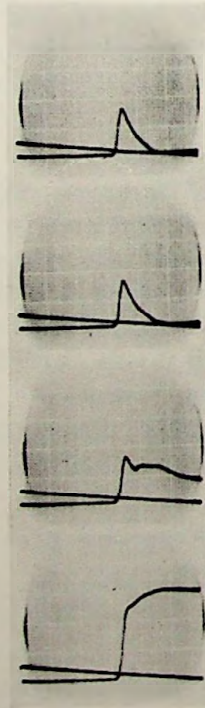


Fig. 6.5.

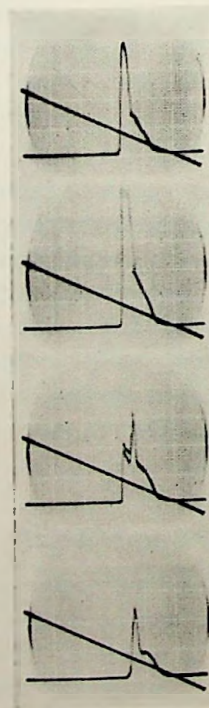


Fig. 6.6.

Fig. 6.5. Spade characteristic II at decreased voltage on the preceding plate.

Fig. 6.6. Spade characteristic I at decreased voltage on the corresponding plate.

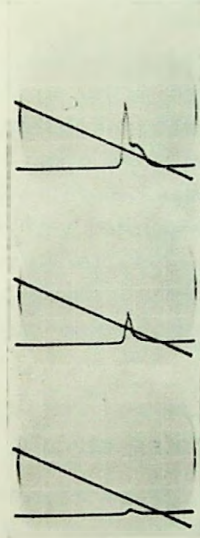


Fig. 6.7.

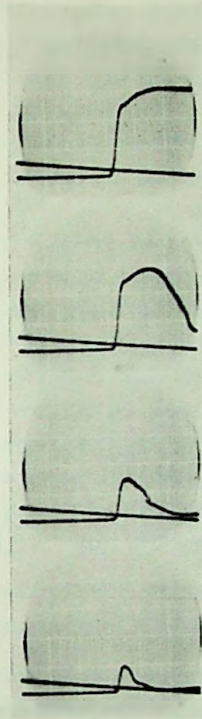


Fig. 6.8.

Fig. 6.7. Spade characteristic I for zero plate voltage and decreased voltage on the following spade.

Fig. 6.8. Characteristic of a spade for preceding plate at zero and increasing voltage of the preceding spade.

supply voltage before s_{n+1} has caught the beam. Then also a set of characteristics is needed for s_{n+1} when $V_{pn} = 0$ and $V_{sn} = 0 + 5, + 10, + 20$ volts, fig. 6.8 (current scale 1 mA/div.).

Consequently the dynamic stepping process is very complicated. The course depends greatly on the plate voltage waveform and the capacitances of the involved spades. The conditions are most unfavorable if the capacitance of s_{n+1} is enlarged and the spade resistances are small. The beam may then become diverted out of the box. In a plane trochotron, the beam then shifts to the first box, instead of stepping further, a fact which can be utilized for fast re-setting of the beam. A cylindrical tube goes cut-off when this

happens, but if the cathode resistance is great, the voltage over the tube increases and leak current to some spade may cause it to catch the beam again. In any case it will count erroneously. In the same way the great sensitivity to capacitive load on the spades is explained. This discussion is only intended to clarify the stepping mechanism, and the lower limit for spade resistances has to be found by experiments.

Another source of trouble encountered in cylindrical trochotrons when too small spade resistances are used, is due to the high locking voltage. If it is too high, the beam is not completely deflected, the degeneration becomes excessive, and the tubes operates in the range where noise and leak currents have peaks according to fig. 4.7 and 4.9. The high leak currents are also associated with the occurrence of discontinuities in the second order characteristic, mentioned in 5.5, fig. 5.17 *a*, which may cause erroneous operation. In tubes of bad design these effects may cause an instable range within the normal operating region.

6.4. Continuously stepping circuits

If the plate supply voltage is reduced below the stepping voltage the trochotron will become self-stepping. When the beam arrives to a box, current begins immediately to flow to the next spade, charging its capacitance and pulling its voltage down. Then the beam is shifted over to the next box and the same process repeated. The spades left behind the beam become currentless and rise in potential.

The process is illustrated in fig. 6.9, which gives an instantaneous picture of the state at a particular moment. On characteristics selected from fig. 6.7 and 6.8 small circles, denoted A, indicate the instantaneous voltage and current of a series of spades. The arrows indicate motion of the operating points. The spades are loaded by large resistors, some 100 k Ω , the supply voltage being 20 volts, and the plates are at zero voltage.

At the moment illustrated the spade s_n is at 10 volts and decreasing. The characteristic for s_n is that of the second picture in fig. 6.8., as the spade behind, s_{n-1} , is locked down to 5 volts, and the next spade, s_{n+1} , is at about 20 volts. The characteristic of s_{n+1} corresponds to the third in fig. 6.8 (the spade behind at 10 volts), and s_{n+2} has the last characteristic of the same figure (the spade behind at 20 volts). The characteristic of s_{n-1} corresponds most

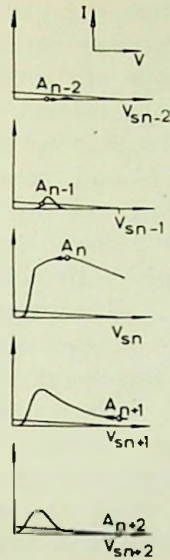


Fig. 6.9. Illustration to the self-stepping process.

closely to the second of fig. 6.7 because the spade in front of it is at 10 volts. For s_{n-2} the last characteristic of fig. 6.7 can be regarded as valid, as this spade is behind a spade at 5 volts.

The rate of change of the spade voltage is in direct proportion to the current flowing into the spade capacitance. The operating point A_{n+1} is thus moving slowly and A_n is rapidly decreasing. A_{n-1} is at rest and A_{n-2} is moving upwards. When the operating points move the shape of the characteristics changes and the stepping speed is thus very difficult to predict.

When the plate voltage is low as in fig. 6.9 the rise time of the spades becomes indirectly the limiting factor. If, for instance, the plates are suddenly brought from a positive voltage to zero the tube begins selfstepping with great speed. Before the first cycle is completed however, many spades are at low potential, the beam current decreases and the fall time of the spade voltage increases. The stepping action is slowed up and an equilibrium speed establishes itself. Under these conditions however, the tube is automatically transferred to a rather critical operation range. The spade characteristics become very low and there is a great risk for erroneous stepping.

When the plate voltage is high, *i. e.* just below the stepping voltage, the fall time is the slowest process determining the stepping speed. The characteristics of the tube are considerably different to those in fig. 6.9. They approach the normal static characteristics I and II. The characteristic corresponding to that for s_n in fig. 6.9 is the ordinary characteristic II and those for s_{n+1} and s_{n+2} approach characteristic I. The charging current to the spade capacitances and consequently the stepping speed, is now very sensitive to the plate voltage. Synchronizing is easily achieved by means of negative pulses applied to the plates. The stepping can be stabilized by introducing RC-combinations in the plate circuits, similar to the RC-coupled plate circuit arrangement for pulsed circuits. Usually it is sufficient to connect the plates to two groups and provide each of the groups with an RC-combination.

In applications where the trochotron is to be run continuously within a certain frequency range the self-stepping technique can be used to advantage. As there is no need to keep the leak current to the next spade very small the strength of the magnetic field can be reduced and thus larger current obtained. The magnetic field can be reduced to about a point where an ordinary first order characteristic (at the plate voltage proper) exhibits a tail going above the spade resistor load line. After this no ordered stepping is possible. The optimum magnetic field with regard to the speed is that for which the steepness of the higher order characteristics is a maximum. As there is no need to lock the beam by means of a first order characteristic the spade resistors can be much smaller than those used in ordinary stepping circuits. Hence the time constant of the spade circuits can be kept small, enabling dependable operation at high speeds.

6.5. Tuned circuits

When a trochotron is to be used at a constant frequency the reliability can be much increased by using tuned circuits. When the spades are connected to resonant circuits tuned to the cycling frequency the risk for erroneous stepping is eliminated within reasonable limits of voltage and magnetic field strength. Thus the tube can operate under conditions of widely varying loads and supply voltages.

Fig. 6.10 is the circuit diagram of such an arrangement. Opposite spades are connected to the ends of five independent LC-circuits,

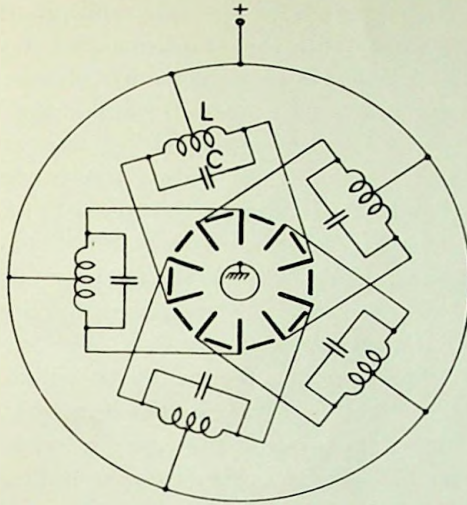


Fig. 6.10. Trochotron with tuned spade circuits.

all tuned to the same frequency, this frequency being near the actual cycling frequency. The coupling between the resonant circuits may be only *via* the electron beam. The strong preference for only one beam to be formed within the tube is the prime advantage of this circuit.

The principle of operation is illustrated in fig. 6.11. The voltage distribution of the spades is shown in *a* and the corresponding spade currents in *b*. The spade currents are obtained from a set of charac-

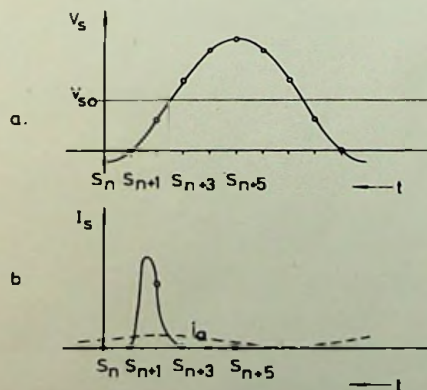


Fig. 6.11. Voltage and current distribution of the spades at tuned circuit operation.

teristics recorded for the spades on this voltage distribution. As every spade runs through all the stadiums pictured, a and b can also be regarded as voltage and current waveforms for one spade.

The LC-circuits are driven by current pulses the peak amplitude and duration of which can be obtained by the graphical method indicated in fig. 6.11. From these pulses the fundamental current wave, i_a , is determined. As evident from fig. 6.11 this current wave leads the voltage drop in the spade impedances. (Note: Time reads from right to left in fig. 6.11). The reactive component of the current supplied to the spade impedances increases the frequency beyond the natural frequency of the LC-circuits. The cycling frequency obtained is thus higher than the frequency to which the LC-circuits are tuned unless the Q-factor of the circuits is very high. At moderate Q-values there is thus a regulating mechanism, which automatically synchronizes the five LC-circuits. However, as indicated in fig. 6.11 a the spades will at the negative voltage peak go down below the cathode potential. This is favorable to the operation of the trochotron as then the beam is completely deflected and the internal feedback interrupted. The higher the Q-value the more negative the spades will go, and thus the Q is to be chosen as a compromise between stable synchronism and stable electronic discharge. In experiments Q-values of about 20 have been used.

In a circuit arrangement according to fig. 6.10 the plate current pulses will be overlapping, more or less depending on tube construction and running conditions. The plate pulses can be separated from each other by inserting resistors in series with the spade leads. In this way a locking of the beam is obtained during a certain interval of the spade voltage.

CHAPTER 7

THE BINARY TROCHOTRON AND ITS USE IN CALCULATING MACHINES

BY

L. LINDBERG

7.1. General remarks

In the rapid development of calculating machines of recent years, a general trend has been to reduce the number of tubes as far as possible in order to reduce the number of sources of error. The trochotron also represents a progress in this direction. In the first place, the ten-box-trochotrons constitute natural elements for small calculating machines working in the decade system, but the trochotron principle is also readily adaptable to the binary system of numbers.

The binary trochotron, an invention by Prof. H. ALFVÉN, is in principle an electronic switch with eight positions, controlled by the voltages on three terminals. It offers straight-forward solutions to many problems in pulse technique, such as coincidence and anticoincidence circuits and may find use in calculating machines as pyramid selector and adder for binary numbers. The number of tubes then becomes greatly reduced, and consequently the number of cathodes reducing the probability of tube failure. The cost may possibly not be smaller, but it may be of less importance if a considerable increase in reliability is achieved.

7.2. Tube properties and operation

The principle was briefly mentioned in 1.2. A schematic cross-section of the electrode system, perpendicular to the magnetic field B , is also shown by fig. 7.1. The electron beam is produced by a

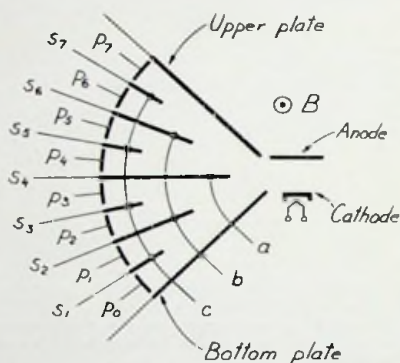


Fig. 7.1. Nomenclature in binary trochotron.

cathode and an anode. It travels between an upper plate at anode potential and a bottom plate at cathode potential. Between them there are three sets of control electrodes, a, b and c, also called «spades», $s_1 \dots s_7$. Each control electrode may shift the position of the beam so that when it is positive the beam continues below it and when negative, the beam passes above it. Ultimately the beam reaches one of the eight plates $p_0 \dots p_7$.

Fig. 7.2 shows the beam in the eight positions corresponding to the eight possible combinations of control voltages on the terminals a, b, c. These photos were taken in a large-scale model tube in which some gas was left to make the beam visible. (Pressure about 10^{-4} mm Hg). The same tube was also utilized for the investigations of the space charger barrier and the distribution of the emission, mentioned in 4.3 and 4.4.

During the development some thirty tubes were built a couple of which are shown by fig. 7.3 and 7.4. Fig. 7.8 is a drawing of the electrode system. The magnetic field is produced by a coil around the tube or a permanent magnet.

These tubes operate well at an anode voltage of 20 volts and a magnetic field of 180 gauss giving a beam current of 2 mA. In order to shift the beam, the control electrode voltage must be shifted between 0 and 20 volts with respect to the cathode. For voltages between these values the beam is divided between the plates and the control electrode as shown by fig. 7.5 and 7.6, the transfer and spade-

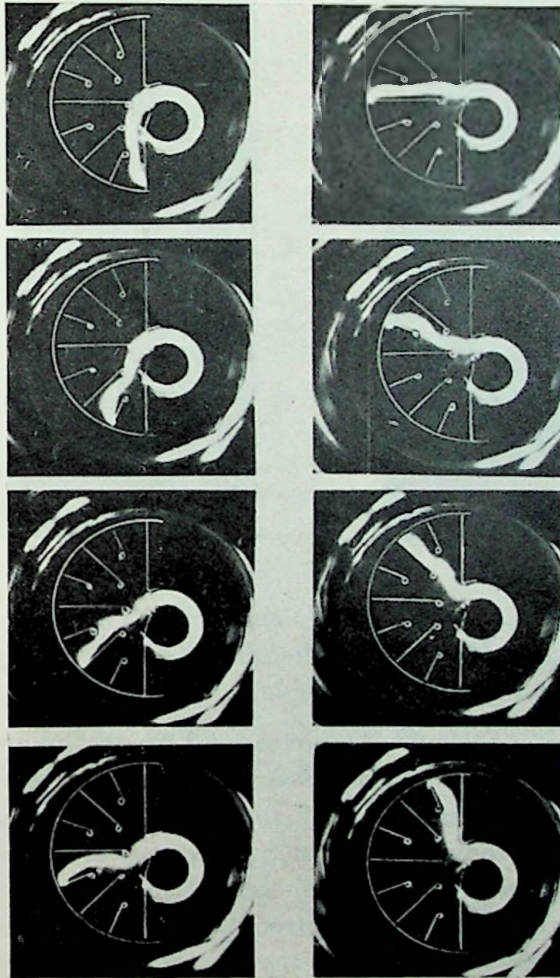


Fig. 7.2. The beam in its different positions in a binary trochotron.

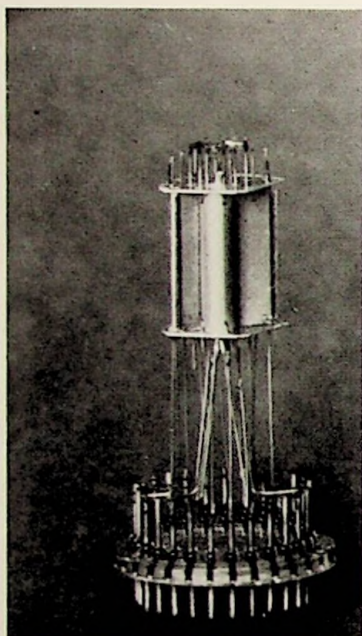


Fig. 7.3.

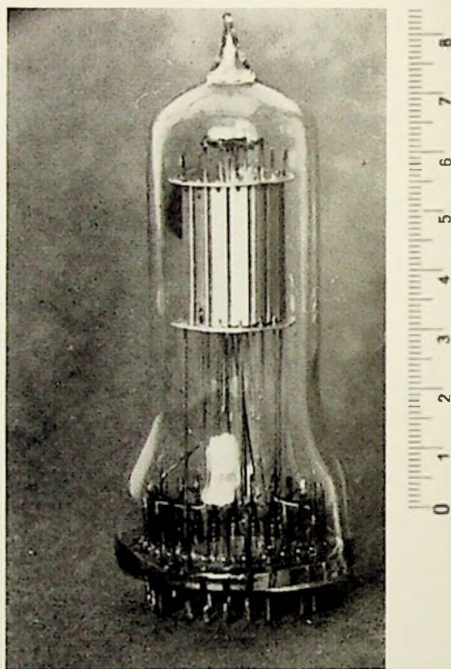


Fig. 7.4.

Figs. 7.3. and 7.4. Binary trochotrons.

characteristics of the tube, here measured for the b-group of spades. If the spade is made too negative, the beam is pressed up against the positive spade next above it, in this case belonging to group c, and if it is made too positive, it may take up part of the beam which should pass beneath it. The tolerances of the control voltages depend on the choice of magnetic field strength. In the stronger field of fig. 7.6 the tolerances are greater at the cost of a reduced beam current. The characteristics of the other control electrodes have the same general character as those shown.

A plate-characteristic is shown by fig. 7.7. It is measured with the spades at normal voltages, i. e. either 0 or 20 volts. When the plate voltage drops to zero, the beam is transferred to the positive spade next above it. In many applications this characteristic may

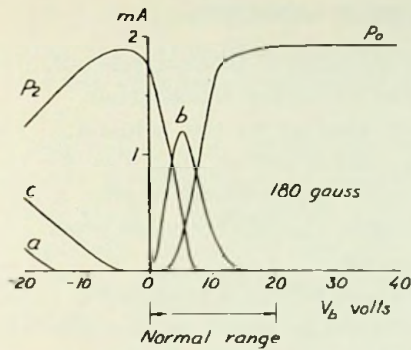


Fig. 7.5.

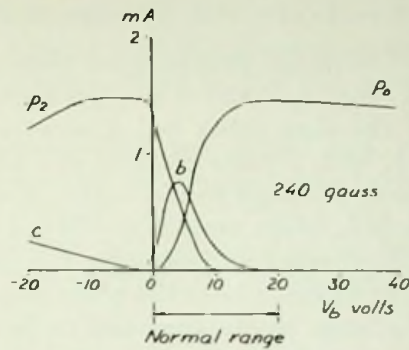


Fig. 7.6.

Figs. 7.5. and 7.6. Current distribution characteristics.

be used to limit the output voltage waveform by «bottoming» of the plate voltage, using a large plate load resistance, as indicated in fig. 7.7.

The anode is never reached by the beam and may be used for powerless control of the current.

Binary trochotrons consequently have many features common with plane and cylindrical trochotrons. The similarity principle is especially worth mentioning. The voltage level of operation may thus be arbitrarily chosen, provided all voltages are changed in the same scale and the magnetic field is changed in proportion to the square root of the voltage.

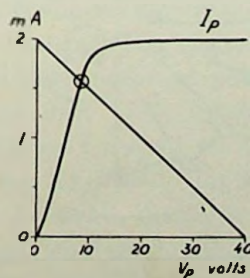


Fig. 7.7. Plate characteristic.

7.3. Design of binary trochotrons

The design principles for plane and cylindrical trochotrons outlined in chap. 1, 2 and 5 are also applicable to binary trochotrons.

The first tubes had a construction similar to the schematic fig. 7.1, with a plane cathode and anode, and a rather long way for the beam to travel to the boxes. Since most applications require a high ratio of beam current to control voltages, the efforts were especially concentrated on increasing the perveance.

In order to keep the beam degeneration within a reasonable value, the beam length then had to be shortened as much as possible, and the tube must be designed to work in a relatively weak magnetic field, utilizing a trochoidal beam of flat character. By increasing the angular space of the electrode system to 180 degrees, the beam length could be shortened, whilst the width of the boxes was maintained unchanged.

Inhomogenities in the electric field, encountered by the beam during its passage, must be kept as small as possible in order to avoid disturbances of the electron paths and widening of the beam. The most suitable position of the spades was found by estimations of the field structure and by experiments. The construction shown in fig. 7.8 is the best compromise hitherto found. The guiding power of the spades is still sufficient owing to the strong action of the space charge barrier (see 4.3). It was found that the spade edges must be

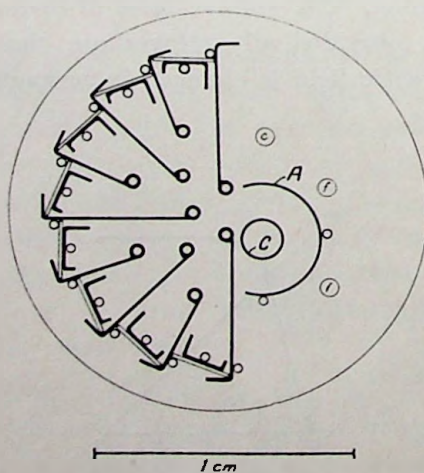


Fig. 7.8. Cross-section of binary trochotron.

rigidly clamped in their correct positions, and this was done by rolling each edge around a piece of straight wire of 0,5 mm diameter, the ends of which protrude through holes drilled in the end plates of mica.

The cylindrical cathode-anode arrangement was found superior since it gives a beam of smooth structure and requires less heater power than a large plane cathode. Coupling around the cathode is completely eliminated by the presence of the negative bottom electrode. The cathode diameter can therefore be much smaller than in a cylindrical trochotron.

7.4. Applications in calculating machines

The following description of a pyramid selector and an adder gives an idea of circuit arrangements. The machine in which these units operate is assumed to be working with serial representation in the binary system, a negative pulse representing the digit one and the absence of a pulse representing zero. The pulse amplitude is assumed about 20 volts and its duration about half the pulse interval. This implies a good utilization of the available bandwidth and secures the possibility of bringing pulses through capacitive couplings followed by d-c restoring elements. To keep the number of tubes to a minimum and simplifying the circuits as far as possible several d-c supply voltages are assumed to be available. The adder is further fed from circuits of low impedance and designed to have a low output impedance itself.

7.5. A pyramid selector

A cascade connection of 9 trochotrons to a selector with 64 positions is schematically shown by fig. 7.9. The control voltages enter on six lines from the top to the spades and the pulses that shall pass the selector are fed with reversed polarity to the anode of the single trochotron to the left. The interconnections between the trochotrons are accomplished by eight triodes each performing phase reversal, restoration of d-c level and amplification. Thanks to them all load resistances may be small, giving a rapid response. Alternatively the plates of the left trochotron could be directly connected to the cathodes of the right trochotrons.

If a selector working in the opposite direction is wanted, that is,

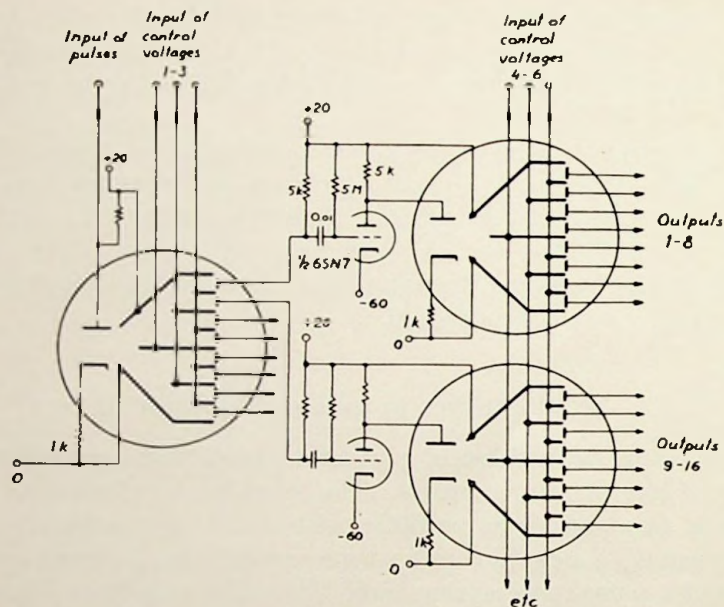


Fig. 7.9. Pyramid selector.

when pulses should be taken from one of 64 input lines, the trochotrons could be furnished with «by-spades» in the boxes, all connected to a common output line. Such by-spades have proved valuable in plane trochotrons.

7.6. A binary adder

A simple circuit of a binary adder is shown in fig. 7.10. The two numbers to be added are synchronously fed to the spade groups c and b. The carry pulses occurring during addition are, after delay for one pulse interval amplified and fed to the spade a, as positive pulses.

Those plates in the trochotron that correspond to the binary sum 01 are connected to a common load resistance of $20\text{ k}\Omega$, large enough to secure bottoming of the plate voltage to set the amplitude of the output pulses. After d-c restoration by a diode the pulses pass a cathode follower and enter the output line.

The plates corresponding to the sum 10 are directly connected to a delay line ($Z_0 = 10\text{ k}\Omega$, $\tau = 8\text{ }\mu\text{s}$). After delay the pulses pass a capacitive coupling to a pentode with positive grid bias and series

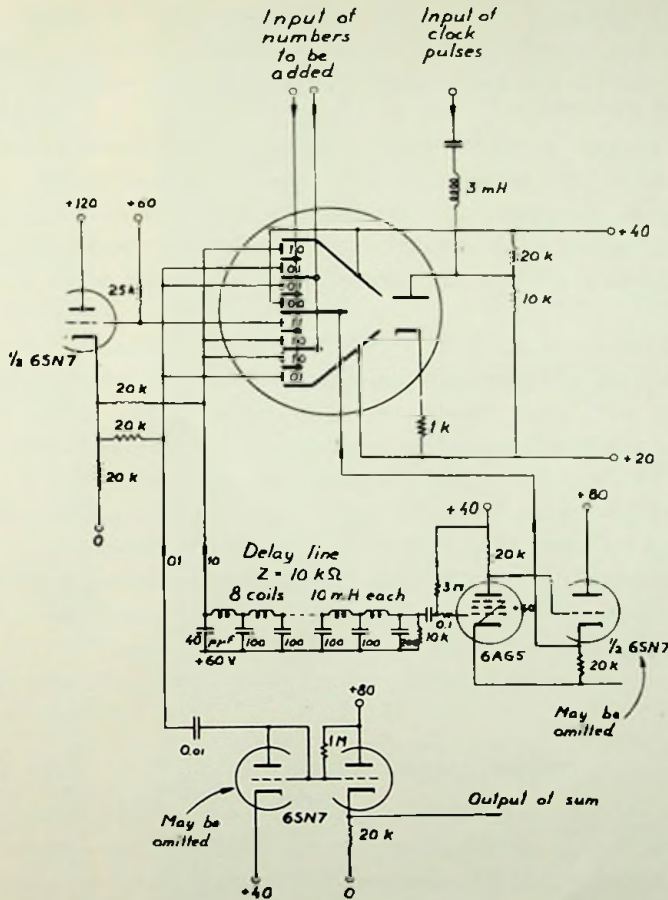


Fig. 7.10. Binary adder.

grid resistance, which slices the pulse between two limits and sets the d-c-level. The anode resistance is large to secure bottoming and a cathode follower is inserted to lower the impedance seen from the trochotron.

The sum 11 is represented by one plate. A pulse on it is divided by a triode connected as a cathode follower to give an output pulse, 01, and a carry pulse, 10.

To avoid false output pulses which would occur during the changes of the control voltages, the emission is cut off during the changes by a square wave applied to the anode.

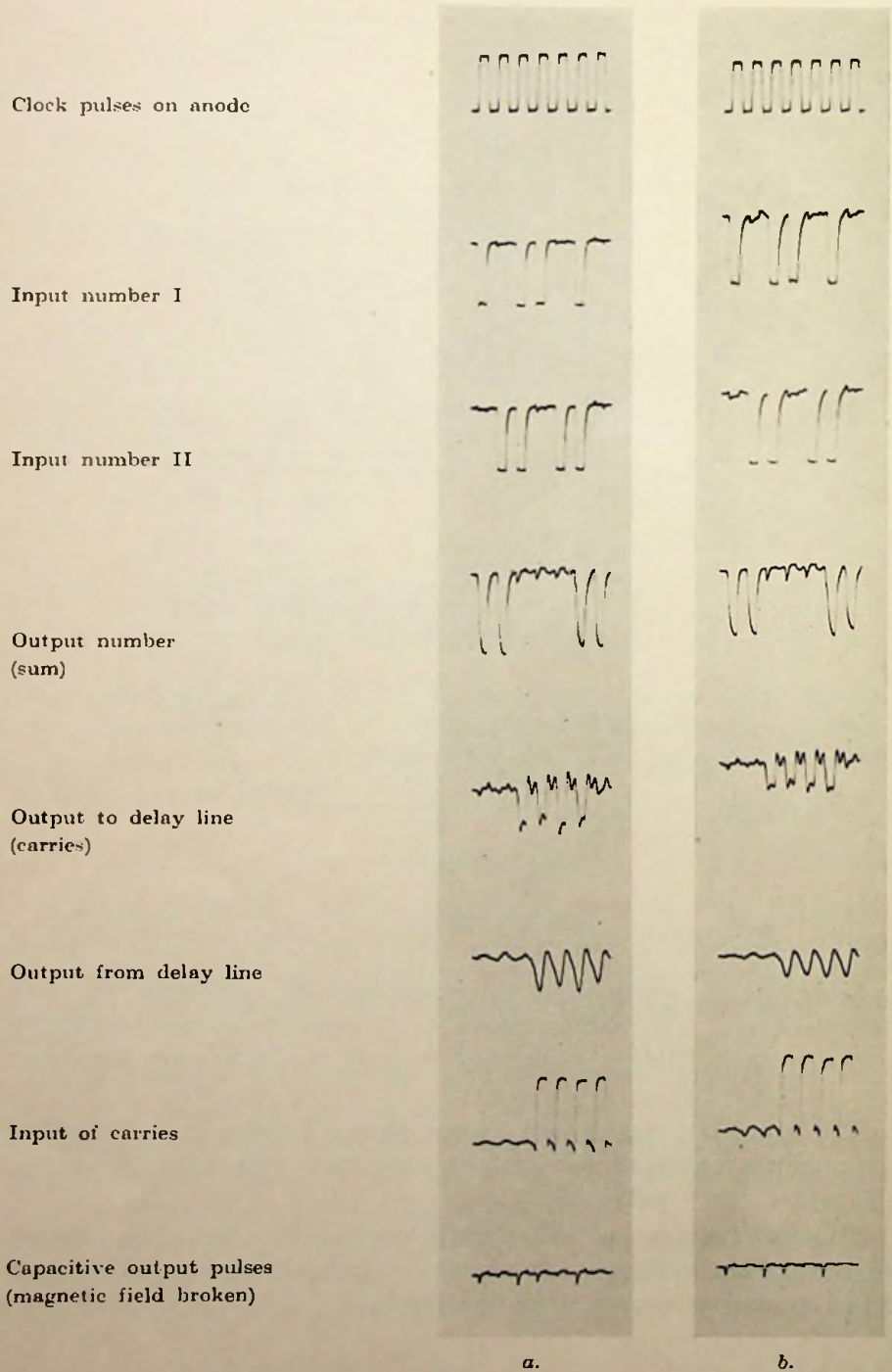


Fig. 7.11. Pulse oscillograms in adder.

The trochotron here operates at 20 volts in a magnetic field of 170 gauss, giving a plate current of about 2 mA. The cathode resistance of $1\text{ k}\Omega$ gives the cathode a small positive bias and serves to stabilize the emission.

For experimental investigation of the adder a special generator was built to give two numbers to the adder. It consisted of a cylindrical ten-box trochotron, continually stepping around, from which pulses were taken from certain boxes. The two numbers were selected to give the binary trochotron all possible combinations of control voltages.

The oscillograms to the left of fig. 7.11 show the pulses on input and output terminals and on the delay line with the least significant digits at left. The memory pulses must enter the trochotron somewhat before the anode pulses and leave somewhat after it to avoid cumulative errors in the output pulses, which would otherwise occur at additions that have long series of carry digits. In the experimental circuit no special attention was paid to the delay line. With a more careful design the number of sections may be reduced. The input pulse width could be reduced somewhat below $2\ \mu\text{s}$ without decrease in the output pulse amplitude. This implies that the pulse frequency may be increased until some 300 kc/s with the same circuit.

7.7. A simplified binary adder

If a fast multiplier is to be composed from a number of adders, it is of course desirable that they should be as simple as possible. The number of tubes may be further reduced if the input terminals to the trochotron are allowed to have high impedance. In a special experiment the output impedance was increased to $20\text{ k}\Omega$, the cathode follower in the carry line was omitted, and the d-c level of the output line was reset by a voltage divider instead of the diode. The remaining tubes are thus one binary trochotron, one triode and one pentode. To avoid leak currents the magnetic field had to be increased to 200 gauss and was a little more critical, but not seriously. The emission correspondingly decreased to 1 mA. The output pulse amplitude is now set by the product of emission times load resistance, since the plate voltage may never bottom. The oscillograms to the right of fig. 7.11 show the voltage waveforms. It is obvious that the speed of response is decreased, but at the actual frequency of 100 kc/s it is still sufficient.

Appendix

CHAPTER 8

MEASURING TECHNIQUE

BY

L. LINDBERG

In the development different kinds of measurements are necessary for the analysis and solution of the problems. Four types of measurements are essential: static characteristics of spades and plates, leak currents, noise and oscillations, and finally operating data in a counting circuit.

In our measurements certain precautions had to be taken causing the conditions to differ considerably from the conditions in practical use. The magnetic field was produced by a large coil around the tube and in order to avoid disturbances in the magnetic field from the chrome-iron base pins, the electrode systems were mounted on rather long leads from the base. The variation of the magnetic field along the axis of the coil was less than three percent within the utilized region. The high transconductances of the tubes easily produce oscillations of different kinds, which must be suppressed as far as possible by the methods discussed in 4.9.

8.1. Photographic recording of static characteristics

Oscilloscopic visualization of tube characteristics has been utilized as far as possible. It is preferable to point-by-point plotting not only because it saves time, but because it gives more true and detailed characteristics, in which all changes can be immediately observed when any parameter is altered. It therefore gives enormously more information about what happens in the tube than a point-by-point plot, in which most details would certainly be lost. Besides, the

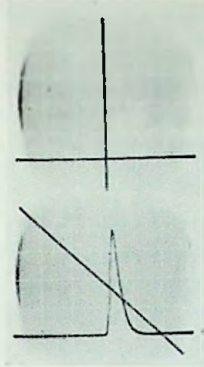


Fig. 8.1.

equipment is not damaged by shorts occurring in the tube, a valuable property in experimental work like this.

As mentioned in 1.5, the similarity principle is valid both for the normal behavior of the electrons and for the noise, and is also experimentally confirmed in 4.10. Thus, it is sufficient to make most measurements at one standardized voltage level without loss in generality. The value chosen for all photographed characteristics was 20 volts. The coordinate axes are always situated as in the top picture of fig. 8.1, and the horizontal voltage scale always runs from -30 to $+30$ volts. The vertical current scale is frequently changed and is given in each case by denoting the current corresponding to one division of the coarse network.

The bottom picture of fig. 8.1 is an example of a spade characteristic and a load line. The current scale is $1 \text{ div.} = 0,2 \text{ mA}$, thus, the height of the characteristic is $0,75 \text{ mA}$ and the load line corresponds to $50 \text{ k } \Omega$.

8.2. Equipment

A scheme of the complete equipment is shown by fig. 8.2. The trochotron in the center is placed in a special holder and is connected to stabilized supply voltages through a switch-box permitting any electrode to be connected to a desired voltage or to the measuring equipment in the upper right corner.

The special holder is provided with decoupling capacitors and damping resistors in direct contact with the tube pins. The capacitors of about 100 pF are formed by thin sector-shaped phosphor-

bronze springs radially clamped between a heavy aluminium plate and an aluminium ring from which they are insulated by thin «telcothene» sheets. The damping resistors are ordinary 0,5 watt, 80Ω carbon resistors, the leads of which are cut to 5 mm length.

In fig. 8.2 the equipment is connected for recording of a spade characteristic. The spade voltage is swept by a 50-cps voltage applied via a transformer. The midpoint of the transformer winding is connected to ground through a small resistance, r_s , in fig. 8.2, over which the current flowing to the spade develops a voltage proportional to the current. This voltage is amplified and fed to the y -plates of an oscilloscope, whilst the x -deflection is made proportional to the spade voltage. The characteristic of the spade is then recorded. Capacitive current to the spade flowing in the decoupling capacitor is balanced by an adjustable capacitor C fed in opposite phase from the transformer.

Cut-off-characteristics are obtained by connecting all spades and plates to the alternating voltage.

Transfer characteristics, *e. g.* the current to a plate as function of the voltage of a spade, is obtained by observing the voltage developed across a small resistor r_p in series with the plate whilst the spade is fed with the alternating voltage. The deflection characteristics are recorded in a similar way.

Small leak currents cannot be observed on the oscilloscope but must be measured with a galvanometer and plotted point by point. For measurements down to 10^{-9} A an *RCA* «Ultrasensitive» tube microammeter has been used. Leak currents due to bad insulation had in some tubes to be eliminated by keeping the electrode to which the current was measured at the same voltage as adjacent electrodes.

8.3. Detection of noise and h. f. oscillations

During most measurements, a video detector was connected to the cathode of the trochotron. It is shown in fig. 8.2 below the trochotron. Any h. f. voltage occurring across the cathode resistor of 50Ω is detected by a silicon crystal, (type 1 *N* 21) operating as a square law detector at zero d. c. current. One pole of the crystal is grounded through a shorted 50Ω coaxial stub of variable length. In its shortest position it acts as a simple short circuit for frequencies below a few hundred megacycles. Above 150 Mc it may be used for approximate wavelength estimations and for tuning the crystal

detector to a certain frequency. The other pole of the crystal is through a low-pass filter connected to a high gain audio amplifier (75—100 dB) A d. c. amplifier with stabilized zero level would be preferable. Now only changes in the h. f-voltage level can be detected. However by applying the same 50-cps voltage to a spade as used when measuring characteristics, the operating conditions are periodically and completely changed and so are the generated oscillations and noise too. The detected signal is then displayed on the oscilloscope as function of the spade voltage. At least during some portion of the cycle the signal is likely to be zero, thereby indicating the zero level. Noise and oscillations are of quite different appearance, the oscillations localized to relatively sharply defined voltages and often of high amplitude, the pure noise rather insensitive to voltage and of lower amplitude. This arrangement is of great value since it indicates whether oscillations occur at all or not, irrespective of their particular frequency within a very wide range.

When measuring the frequency spectrum in fig. 4.14 a radar receiver (type AN/APR 4) was used. It covered with three tuning units the range 38—1000 Mc/s.

Acknowledgement

We wish to acknowledge our sincere thanks to Prof. H. ALFVÉN, the inventor of the trochotron, who was a source of inspiration and encouragement during the work. We are very thankful to the State Council of Technical Research for the financial support of the work. We also wish to thank our colleagues, especially Mr D. ROMELL and Mr E. ÅSTRÖM for many valuable suggestions and comments, and all others in the laboratory and the workshop for their valuable assistance. We wish to extend our thanks also to Mr O. STERNBECK and Mr H. NETTELBLADT of Telefonaktiebolaget L. M. ERICSSON and finally to Mrs M. WALLMARK for her linguistic corrections.

JONAS BJÖRKMAN · LENNART LINDBERG
The Royal Institute of Technology, Stockholm
Division of Electronics
November 1953

Literature

- ALFVÉN, H. and ROMANUS, H. 1947. Valve with trochoidal electronic motion. *Nature*, 160, p. 614, 1947.
- ALFVÉN, H., LINDBERG, L., MALMFORS, K. G., WALLMARK, T. and ÅSTRÖM, E. 1948. Theory and Applications of Trochotrons. *Transact., Roy. Inst. Techn., Stockholm*, No 22, 1948. [Also *Acta Polytechnica* 34 (1949) *El. Eng. Ser. 2 nr 2*].
- ALFVÉN, H. 1950. *Cosmical Electrodynamics*, Oxford 1950.
- COLLINS *et al.* 1948. *Microwave Magnetrons*, Rad. Lab. Series, MIT, vol. 6.
- ENGBERT, W. 1938. Die Potentialverteilung im Magnetron. *Hochfrequenztechnik und Elektroakustik*, 51, p. 44 (1938).
- HARVEY, A. F. 1943. *High Frequency Thermionic Tubes*, Wiley, N. Y. 1943.
- MOULLIN, E. B. 1940. Considerations of the Effect of Space Charge in the Magnetron. *Proc. Cambr. Phil. Soc.* 36, p. 94, 1940.
- REVERDIN, D. L. 1951. Electron Optical Exploration of Space Charge in a Cut-Off Magnetron. *J. Appl. Phys.* 22 p. 257 (1951).
- SPANGENBERG, K. 1948. *Vacuum Tubes*, Mc Graw-Hill, N. Y. 1948.

Table of contents.

	Page
Summary	3
Chapter 1. Basic Trochotron Technics	5
1.1. Trochoidal electronic beams	5
1.2. Trochotrons	6
1.3. Tube characteristics	9
1.4. Degeneration in trochoidal beams	12
1.5. The similarity principle	14
1.6. Trochotron circuits	16
1.7. Scale-of-ten	18
1.8. The plane trochotron as a scale-of-ten	19
Chapter 2. The Cylindrical Trochotron	21
2.1. Comparison of the plane and the cylindrical trochotron designs	21
2.2. Electrode arrangement	21
2.3. The discharge mechanism	23
2.4. Characteristics and circuits	26
2.5. The design problem	28
2.6. Hybrid tube types	32
Chapter 3. Theoretical Considerations	39
3.1. General differential equations for a plane magnetron	39
3.2. Laminar streaming	40
3.3. The general cut-off relation	41
3.4. The translation current	42
3.5. Graphic representation for a plane magnetron	45
3.6. Space charge influence on electron paths	47
3.7. Disturbed electron paths	47
3.8. Influence of nonhomogeneous electric field	49
3.9. Field distribution and circulating current in a cylindrical magnetron	50
3.10. Graphic representation	51
Chapter 4. Experimental Investigations	54
4.1. Fundamental phenomena	54
4.2. Effect of space charge on beam position	54
4.3. Deflection by space charge barrier	55
4.4. Distribution of the emission	57
4.5. Cut-off in cylindrical trochotrons	58

	Page
4.6. Deflection characteristics and noise	60
4.7. Spade characteristics and the beam length	62
4.8. Leak currents	64
4.9. Oscillations and noise	67
4.10 Control of the similarity principle	70
Chapter 5. Design of Cylindrical Trochotrons	72
5.1. Experimental tubes	72
5.2. Mechanical construction	72
5.3. Data and characteristics of the experimental tubes	75
5.4. Design of the boxes and influence of the plate voltage	85
5.5. A cathode for distributed emission	88
5.6. Theory and design	92
5.7. Discussion	95
Chapter 6. Design of Circuits	98
6.1. Considerations for maximum reliability	98
6.2. Considerations for maximum speed	100
6.3. Some details of the stopping process	105
6.4. Continuously stepping circuits	108
6.5. Tuned circuits	110
Chapter 7. The Binary Trochotron and Its Use in Calculating Machines	113
7.1. General remarks	113
7.2. Tube properties and operation	113
7.3. Design of binary trochotrons	118
7.4. Applications in calculating machines	119
7.5. A pyramid selector	119
7.6. A binary adder	120
7.7. A simplified binary adder	123
Appendix	
Chapter 8. Measuring Technique	124
8.1. Photographic recording of static characteristics	124
8.2. Equipment	125
8.3. Detection of noise and h. f. oscillations	127
Acknowledgement	129
Literature	129

36. TISCHER, F., *Die Genauigkeit der Impedanzmessung bei Mikrowellen*. 31 s. 1950. Kr. 2: 50.
37. WRANGLÉN, COSTA, *On the Principles of Electrodeposition of Metal Powders*. 31 s., 8 pl. 1950. Kr. 2: 50.
38. DAHLGREN, F., *Some Remarks on the Energy Flow in Rotating Electric Machines*. 16 s. 1950. Kr. 2: 50.
39. ÅSLANDER, ALFRED, *Relation between Geologic Formation and Content of Easily Soluble Plant Nutrients in Clays of the Uppsala Region*. 44 s. 1950. Kr. 4: —.
40. HELLSTRÖM, NILS, *On Distillates from Fir Stumps*. Part. III. Investigation of Rosin Acids. 44 s. 1950. Kr. 4: —.
41. HELLSTRÖM, B., and RUNDGREN, L., *Model Tests for Port of Malmö Improvements*. (Bulletin No. 25 of The Institution of Hydraulics). 56 s. 1950. Kr. 5: —.
42. HILTSCHER, RUDOLF, *Ein praktisches Lateralexensometer zur Bestimmung der Spannungssumme*. 22 s. 1950. Kr. 2: 50.
43. BRIMBERG, STIG, *Influence of Losses on Attenuation of Four-Terminal Impedance Networks*. 30 s. 1950. Kr. 3: —.
44. ZACHRISSON, L. E., *On the Membrane Analogy of Torsion and its Use in a Simple Apparatus*. 40 s. 1951. Kr. 4: —.
45. TISCHER, F., *Induktive Sonde für Messleitungen und Nahfeldprüfer bei Mikrowellen*. 18 s. 1951. Kr. 3: —.
46. *Supplement No. 1 to List of Publications of Members of the Staff of The Royal Institute of Technology, Stockholm*. 75 s. 1951. Kr. 5: —.
47. DAHLGREN, F., and LITCKE-PERSSON, A. K., *Static Frequency Transformers for Small Electric Motors*. 27 s. 1951. Kr. 3: 50.
48. BOLINDER, FOLKE, *Fourier Transforms in the Theory of Inhomogeneous Transmission Lines*. 84 s. 1951. Kr. 6: —.
49. BJERHAMMAR, ARNE, *Application of Calculus of Matrices to Method of Least Squares With special Reference to Geodetic Calculations*. 86 s. 1951. Kr. 10: —.
50. PIERIE, BO, *Influence of Frames on Insulation of Cold Storage Chambers on Board Ship*. 65 s. 1951. Kr. 7: —.
51. DAHLGREN, F., *Theory and Applications of Wave Vectors*. 68 s. 1951. Kr. 7: 50.
52. LARSSON, GERHARD, *Income Value of Marginal Areas on Farms*. 61 s. 1951. Kr. 7: —.
53. DAHLGREN, F., and BIRINGER, P., *Speed Regulation of Slip-Ring Induction Motors for Special Purposes*. 39 s. 1951. Kr. 4: 50.
54. WIDELL, T. A., and JUHÁSZ, S. I., *Metal Temperature in Regenerative and Recuperative Air Preheaters*. 50 s. 1952. Kr. 6: 50.
55. FANT, GUNNAR, *The Heterodyne Filter*. 78 s. 1952. Kr. 10: —.
56. VOIPIO, ERKKI, *Voltage Stability of Synchronous Alternators with Capacitive Loads*. 64 s. 1952. Kr. 8: —.
57. NIORDSON, FRITHOF I. N., *Transmission of Shock Waves in Thinwalled Cylindrical Tubes*. 24 s. 1952. Kr. 3: 50.
58. MEYERSBERG, G., *Grösseneinfluss und Randeinfluss auf die Festigkeit der Werkstoffe*. 123 s. 1952. Kr. 12: —.
59. BJÖRLING, G., *The Conductivity of some Molten Silicates on Fayalite Basis*. 32 s. 1952. Kr. 4: —.
60. BRUNDELL, P.-O. and ENANDER, B., *The Neutron-Proton System with a Central Exponential Potential, I*. 14 s. 1952. Kr. 3: —.
61. WINQVIST, GUSTAV, *Ground Water in Swedish Eskers*. 91 s. 1953. Kr. 10: —.
62. PETERSSON, S., *Investigation of Stress Waves in Cylindrical Steel Bars*. 22 s. 1953. Kr. 3: 50.
63. TISCHER, F., *The Effective Bandwidth of Video Amplifiers*. 32 s. 1953. Kr. 4: —.
64. FALKEMO, CURT, *On the Possibilities of Estimating the Towing Resistance of Ships by Tests with Small Models*. I. (Publication no 2 of the Ship Testing Laboratory.) 61 s. 1953. Kr. 7: —.
65. PRAGER, WILLIAM, *A Geometrical Discussion of the Slip Line Field in Plastic Flow*. 27 s. 1953. Kr. 4: —.
66. ODQVIST, FOLKE K. G., *Influence of Primary Creep on Stresses in Structural Parts*. 18 s. 1953. Kr. 2: 50.
67. ALM, EMIL, *Small Self-excited and Self-compounded Three-phase Generators*. 42 s. 1953. Kr. 6: —.
68. HÅMOS, L. v., *An X-Ray Microanalyzer Camera*. 68 s. 1953. Kr. 9: —.
69. KNUDSEN, NIELS H., *Abnormal Oscillations in Electric Circuits Containing Capacitance*. 134 s. 1953. Kr. 12: —.
70. ÅLLANDER, CLAES GUSTAF, *Untersuchung des Adsorptionsvorganges in Adsorbentenschichten mit linearer Adsorptionsisotherme*. 160 s. 1953. Kr. 10: —.
71. RAHM, LENNART, *Flow Problems with Respect to Intakes and Tunnels of Swedish Hydro-Electric Power Plants*. 219 s. 1953. Kr. 18: —.
72. NILSSON, SVEN GÖSTA, *The Motion of Electrons in two combined Magnetic Fields*. 23 s. 1953. Kr. 4: —.

73. FRITHIOF I. N. NIORDSON, *Vibrations of a Cylindrical Tube Containing Flowing Fluid.* 28 s. 1953. Kr. 4:—.
74. SCHNITTOER JAN, R., *Vortex Flow in Axial Turbo Machines.* 62 s. 1954. Kr. 8:—.
75. VON DARDEL, G. F., *The Interaction of Neutrons with Matter Studied with a Pulsed Neutron Source.* 104 s. 1954. Kr. 10:—.
76. B. HELLSTRÖM and L. RUNDGREN, *Model Tests on Ölands södra grund Lighthouse.* 66 s. 1954. Kr. 8:—.
77. BROWN, GÖSTA, *Theory of Moist Air Heat Exchangers.* 33 s. 1954. Kr. 5:—.
78. FORSELL, CARL, *Schubfestigkeit und Schubwehrrung der Betonbalken.* 65 s. 1954. Kr. 10:—.
79. *Basorganisation för forskning vid de tekniska högskolorna.* 154 s. + 6 tabellbilagor. 1954. Kr. 12:—. (Not for exchange).
80. J. BJÖRMAN and L. LINDBERG, *Development of trochotrons.* 131 s. 1954. Kr. 12:—.